NON-LINEAR FINITE ELEMENT SIMULATIONS OF HYDROGEN DIFFUSION AND HYDROGEN-DISLOCATION INTERACTIONS

by

Zara Molaeinia

A dissertation submitted to Johns Hopkins University in conformity with the requirements for the degree of Master of Science

Baltimore, Maryland

May, 2015

NON-LINEAR FINITE ELEMENT SIMULATIONS OF HYDROGEN DIFFUSION AND HYDROGEN-DISLOCATION INTERACTIONS

Abstract

The effect of hydrogen on dislocation-Impurity atom interactions is studied under conditions where hydrogen is in equilibrium with local stresses and in systems where hydrogen increases the elastic modulus.

The problem is investigated for the plane strain case, where the effect of hydrogen is modeled by a continuous distribution of dilatation lines whose strength depends on the local hydrogen concentration.

The iterative finite element analysis used to calculate the hydrogen distribution accounts for the stress relaxation associated with the hydrogen Induced volume and the elastic moduli changes due to hydrogen.

Modeling of the hydrogen effects on the edge dislocation-interstitial solute atom interaction is discussed using a finite element analysis and the atom interaction energies are calculated in the presence of hydrogen.

The interaction includes the effect of both the first and the second order terms of interaction energies, effects of initial concentration of hydrogen on diffused concentration near and far away from the dislocations.

The models have been employed to evaluate all effects on a single dislocation, two dislocations in a same slip planes, and randomly-distributed.

The computational scheme is compared to literature with a very good agreement.

Readers

Stefanos Papanikolaou, Jaafar El-Awady (Advisor)

Acknowledgements

I thank my advisor, Professor Jaafar El-Awady, for all of his guidance.

I am very appreciative to Professor Stefanos Papanikolaou for reviewing my thesis, and most helpful comments are tremendously valued.

I thank to administrative staff who were always sincerely helpful and caring, Mike Bernard, Kevin Adams, and Cindy Larichiuta.

I am extremely grateful of my family and friends for unconditionally supporting me in the entire time of my life, in happiness and pain.

I dedicate this work to my family

Contents

Abstract ..... **ii**

Acknowledgements ..... **iv**

CHAPTER 1: Hydrogen Embrittlement **1**

1-1 Types of Hydrogen embrittlement **2**

1-1-1 Internal hydrogen embrittlement **2**

1-1-2 Environmental hydrogen embrittlement **3**

1-2 Hydrogen embrittlement mechanism in macroscopic level **3**

1-2-1 Hydrogen-induced cracking 3

1-2-2 Delayed failure 5

1-2-3 Flaking and shatter cracking 6

1-2-4 Hydrogen attack 6

1-3 Hydrogen embrittlement mechanism at the microscopic level **7**

1-3-1 Hydride-induced embrittlement (HIE) 7

1-3-2 Interstitial mechanisms - Hydrogen-Enhanced Decohesion (HEDE) … 9

1-3-3 Interstitial mechanisms - Hydrogen-Enhanced Localized Plasticity (HELP) ……...……. 11

1-4 Point Defects in Crystalline Materials ……..…….. 13

1-5 Interstitial sites in bcc and fcc unit cells ……..… 14

CHAPTER 2: Diffusion ……..…… 17

2-1 Interdiffusion mechanism ……..... 17

2-2 Diffusion and Gibbs free energy-Fick's first law ……. 19

2-3 Diffusion and Gibbs free energy- Fick's second law ……... 22

2-4 Steady state diffusion and Fick's first law ……. 23

2-5 General solution of the diffusion equation ……... 24

CHAPTER 3: General Solution for the Diffusion Equation in the Steady State due to Dislocation Stress Fields ……...…..…… 25

3-1 The interaction energy ……..... 26

3-2 Dislocation singularity …….. 27

3-3 The general inclusion ……. 29

3-4 The interaction energy between dislocations and solute atoms ……..... 36

3-5 Screw dislocation stresses ……. 37

3-6 Edge dislocation stresses ……... 38

3-7 Slip systems in body centered crystal structure …… 40

3-8 The interaction energy- Screw dislocation …… 42

3-9 The interaction energy – Edge dislocations …… 43

3-10 The first and the second order interaction energies ……...… 45

CHAPTER 4: The force on a singularity by surface tractions …….. 47

4-1 Force between two dislocations ……... 51

4-2 Hydrogen Effect on the interaction between two edge dislocations ……. 54

4-3 The stress field of a single hydrogen dilatation line …… 54

4-4 Plane strain condition ……... 56

4-5 Interaction of a single dilatation line with an applied stress ……..... 58

4-6 shear stress of hydrogen dilatation lines on a dislocation …….. 59

CHAPTER 5: General finite element approach ……..…….. 63

5-1 Four-Node rectangular elements …….. 71

5-2 Implicit integration to solve non-linear equations ……... 73

5-2-1 Newton–Raphson method ……. 73

5-3 Hydrogen effect on the elastic moduli of niobium ……..… 75

CHAPTER 6: Simulations and results ……..……..…….. 77

6-1 Finite element simulation cell and imposed boundary conditions ……..… 77

6-2 Verification of computational scheme ……..... 79

6-2-1 Single edge dislocation …….. 80

6-2-2 Two parallel edge dislocations with equal Burgers vectors …… 80

6-2-3 Two parallel edge dislocations with opposite Burgers vectors …….. 83

6 -3 Extended studies …… 98

6 -3-1 Effect of initial hydrogen concentration ……..… 98

6 -3-2 Effect of the second order interaction energy ……..…… 101

6 -3-3 Randomly-distributed dislocations ……..…….. 105

6 -4 Closure ……...…… 110

References ……...…….. 111

List of Figures

Figure 1-1 Blistering of the surface of a pressure vessel due to hydrogen existence [12] ……..…...4

Figure 1-2 Stepwise cracking due to the presence of hydrogen [14] ……...…5

Figure 1-3 Delayed failure at a lower stress level [16] ……...…5

Figure 1-4 brittle failure during forging metals [18] ……..6

Figure 1-5 Hydrogen attack at high temperature [19] ……...7

Figure 1-6 Hydride field causing crack growth [23] ……..8

Figure 1-7 Reduction of cohesion in solute matrix [27] ……...11

Figure 1-8 Hydrogen manifested as a point defect in materials ……14

Figure 1-9 a) Octahedral and b) Tetrahedral sites in a bcc unit cell ……..15

Figure 1-10 a) Octahedral and b) Tetrahedral sites in a fcc unit cell …….16

Figure 2-1 Vacancy diffusion ……...18

Figure 2-2 Interstitial diffusion ……...19

Figure 2-3 Diffusion in solvent from position x to $x+a$ ……20

Figure 3-1 Removing the inclusion from the matrix ……30

Figure 3-2 Putting back the inclusion to the matrix ……..31

Figure 3-3 Relaxing body forces and converting to self-stress state ……..….31

Figure 3-4 Body with singularity-S ……35

Figure 3-5 Elastic distortion produced by screw dislocation ……...……..38

Figure 3-6 Elastic distortion produced by edge dislocation …….……..39

Figure 3-7 bcc slip systems ……..……41

Figure 4-1 Two parallel edge dislocations ……52

Figure 4-2 Two parallel screw dislocations ……..……..53

Figure 4-3 The shear stress $d\tau_H$, induced at the core of the dislocation 2 by the hydrogen dilatation lines [49] ……..…….63

Figure 5-1 Element local coordinate system ……..71

Figure 6-1 schematic of the simulation cell ……...79

Figure 6-2 Contours of the normalized hydrogen concentration $\frac{c}{c_0}$ around a single edge dislocation at a nominal hydrogen concentration $c_0 = 0.1$ and temperature 300 K ……..81

Figure 6-3 Contours of the normal and shear stresses around a single edge dislocation at a nominal hydrogen concentration, $c_0 = 0.1$, and temperature, 300K a) Normal stress in the x direction b) Normal stress in the y direction c) Shear stress on the xy plane ……83

Figure 6-4 Contours of the normalized hydrogen concentration $\frac{c}{c_0}$ around two parallel edge dislocations with equal Burgers vectors at a nominal hydrogen concentration, $c_0 = 0.1$, and temperature, 300 K The separation distances are a) 6b b) 8b c) 10b ……..85

Figure 6-5 Contours of the normal stresses in the x direction around two parallel edge dislocations with equal Burgers vectors at a nominal hydrogen concentration, $c_0 = 0.1$, and temperature, 300 K The separation distances of a) 6b b) 8b c) 10b ……..87

Figure 6-6 Contours of the normal stress in y direction around two parallel edge dislocations with equal Burgers vectors at a nominal hydrogen concentration, $c_0 = 0.1$, and temperature, 300 K The separation distances are a) 6b b) 8b c) 10b ……88

Figure 6-7 Contours of the shear stress on the xy plane around two parallel edge dislocations with equal Burgers vectors at a nominal hydrogen concentration, $c_0 = 0.1$, and temperature, 300 K The separation distances are a) 6b b) 8b c) 10b ……90

Figure 6-8 Contours of the normalized hydrogen concentration $\frac{c}{c_0}$ around two parallel edge dislocations with opposite Burgers vectors at a nominal hydrogen concentration, $c_0 = 0.1$, and temperature, 300 K The separation distances are a) 6b b) 8b c) 10b ……..92

Figure 6-9 Contours of the normal stresses in x direction around two parallel edge dislocations with opposite Burgers vectors at a nominal hydrogen concentration, $c_0 = 0.1$, and temperature, 300 K The separation distances are a) 6b b) 8b c) 10b ……..94

Figure 6-10 Contours of the normal stress in the y direction around two parallel edge dislocations with opposite Burgers vectors at a nominal hydrogen concentration, $c_0 = 0.1$, and temperature, 300 K The separation distances are a) 6b b) 8b c) 10b ……..96

Figure 6-11 Contours of the shear stress on the xy plane around two parallel edge dislocations with opposite Burgers vectors at a nominal hydrogen concentration, $c_0 = 0.1$, and temperature, 300 K The separation distances are a) 6b b) 8b c) 10b ……..97

Figure 6-12 Contours of the normalized hydrogen concentration $\frac{c}{c_0}$ around a single edge dislocation for temperature 300 K and different nominal hydrogen concentrations a) $c_0 = 0.1$ b) $c_0 = 0.01$ c) $c_0 = 0.001$ ……100

Figure 6-13 Contours of the normalized hydrogen concentration $\frac{c}{c_0}$ around a single edge dislocation with first and second order interaction energies for temperature, 300 K The initial concentrations are a) $c_0 = 0.1$ b) $c_0 = 0.01$ c) $c_0 = 0.001$ ……...103

Figure 6-14 Contours of the ratio of the second order to the first interaction energy around a single edge dislocation for temperature, 300 K The initial concentrations are a) $c_0 = 0.1$ b) $c_0 = 0.01$ c) $c_0 = 0.001$ ……105

Figure 6-15 Contours of the normalized hydrogen concentration $\frac{c}{c_0}$ around randomly-distributed dislocations with the first and second order interaction energies and for initial concentration, 0.1 and temperature, 300 K a) Only the first order interaction energy b) Both the first and the second order interaction energies ……..107

Figure 6-16 Contours of the normalized hydrogen concentration $\frac{c}{c_0}$ around randomly-distributed dislocations with the first and the second order interaction energies for initial concentration, 0.01 and temperature, 300 K a) Only the first order interaction energy b) Both the first and the second order interaction energies ……..109

List of Tables

Table 1-1 Interstitial sites in bcc and corresponding planes …….15

Table 1-2 Interstitial sites in fcc and corresponding planes ……..16

CHAPTER 1

Hydrogen Embrittlement

Hydrogen embrittlement (HE) is the degradation of structural properties of solids due to the presence of hydrogen resulting in a decrease of the toughness or ductility and reduced load carrying capacity of a material. Consequently there would be a brittle failure below the yield stress of the susceptible material [1]. Hydrogen embrittlement occurs in most metals, and the most vulnerable materials for hydrogen embrittlement are high strength steels, however, this effect can be ignored usually in copper, gold, silver, and tungsten [2].

General effects of hydrogen presence in materials can be observed on the strain hardening rate, tensile strength, fracture toughness, elongation to failure, and crack propagation rate [1-3].

As little as 0.0001 weight percent of hydrogen can cause cracking in steel, yet alloying high strength steels with Ni or Mo reduce this effect [4]. Furthermore,

hydrogen embrittlement is more severe at room temperature than at high and low temperature [5].

Several factors should be taken into account for studying the effects of hydrogen on materials, such as the concentration of hydrogen in the environment, the speed at which the hydrogen molecules move in the material, type of material, and the applied load on the system. If a combination of these parameters attains a critical value, the material will fail [3, 6].

There are some situations susceptible to hydrogen contact:

- Damp conditions due to the existence of H_2O
- The presence of hydrogen or hydrogenated gas near materials
- Corrosion in an aqueous environment followed by hydrogen origination

1-1 Types of Hydrogen embrittlement

1-1-1 Internal hydrogen embrittlement

This case occurs when the hydrogen enters molten materials which become supersaturated with hydrogen immediately after solidification [7].

1-1-2 Environmental hydrogen embrittlement

This instance results from hydrogen being absorbed by solid materials, and can take place during thermal treatments at elevated-temperature, being in contact with maintenance chemicals, corrosion reactions, cathodic protection, and operating in high-pressure hydrogen [8, 9].

1-2 Hydrogen embrittlement mechanism in macroscopic level

The effects of hydrogen embrittlement can be observed in many forms. With a tensile stress or stress-intensity factor exceeding a specific threshold, the atomic hydrogen interacts with the metal to induce subcritical crack growth leading to fracture. In the following, a few macroscopically observed failure mechanisms associated with hydrogen embrittlement are summarized.

1-2-1 Hydrogen-induced cracking

Hydrogen-induced cracking occurs when two H atoms form an H_2 molecule inside the metal matrix, in abundance, leading to increased pressure locally. This phenomena can be divided in two categories, Blistering, and Crack formation and growth [10].

a) Blistering

If the pressure increase is located near the surface of the material, blistering will occur near the surface [11], see Figure (1-1).

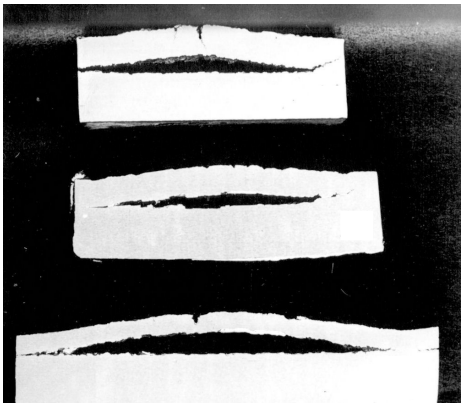

Figure 1-1 Blistering of the surface of a pressure vessel due to hydrogen existence [12]

b) Crack formation and growth

If the pressure increase is far from the surface, the material will experience crack formation and growth. The cracking may resemble steps ("stepwise cracking"). Stepwise cracking shown in Figure (1-2), is a series of events whereby the crack-front region of one void connects with the crack-front of another void on a parallel plane [10,13].

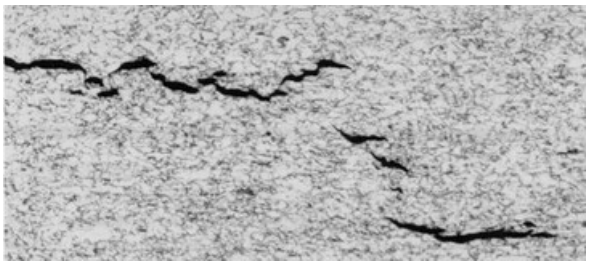

Figure 1-2 Stepwise cracking due to the presence of hydrogen [14]

1-2-2 Delayed failure

Delayed failure is a phenomenon whereby a metal containing hydrogen fails at a lower stress level than its tensile stress as measured in a notched tensile test due to increase of diffusion of hydrogen which yields high concentrations in regions of localized stress. It is also referred to as hydrogen-stress failure and low-stress brittle failure [15]. An example is shown in Figure (1-3).

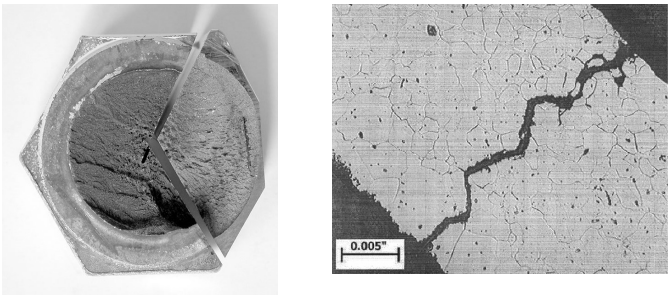

Figure 1-3 Delayed failure at a lower stress level [16]

1-2-3 Flaking and shatter cracking

This case as shown in Figure (1-4), occurs during forging of metals caused by hydrogen being picked up during the melting and precipitating at voids [17].

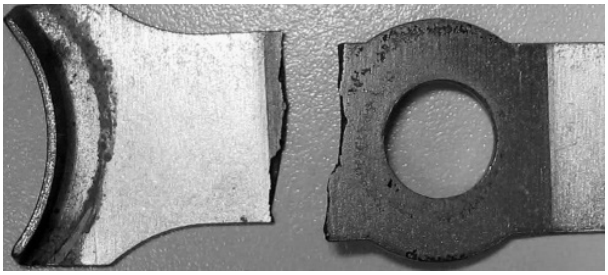

Figure 1-4 brittle failure during forging metals [18]

1-2-4 Hydrogen attack

This case take places at elevated temperatures (above 200^0C). Hydrogen combines with carbon to form methane at grain boundaries, and the internal pressure caused by the methane leads to enlarged pores in the metal [19]. The damage caused by hydrogen attack cannot be reversed by a low-temperature annealing process; the reduction of strength and ductility are permanent, see Figure (1-5).

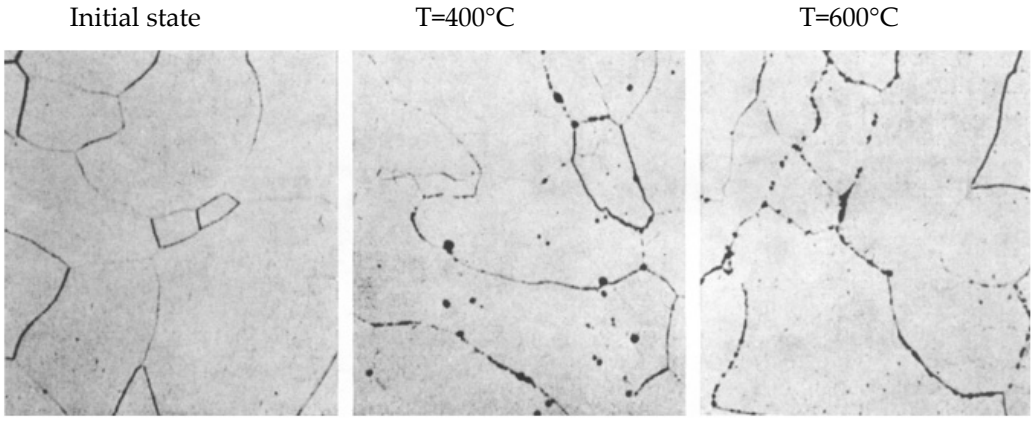

Figure 1-5 Hydrogen attack at high temperature [19]

1-3 Hydrogen embrittlement mechanism at the microscopic level

1-3-1 Hydride-induced embrittlement (HIE)

This mechanism involves the nucleation and growth of an extensive hydride field in the tip of a crack. As shown in Figure (1-6), hydrides first nucleate in the stress field of a crack and then grow to large sizes. The formation of brittle hydrides both in the grain matrix and at the grain boundaries can be detrimental to the mechanical properties of the metal. A flux of hydrogen is created toward stress concentrators. Once the particular terminal solid solubility (*CTS*) of hydrogen is reached, a hydride will precipitate [20,21]. The terminal solid solubility is dependent also on temperature and applied stress. As derived by Varias and Massih [22], the terminal solid solubility for a system is:

$$C_{TS} = C_{TS,0} \exp\left(\frac{W_{acc} + W_{int}}{N_H RT} \right) \exp\left(\frac{V_H}{RT} \left(\frac{\sigma_{mm}}{3} - \frac{1}{2} M_{ijkl}\, \sigma_{ij}\, \sigma_{kl} \right) \right) \quad \text{3-1}$$

where $C_{TS,0}$ is the terminal solid solubility in the absence of applied stress, W_{acc} is the material strain energy per mole of hydride in the absence of applied stress, W_{int} is the interaction energy per mole of hydride while under applied stress, N_H is the number of hydrogen atoms in the metal hydride molecule, R is the ideal gas constant, T is the temperature, V_H is the partial molar volume of hydrogen, M_{ijkl} is the elastic compliance tensor, and σ_{ij} , σ_{kl} are the applied stress tensors .

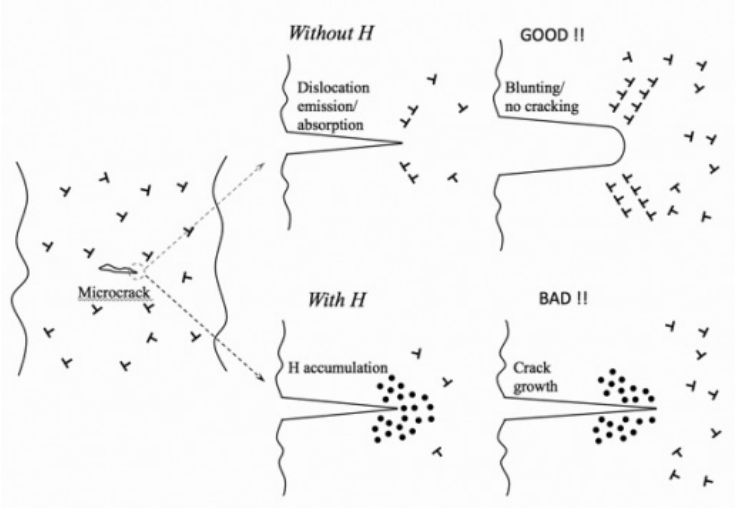

Figure 1-6 Hydride field causing crack growth [23]

Crack propagation is assisted through the repeated formation and cleavage of hydrides in the stress zone at the crack tip [25]. A hydride nucleates in an area reaching terminal solid solubility, and creates an additional stress concentration

at its tip. The stress field between the hydride and crack tips facilitates the growth of the precipitate toward the crack [24,26].

1-3-2 Interstitial mechanisms

Hydrogen-Enhanced Decohesion (HEDE)

Hydrogen accumulates within the crack tip and reduces the cohesion and bonding strength between metal atoms in that part which results in premature brittle fracture. As hydrogen is absorbed at an atomically sharp crack tip, there is a decrease in electron charge density between metal atoms. It has been claimed that there exists an electron transfer from the 1s band of hydrogen to the 3d and 4s bands of the metal that decreases the cohesive energy. The final decohesion results from tensile separation of the atoms, which is planar in nature. Fracture by the HEDE mechanism is characterized by limited activity of dislocations. By performing scanning electron microscopy, this becomes evident by the appearance of atomically flat fracture surfaces (i.e. the absence of microvoids and dimples)[28].

Diffusion of hydrogen is influenced both by temperature and chemical potential gradients. In this case, the chemical potential gradient refers to the force imposed on the atoms due to a concentration gradient. A lattice expansion

caused by the hydrostatic tensile stress surrounding a crack tip locally reduces the effective hydrogen concentration and, thus, the chemical potential, resulting in a flux of hydrogen toward it. The elevated hydrogen content lowers the resistive force between the atoms, so the crack will propagate when the resistive force reaches a value causing the local maximum tensile stress normal to the plane of the crack to equal the maximum lattice cohesive force, given by the following equation

$$\sigma_z = n F_m C \qquad 3\text{-}1$$

where σ_z is the local maximum tensile stress, n is the number of atoms per unit area of crystallographic plane, F_m is the resistive force, and C is the local concentration of hydrogen [24,26].

Hydrogen-enhanced decohesion can be detected by measuring changes in elastic constants, atomic force constants (measured as a function of the interaction forces between atoms' nuclei and their displacements from one equilibrium position to another), and surface energy. The HEDE mechanism is often coupled with a less widespread proposal, the hydrogen adsorption method. Because chemical reactions at grain boundaries behave similarly to free surfaces in some respect, the local affinity for hydrogen at grain boundaries may

lower the free energy, thus, promoting fracture. The segregation of hydrogen along a developing fracture path can, thus, reduce the cohesive energy, resulting in a reduction in atomic binding [25, 26], see Figure (1-7).

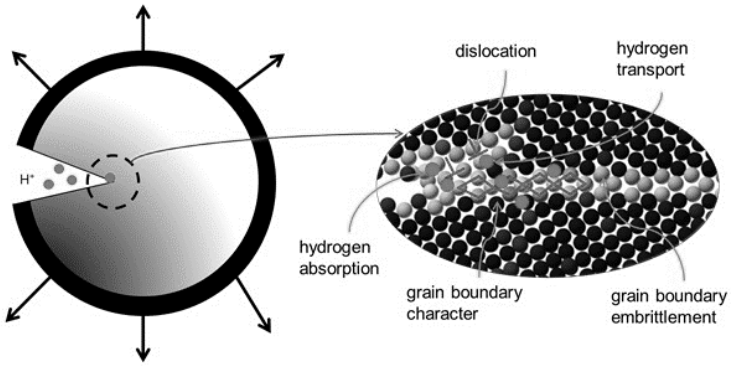

Figure 1-7 Reduction of cohesion in solute matrix [27]

1-3-3 Interstitial mechanisms

Hydrogen-Enhanced Localized Plasticity (HELP)

Hydrogen eases dislocation movement by shielding the dislocation stress fields against each other as well as against other grid defects. This local drop of yield stress due to hydrogen causes local dislocation movement at low levels of shearing stress. Hydrogen enhances the mobility of dislocations and decreases the separation distance between dislocations, thereby, enhances crack propagation rates [29].

The main principal behind the HELP mechanism is that increases in hydrogen concentration on a local scale can increase dislocation activity in the immediate vicinity. As reported by Abraham and Altstetter [20], it has been suggested that absorbed hydrogen at a crack tip will facilitate the injection of dislocations. The increase in local dislocation activity causes local stress concentration, contributing to failure initiation at planar defects where hydrogen is not present. A brittle fracture surface facilitated by the HELP mechanism will have evidence of slip, dimples, and tear ridges [30,32]. The increase in dislocation activity stems from the affinity of absorbed hydrogen for dislocations and other defects (e.g. precipitates, interstitial impurities, grain boundaries). Hydrogen is attracted to areas of local hydrostatic tensile stress, such as those surrounding defects, therefore, as two dislocations on the same slip plane with the same Burgers vector approach one another, their stress fields merge and the surrounding hydrogen atmosphere is redistributed. As the hydrogen concentration increases, there is a decrease in shear stress experienced by one dislocation due to the other.

The hydrogen atmosphere that develops around dislocations and defects create a shielding mechanism that limits interaction with precipitates and forest dislocations, thus easing dislocation glide and enhancing plasticity. In essence, the repulsive interaction energy with the obstacles is decreased, allowing dislocations to move at lower levels of applied stress. An increase in hydrogen

pressure tends to increase the velocity of dislocations. This mechanism is independent of crystal structure and is the same for edge, screw, mixed, and partial dislocations [34,35].

1-4 Point Defects in Crystalline Materials

Hydrogen in solutes are considered as a point defect in materials. Point defects can be divided into several categories [32, 33], see Figure (1-8):

a) Substitutional impurities: Hydrogen atoms substitute the host atoms by breaking bonds and making new bonds

b) Self interstitial impurities: Hydrogen atoms sit in - between the host atoms

c) Vacancy impurities: Atoms sit in the vacancy created at the host atoms; it can be created intentionally by spending energy for breaking bonds.

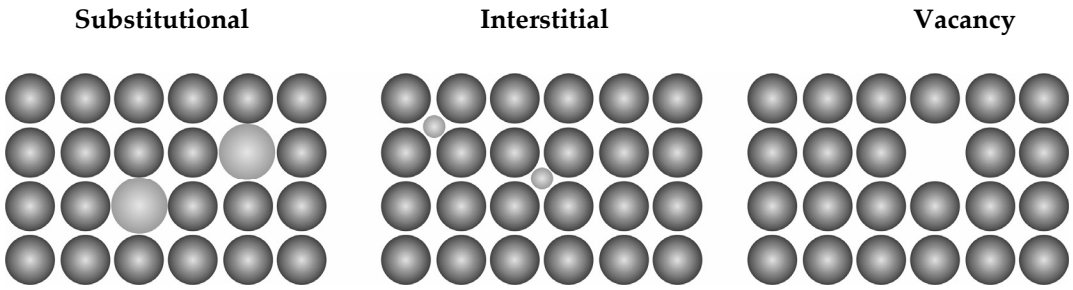

Figure 1-8 Hydrogen manifested as a point defect in materials

1-5 Interstitial sites in bcc and fcc unit cells

There are two probable matrix sites for hydrogen interstitial based on minimization of potential energy, namely, octahedral and tetrahedral sites, which are shown in Figure (1-9) and (1-10) for bcc and fcc unit cell structures, respectively. The summary of interstitial sites and corresponding planes has been shown in Table (1-1) and (1-2).

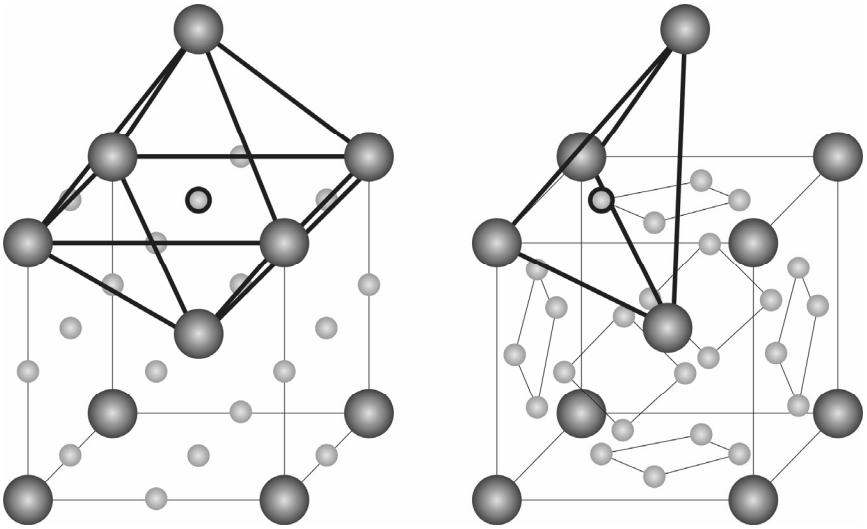

Figure 1-9 a) Octahedral and b) Tetrahedral sites in a bcc unit cell

Interstitial sites in bcc	
Octahedral interstices	Tetrahedral interstices
6 on faces at $\left(\frac{1}{2},\frac{1}{2},0\right)$ 12 on faces at $\left(\frac{1}{2},0,0\right)$ Total of 3 per atoms	24 on faces at $\left(\frac{1}{2},1,0\right)$ Total of 6 per atoms

Table 1-1 Interstitial sites in bcc and corresponding planes

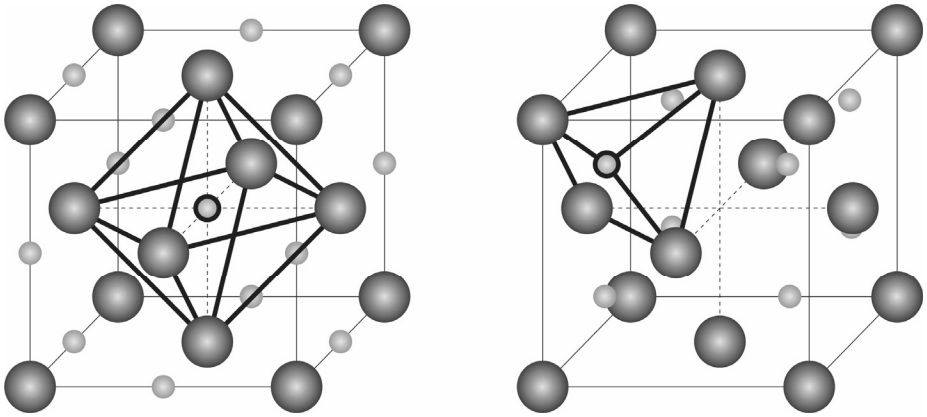

Figure 1-10 a) Octahedral and b) Tetrahedral sites in a fcc unit cell

Interstitial sites in fcc	
Octahedral interstices	Tetrahedral interstices
Four-fold coordination Sites: $\left(\frac{1}{2},\frac{1}{2},\frac{1}{2}\right),\left(\frac{1}{2},0,0\right)$	Four-fold coordination Sites: $\left(\frac{1}{4},\frac{1}{4},\frac{1}{4}\right)$

Table 1-2 Interstitial sites in fcc and corresponding planes

CHAPTER 2

Diffusion

Diffusion describes the spread of particles through random motion usually from regions of high concentration to regions of low concentration. This phenomenon in materials is also known as interdiffusion [34].

2-1 Interdiffusion mechanism

Interdiffusion is due to the high concentration gradient, and as a result atoms of one material diffuse into another one. To move from lattice sites, atoms need adequate energy, coming from atomic vibrations, to break bonds causing fluctuation and distortions during motion. There are two important types of interdiffusion in solid materials, [34, 36], Vacancy diffusion, and Interstitial diffusion.

a) Vacancy diffusion

This mechanism involves the interchange of an atom from a normal lattice position to an adjacent vacant lattice site or vacancy [34], shown in Figure (2-1).

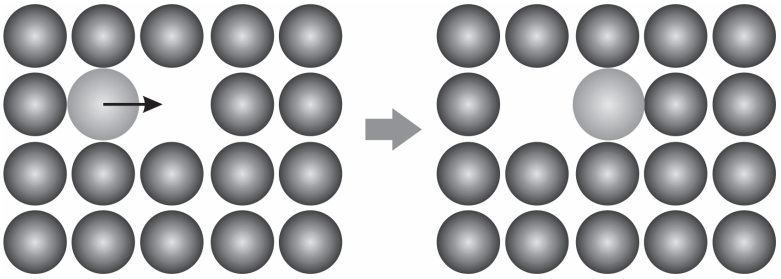

Figure 2-1 Vacancy diffusion

Vacancy diffusion is dependent on the number of vacancies in the matrix. The amount of vacancy increases with the increase of temperature in metals. Since diffusing atoms and vacancies exchange positions, the diffusion of atoms in one direction corresponds to the motion of vacancies in the opposite direction [36, 37].

b) Interstitial diffusion

Atoms migrate from an interstitial position to an empty nearby one, displayed in Figure (2-2). This mechanism is the main process in hydrogen embrittlement due to small size of hydrogen atoms for fitting into the interstitial positions [34].

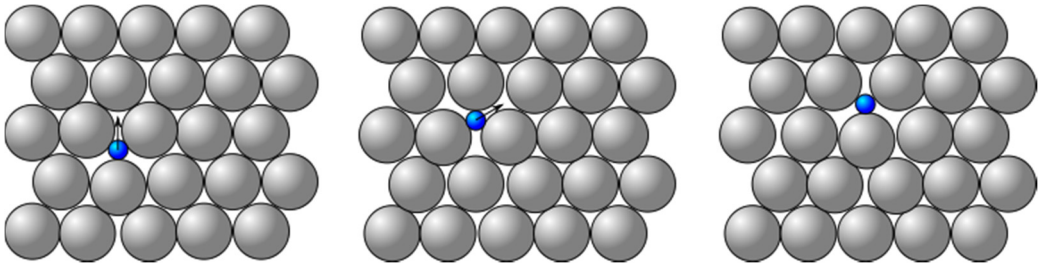

Figure 2-2 Interstitial diffusion

In most metal alloys, interstitial diffusion occurs much more rapidly than vacancy diffusion, since the interstitial atoms are smaller and thus more mobile [36]. Furthermore, there are more empty interstitial positions than vacancies; hence, the probability of interstitial atomic movement is greater than for vacancy diffusion [24, 37].

Atomic motion needs to satisfy:

- There must be an empty adjacent site
- The atom must have sufficient energy to break bonds with its adjacency

2-2 Diffusion and Gibbs free energy-Fick's first law

Diffusion is driven by the decrease in Gibbs free energy or by the chemical potential difference [37]. As shown in Figure (2-3), by considering atomic motion from position x to $x+a$, and C as the concentration of the solute, P as potential energy, and H as activation energy [36], we can write

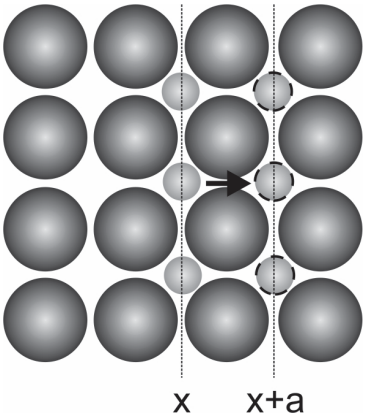

Figure 2-3 Diffusion in solvent from position x to $x+a$

$$P(x+a) = P(x) + a\frac{dP(x)}{dx}$$
$$C(x+a) = C(x) + a\frac{dC(x)}{dx} \qquad 2\text{-}1$$

From Thermodynamics first and second laws it can be shown that

$$\frac{\Delta H}{RT} = \frac{P(x+a) - P(x)}{RT} = \frac{a}{RT}\frac{dP(x)}{dx} \qquad 2\text{-}2$$

where R is the gas universal constant and T is temperature.

By having f as vibration frequency of the motion, and $n(x)$ the number of solute atoms per unit area at x, the net flux J along x showing the number of atoms passing through the unit area in the unit time along x is

$$J = \frac{1}{6} f\, n(x)\left(-\frac{a}{RT}\frac{dP}{dx}\right)\exp\left(-\frac{\Delta H}{RT}\right) \qquad 2\text{-}3$$

Since $n(x) = \mathrm{a}\,C(\mathrm{x})$ one can write

$$J = -\frac{1}{6}a^2 f\left(\frac{C(x)}{RT}\frac{dP}{dx}\right)\exp\left(-\frac{\Delta H}{RT}\right) \qquad 2\text{-}4$$

From thermodynamics laws and Helmholtz free energy we get

$$P(x) = P_0 + RT\ln C(x) \qquad 2\text{-}5$$

and by $\frac{dP(x)}{dx} = \frac{RT}{C(x)}\frac{d\,C(x)}{dx}$ it may be written as

$$J = -\frac{1}{6}a^2 f\left(\frac{dC(x)}{dx}\right)\exp\left(-\frac{\Delta H}{RT}\right) \qquad 2\text{-}6$$

Here, $D = -\frac{1}{6}a^2 f\exp\left(-\frac{\Delta H}{RT}\right)$ is the diffusion coefficient or diffusivity, then Fick's first law takes the form

$$J = -D\,\frac{dC(x)}{dx} \qquad 2\text{-}7$$

By considering diffusion in a three-dimensional space in the form of random motion of an atom, for the number of jumps of an atom per second, *N*, we can write

$$N = f\exp(-\frac{\Delta H}{RT}) \qquad 2\text{-}8$$

Based on the expression for the diffusion coefficient, D, number of jumps per second will be

$$N = \frac{6D}{a^2} \qquad 2\text{-}9$$

Thus, for a random motion in three-dimensions, an atom travels N steps with an average distance of $a\sqrt{N}$ per second, therefore after passing time t, diffusion length will be [37]

$$d = a\sqrt{Nt} = a\sqrt{\frac{6D}{a^2}t} = \sqrt{6Dt} \qquad 2\text{-}10$$

2-3 Diffusion and Gibbs free energy- Fick's second law

If local concentration $C(x)$ through a unit area A at position x changes in terms of time as well, we will have [34]

$$dC(x,t) = \frac{\left(J(x) - J(x+dx)\right) A\, dt}{A dx} \quad ; \quad J(x+dx) = J(x) + \frac{dJ(x)}{dx}dx$$
$$\frac{\partial C(x,t)}{\partial t} = -\frac{dJ(x)}{dx} \qquad 2\text{-}11$$

Then by Fick's first law, Fick's second law in one dimension can be expressed as [35,36]

$$\frac{\partial C(x,t)}{\partial t} = D\frac{\partial^2 C(x,t)}{\partial x^2} \qquad 2\text{-}12$$

While in three-dimensional space, it takes the form

$$\frac{\partial C(x,t)}{\partial t} = D\nabla^2 C(x,t) \qquad 2\text{-}13$$

2-4 Steady state diffusion and Fick's first law

In this case the flux and solute concentration do not change as a function of time which leads to

$$\frac{\partial C(x,t)}{\partial t} = 0 \;\Rightarrow\; \nabla^2 C(x) = 0 \qquad 2\text{-}14$$

Solving the equation in one dimension results in

$$\frac{\partial C(x)}{\partial x} = const \qquad 2\text{-}15$$

By bearing in mind the Fick's first law it can be deduced that the steady state diffusion equation, is in fact, Fick's first law or it can be interpreted that the Fick's first law is the special form of Fick's second law when there is no dependency on time [35,36,37].

2-5 General solution of the diffusion equation

The general diffusion equation $\frac{\partial C(x,t)}{\partial t} = D\nabla^2 C(x,t)$ can be solved under specific initial and boundary conditions. For this purpose we need one initial condition –single initial condition for all spatial values- and *n* boundary condition(s) for the *n*-dimensional problem as *n=1,2,3*.

For most cases in solid materials, the diffusion equation can be considered in one dimension [28], and become

$$\begin{cases} \frac{\partial C}{\partial t} = D\frac{\partial^2 C}{\partial x^2} \quad ; \quad non-steady\,state \\ \frac{\partial^2 C}{\partial x^2} = 0 \qquad ; \quad steady\,state \end{cases} \qquad 2\text{-}16$$

With *C* being the concentration of the solute.

CHAPTER 3

General Solution for the Diffusion Equation in the Steady State due to Dislocation Stress Fields

The steady state response from the diffusion equation in the stress fields of dislocations is considered. One solution is the Boltzmann approximation and can be stated as [38]

$$c = c_0 \exp(\frac{W_{\text{int}}}{k_B T}) \qquad 3\text{-}1$$

where c, c_0 are the concentration of solute in the dislocation field and far from the dislocation, respectively, in the steady state stage. In addition W_{int} is the interaction energy between solute and a dislocation, and k_B is the Boltzmann constant.

Several experiments have shown [39] that the Boltzmann approximation is not adequate for the case of dislocation cores. Instead, the large ratio of $\frac{W_{\text{int}}}{T}$ requires

the use of the Fermi-Dirac form

$$\frac{c}{1-c} = \frac{c_0}{1-c_0}\exp(\frac{W_{\text{int}}}{k_B T}) \qquad 3\text{-}2$$

For the particular case of interstitially dissolved hydrogen in metals where W_{int} is relatively large and where permeability and diffusivity studies [40] indicate sufficient mobility for appreciable solute atmosphere formation at room temperature and below, reliability of this form of solution have been more noticeable. Knowledge of the amount of hydrogen adsorbed at dislocations is important in assessing permeability and diffusivity of hydrogen, especially as influenced by cold work [41].

3-1 The interaction energy

If stress and strain tensor for a displacement field of u at a point due to two sets of quantities $\left(u_i, \sigma_{ij}, \varepsilon_{ij}\right)$ and $\left(u_i', \sigma_{ij}', \varepsilon_{ij}'\right)$ satisfying equilibrium equation considered, one can write

$$\sigma_{ij}\,\varepsilon_{ij}' = \sigma_{ij}'\,\varepsilon_{ij} = \sigma_{ij}\,u_{i,j}' = \sigma_{ij}'\,u_{i,j} \qquad 3\text{-}3$$

If we form the vector v with components

$$v_j = \sigma'_{ij} u_i - \sigma_{ij} u'_i \qquad 3\text{-}4$$

It can be shown that div $\mathbf{v} = v_{i,j} = 0$. Hence, by Gauss's theorem

$$\int_{\Gamma_1} v_j \, dS_j = \int_{\Gamma_2} v_j \, dS_j \quad or \quad \int_{\Gamma_1 - \Gamma_2} v_j \, dS_j = 0 \qquad 3\text{-}5$$

This equation is known as Betti's reciprocal theorem, where Γ_1 , Γ_2 are two continuous closed surfaces without singularities of **v**. If Γ is a closed surface containing no singularities of **v**

$$\int_{\Gamma} v_j \, dS_j = 0 \qquad 3\text{-}6$$

If **v** has a singularity, the above equation is still satisfied provided $\int v_j \, dS_j$ taken over Γ_1 , Γ_2 where excluded singularity.

3-2 Dislocation singularity

A large range of singularities can be regarded as particular cases of a type of surface singularity and can be generated in the following way [42].

- Make a cut over a surfaces (open or closed) in an unstrained body and give the faces of the cut a small relative displacement, removing material where there would be interpenetration.

- Fill in the remaining gaps and weld together. We are left with a system of internal strain which is completely characterized by giving as a function of position on S the vector d which specifies the final separation of points originally adjacent on opposite sides of the cut.

The stress $\sigma_{ij}n_j$ is continuous across S, but the individual components of σ_{ij} , ε_{ij} are in general discontinuous.

Surface singularity dislocations for which $\mathbf{d} = \mathbf{b} + \mathbf{r} \times \mathbf{c}$ with constant vectors $\mathbf{b}$ and $\mathbf{c}$ are the Weingarten dislocations discussed by Volterra [43]. Dislocations for which $\mathbf{c} = \mathbf{0}$ are physical dislocations

To derive point and line singularities from the general Surface singularity dislocations, a sphere or tube of radius r for *S* and a suitable distribution of d can be considered, then by letting r decrease to zero, at the same time increasing d in such a way that the displacement at a fixed point of observation remains finite. If *S* is a sphere and d is normal to *S*, the center of dilatation $\mathbf{d} = \frac{\mathbf{c}}{\mathbf{r}^2}$ can be obtained, where c is a constant.

We may have a volume distribution of internal stress in which equilibrium equation is satisfied, but the ε_{ij} derived from σ_{ij} with the aid of Hooke's law do not satisfy compatibility condition $S_{ij} = 0$ everywhere. The regions in which $S_{ij} \neq 0$ are to be regarded as the actual seat of the singularity.

3-3 The general inclusion

For small deformation and displacement field **u** the strain can be stated as

$$\varepsilon_{ij} = \frac{1}{2}(u_{i,j} + u_{j,i}) \qquad 3\text{-}7$$

By using Hooke's law the elastic stress will be

$$\sigma_{ij} = \lambda \varepsilon_{kk} \delta_{ij} + 2\mu \varepsilon_{ij} \qquad 3\text{-}8$$

where λ, μ are Lame's constants. The inclusion in the absence of the matrix would undergo into the uniform transformation (strain stress-free) strain ε_{ij}^{T}. The main problem is to find the constrained strain ε_{ij}^{C} in the inclusion when it transforms while it is embedded in the matrix.

If S is the surface separating the matrix and inclusion, and n_i its outward normal, Eshelby [44] suggested to solve the problem as follows:

1) Remove the inclusion and let it undergo ε_{ij}^{T} without altering its elastic constants. The stress according to equation (3-8) will be

$$\sigma_{ij}^{T} = \lambda \varepsilon_{kk}^{T} \delta_{ij} + 2\mu \varepsilon_{ij}^{T} \qquad 3\text{-}9$$

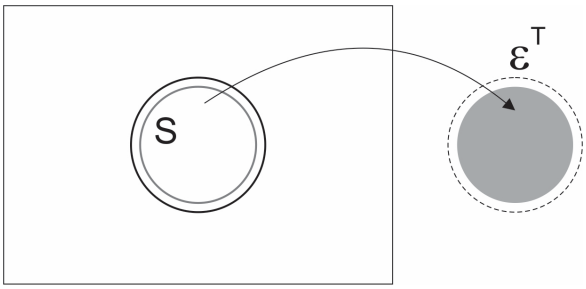

Figure 3-1 Removing the inclusion from the matrix

At this stage the stress in the inclusion and matrix is zero.

2) Apply surface tractions $-\sigma_{ij}^{T} n_j$ to the inclusion. This brings it back to the shape and size it had before transformation. Put it back in the matrix and reweld across *S*. The surface forces have now become a layer of body force spread over *S*.

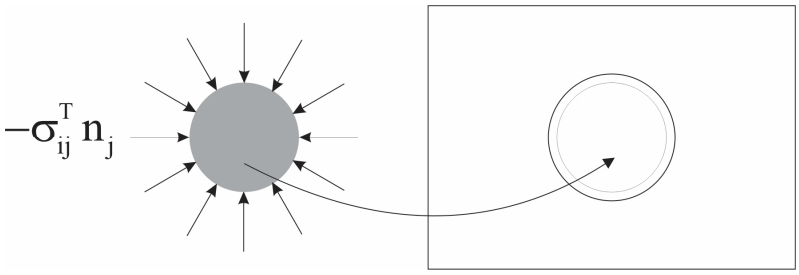

Figure 3-2 Putting back the inclusion to the matrix

3) Let these body forces relax, or, what comes to the same thing, apply a further distribution $\sigma_{ij}^{T} n_j$ over *S*. The body is now free of external force but in a state of self-stress because of the transformation of the inclusion.

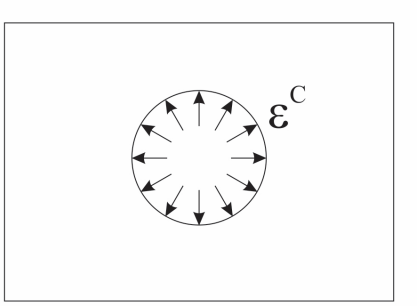

Figure 3-3 Relaxing body forces and converting to self-stress state

Since the displacement at **r** due to a point-force F_i is [45]

$$U_j(\mathbf{r}-\mathbf{r}') = \frac{1}{4\pi\mu}\frac{F_j}{|\mathbf{r}-\mathbf{r}'|} - \frac{1}{16\pi\mu(1-\nu)}F_l\frac{\partial^2}{\partial x_l \partial x_j}|\mathbf{r}-\mathbf{r}'| \qquad 3\text{-}10$$

the displacement impressed on the material in stage 3 is

$$\mathrm{u}_i^C(\mathbf{r}) = \int_S \sigma_{jk}^T U_j(\mathbf{r}-\mathbf{r}')\, dS_k \qquad 3\text{-}11$$

It will be convenient to take the state of the material at the conclusion of stage 2 as a state of zero displacement. This is reasonable, since the stress and strain in the matrix are then zero and the inclusion, though not stress-free, has just the geometrical form which it had before the transformation occurred. u_i^C is then the actual displacement in the matrix and inclusion. The strain in matrix or inclusion is

$$\varepsilon_{ij}^C = \frac{1}{2}(u_{i,j}^C + u_{j,i}^C) \qquad 3\text{-}12$$

The stress in the matrix is derived from ε_{ij}^{C} by Hooke's law. On the other hand, the inclusion had a stress $-\sigma_{ij}^{T}$ even before particular 3, so that the stress in it is

$$\sigma_{ij}^{I} = \sigma_{ij}^{C} - \sigma_{ij}^{T} = \lambda(\varepsilon_{kk}^{C} - \varepsilon_{kk}^{T})\delta_{ij} + 2\mu(\varepsilon_{ij}^{C} - \varepsilon_{ij}^{T}) \qquad 3\text{-}13$$

where, σ_{ij}^{C} is the stress derived by Hooke's law from the strain ε_{ij}^{C} in the inclusion.

By using Gauss's theorem, the displacement in the matrix can be rewritten as

$$u_i^{C} = \frac{1}{16\pi\mu(1-\nu)}\sigma_{jk}^{T}\Psi_{,ijk} - \frac{1}{4\pi\mu}\sigma_{ik}^{T}\Phi_{,k} \qquad 3\text{-}14$$

where

$$\begin{aligned}\Phi &= \int_V \frac{1}{|\mathbf{r}-\mathbf{r}'|}\,dV \\ \Psi &= \int_V |\mathbf{r}-\mathbf{r}'|\,dV\end{aligned} \qquad 3\text{-}15$$

where V is the volume bounded by S.

Following relation between Ψ, Φ can be accordingly shown

$$\begin{aligned}\nabla^2\Psi &= 2\Phi \\ \nabla^4\Psi &= 2\nabla^2\Phi = \begin{cases}-8\pi & inside\,S \\ 0 & outside\,S\end{cases}\end{aligned} \qquad 3\text{-}16$$

For dilatation in the material, when ε_{ik}^{T} is a pure dilatation or $\varepsilon_{ij}^{C} = \frac{1}{3}\varepsilon^{T}\delta_{ij}$, it is enough to know Φ, then by using Ψ, Φ relation

$$\varepsilon^C = u^C_{i,i} = \frac{1}{16\pi\mu(1-\nu)}\sigma^T_{ik}\left(2\Phi_{,ik}\right) - \frac{1}{4\pi\mu}\sigma^T_{ik}\Phi_{,ik} = -\frac{(1-2\nu)}{8\pi\mu(1-\nu)}\sigma^T_{ik}\Phi_{,ik} \qquad 3\text{-}17$$

Using Hooke's law yields in

$$\varepsilon^C_{il} = -\frac{1}{4\pi}\frac{(1+\nu)}{3(1-\nu)}\varepsilon^T_{ik}\Phi_{,\mathrm{il}} \qquad 3\text{-}18$$

for $\Phi_{,ii} = -8\pi$, the dilatation is $\varepsilon^T \frac{(1+\nu)}{3(1-\nu)}$ in the inclusion and zero in the matrix. Thus, for example for $\nu = \frac{1}{3}$, the constraint of the matrix reduces the free expansion of the inclusion by a factor $\frac{2}{3}$.

The strain energy density in the inclusion is $\frac{1}{2}\sigma^I_{ij}\varepsilon^I_{ij}$, where, ε^I_{ij} is the strain derived from σ^I_{ij} by Hooke's law. Thus the elastic energy in the inclusion is

$$\frac{1}{2}\int_V \sigma^I_{jk}\left(\varepsilon^C_{jk} - \varepsilon^T_{jk}\right)dV \qquad 3\text{-}19$$

and the elastic energy in the matrix is

$$-\frac{1}{2}\int_S \sigma^C_{ij}u^C_i\,dS_j = -\frac{1}{2}\int_S \sigma^I_{ij}u^C_i\,dS_j = -\frac{1}{2}\int_V \sigma^I_{ij}\varepsilon^C_{ij}\,dV \qquad 3\text{-}20$$

The first member exhibits it as the work done in setting up the elastic field by applying suitable forces to the surface *S*; the sign is correct if the normal points from inclusion to matrix. The second follows because displacement and normal

traction are continuous across *S*. The third follows from Gauss's theorem, the equilibrium equation $\sigma^I_{ij,j} = 0$ and the symmetry condition $\sigma^I_{ij} = \sigma^I_{ji}$. The total strain energy in matrix and inclusion is thus

$$E_{el} = -\frac{1}{2}\int_V \sigma^I_{ij}\,\varepsilon^C_{ij}\,dV \qquad 3\text{-}21$$

In the special case where ε^C_{ij} is a uniform expansion

$$E_{el} = -\frac{2\mu(\varepsilon^T)^2 V(1+\nu)}{9(1-\nu)} \qquad 3\text{-}22$$

The difference of energy between two bodies of the same size and shape distinguished by unprimed and primed quantities, with different inhomogeneous elastic constants and acted on by the same surface tractions is [46]

$$\delta E = \frac{1}{2}\int\left(\sigma'_{ij}\varepsilon'_{ij} - \sigma_{ij}\varepsilon_{ij}\right)dV \qquad 3\text{-}23$$

But

$$\int\left(\sigma_{ij} - \sigma'_{ij}\right)\varepsilon_{ij}\,dV = \int_{\Sigma_o}\left(\sigma_{ij} - \sigma'_{ij}\right)u_{ij}\,dS_j = 0 \qquad 3\text{-}24$$

since $\sigma_{ij}n_j = \sigma'_{ij}n_j$ at the surface, we can replace $\sigma_{ij}\,\varepsilon_{ij}$ by $\sigma'_{ij}\,\varepsilon_{ij}$ in δW and similarly $\sigma'_{ij}\,\varepsilon'_{ij}$ by $\sigma_{ij}\,\varepsilon'_{ij}$, then

$$\delta E = \frac{1}{2}\int \left(c_{ijkm} - c'_{ijkm}\right)\varepsilon'_{ij}\,\varepsilon_{km}\,dV \qquad 3\text{-}25$$

Correspondingly, we can express the interaction energy between two singularities as an integral over a surface separating them. In Figure (3-4), u_i^S exists in step 2 and u_i^T in step 1 but not vice versa.

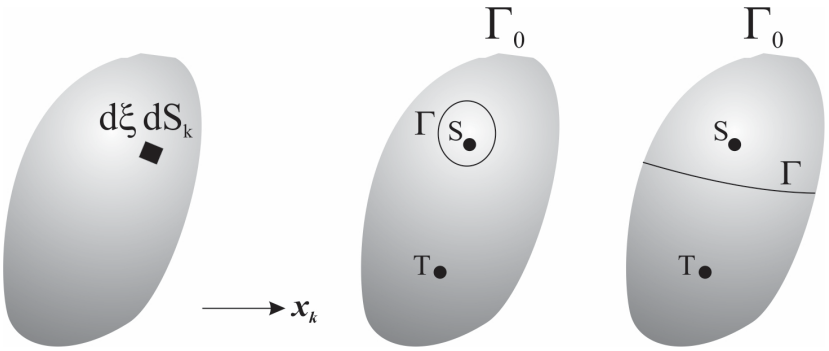

Figure 3-4 Body with singularity-S

The interaction energy in step 1 can be expressed in terms of u_i^T and in terms of u_i^S in step 2. By applying Gauss's theorem, the interaction energy of the elastic field u_i^C with another field u_i^A is

$$E_{\text{int}} = \int_{\Gamma}\left(\sigma_{ij}^C u_i^A - \sigma_{ij}^A u_i^C\right)dS_j \qquad 3\text{-}26$$

taken over any surface Γ enclosing the inclusion. If Γ is a surface just outside S and since u_i^C and the normal stress are continuous across S can be converted into

an integral over a surface just inside *S*, and hence into a volume integral over the inclusion

$$E_{\text{int}} = \int_V \left(\sigma_{ij}^I \varepsilon_{ij}^A - \sigma_{ij}^A \varepsilon_{ij}^I \right) dS_j \qquad 3\text{-}27$$

So

$$E_{\text{int}} = -\int_V \sigma_{ij}^T \varepsilon_{ij}^A \, dV = -\int_V \sigma_{ij}^A \varepsilon_{ij}^T \, dV = -\int_V \sigma_{ij}^A u_i^T \, dS_j \qquad 3\text{-}28$$

Therefore only ε_{ij}^T and not ε_{ij}^C is needed.

3-4 The interaction energy between dislocations and solute atoms

In general the interaction energy in terms of stress field can be written in the form of [47]

$$W_{\text{int}} = \sigma_{ij} \, \varepsilon_{ij} \, V \qquad 3\text{-}29$$

where σ_{ij} is the stress tensor of the dislocation, V is the reference volume containing the solute atom and ε_{ij} is the local internal strain field produced by the solute atom referred to this reference volume.

For either octahedral or tetrahedral site occupancy, the strain field referred to cube axes is $\varepsilon_{xx} > \varepsilon_{yy} = \varepsilon_{zz}$, other $\varepsilon_{ij} = 0$

3-5 Screw dislocation stresses

Figure (3-5) shows a screw dislocation in a distorted cylinder. The cut surfaces in the cylinder are pulled relative to each other along the z axis. Due to this deformation, only strain component of $\varepsilon_{\theta z}$ or shear strain $\gamma_{\theta z}$ is produced in the cylinder, and at the radius r can be stated as

$$\gamma_{\theta z} = \gamma_{z\theta} = \frac{b}{2\pi r} \tag{3-30}$$

where b is the magnitude of the dislocation or Burgers vector. The stress corresponding to this strain by using Hooke's law is

$$\sigma_{\theta z} = \sigma_{z\theta} = \mu \frac{b}{2\pi r} \tag{3-31}$$

where μ is shear modulus. All other stress components are zero. In Cartesian coordinate system, stress tensor will be

$$\sigma = \begin{bmatrix} 0 & 0 & \sigma_{xz} \\ 0 & 0 & \sigma_{yz} \\ \sigma_{zx} & \sigma_{zy} & 0 \end{bmatrix} \tag{3-32}$$

By using shear stress expression in cylindrical coordinates, the shear stresses in the Cartesian stress tensor can be written as [41]

$$\sigma_{xz} = \sigma_{zx} = -\frac{\mu b}{2\pi}\frac{y}{(x^2+y^2)} = -\frac{\mu b}{2\pi}\frac{\sin\theta}{r}$$

$$\sigma_{yz} = \sigma_{zy} = \frac{\mu b}{2\pi}\frac{\mathrm{x}}{(x^2+y^2)} = \frac{\mu b}{2\pi}\frac{\cos\theta}{r} \qquad 3\text{-}33$$

$$\sigma_{xx} = \sigma_{yy} = \sigma_{zz} = \sigma_{xy} = \sigma_{yx} = 0$$

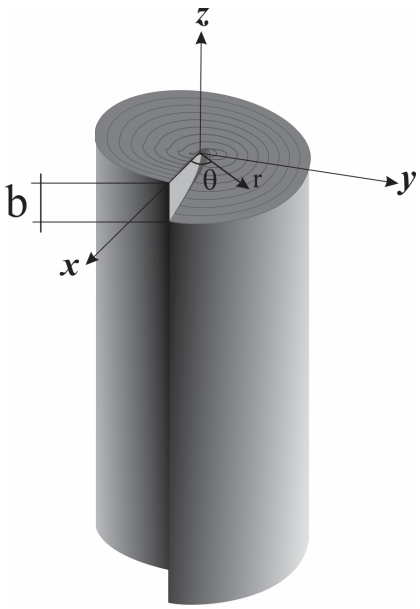

Figure 3-5 Elastic distortion produced by screw dislocation

3-6 Edge dislocation stresses

The stress field around the edge dislocation is more complicated than the stress field of the screw dislocation and can be calculated by linear elastic theory. Therefore the details are omitted and results are given. Considering the edge dislocation with the elastic strain field that can be produced in the cylinder by a rigid displacement of the faces of the slit by a distance b in the x-direction as shown in Figure (3-6). The displacement and strains in the *z*-direction are zero

therefore the case is in the plane strain condition, hence the stress tensor can be stated as

$$\sigma = \begin{bmatrix} \sigma_{xx} & \sigma_{xy} & 0 \\ \sigma_{yx} & \sigma_{yy} & 0 \\ 0 & 0 & \sigma_{zz} \end{bmatrix} \qquad 3\text{-}34$$

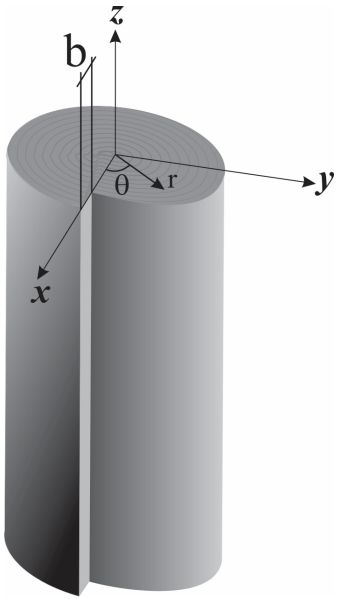

Figure 3-6 Elastic distortion produced by edge dislocation

The stress field has both dilatational and shear components. The largest normal stress is σ_{xx} which acts parallel to the slip vector. Since the slip plane can be defined at *y=0*, the maximum compressive stress (σ_{xx} negative) acts immediately above the slip plane and the maximum tensile stress (σ_{xx} positive) acts immediately below the slip plane [41].

$$\sigma_{xx} = -\frac{\mu b}{2\pi(1-\nu)}\frac{y(3x^2+y^2)}{(x^2+y^2)^2}$$
$$\sigma_{yy} = \frac{\mu b}{2\pi(1-\nu)}\frac{y(x^2-y^2)}{(x^2+y^2)^2}$$
$$\sigma_{zz} = \nu\left(\sigma_{xx}+\sigma_{yy}\right) \qquad \text{3-35}$$
$$\sigma_{xy} = \sigma_{yx} = \frac{\mu b}{2\pi(1-\nu)}\frac{\mathrm{x}(x^2-y^2)}{(x^2+y^2)^2}$$
$$\sigma_{xz} = \sigma_{zx} = \sigma_{zy} = \sigma_{yz} = 0$$

where ν and μ are Poisson's ratio and shear modulus respectively, and b is the magnitude of the Burgers vector.

3-7 Slip systems in body centered crystal structure

In body center cubic (bcc) crystals, there are several planes that are of similar density of packing, and hence there are several families of planes on which slip occurs. However, there is no ambiguity about the slip direction, since the atoms are closest along the $\langle 111 \rangle$ direction and those equivalent to it [48]. The slip systems observed in bcc crystals are shown in Figure (3-7).

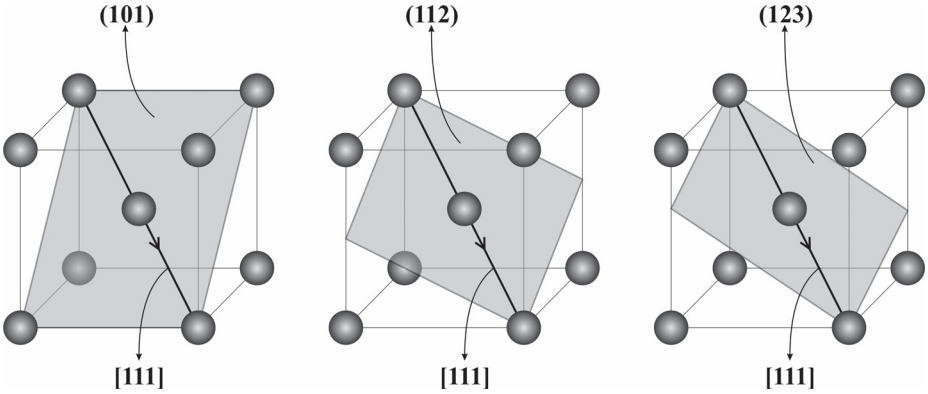

Figure 3-7 bcc slip systems

Thus, there are three families of slip systems as following

{110}<111> ; {112}<111> ; {123}<111>

However {110}<111> family is considered as the primary slip systems. In this case for the dislocation stress field with x parallel to the Burgers vector b, and z parallel to the dislocation line resulted from local slip system $[111],[\bar{1}10],[\bar{1}\,\bar{1}2]$ for bcc structures, the transformation tensor from slip system coordinates to Cartesian coordinate system *xyz* is

$$Q=\begin{bmatrix} \frac{1}{\sqrt{3}} & \frac{1}{\sqrt{3}} & \frac{1}{\sqrt{3}} \\ -\frac{1}{\sqrt{2}} & -\frac{1}{\sqrt{2}} & 0 \\ -\frac{1}{\sqrt{6}} & -\frac{1}{\sqrt{6}} & \frac{2}{\sqrt{6}} \end{bmatrix} \qquad 3\text{-}36$$

3-8 The interaction energy- Screw dislocation

By considering the general tensor transformation for the stress tensor we will have

$$\boldsymbol{\sigma}' = \mathbf{Q}^{\mathrm{T}}\boldsymbol{\sigma}\mathbf{Q} = \begin{bmatrix} \frac{1}{\sqrt{3}} & -\frac{1}{\sqrt{2}} & -\frac{1}{\sqrt{6}} \\ \frac{1}{\sqrt{3}} & -\frac{1}{\sqrt{2}} & -\frac{1}{\sqrt{6}} \\ \frac{1}{\sqrt{3}} & 0 & \frac{2}{\sqrt{6}} \end{bmatrix} \begin{bmatrix} 0 & 0 & \sigma_{xz} \\ 0 & 0 & \sigma_{yz} \\ \sigma_{zx} & \sigma_{zy} & 0 \end{bmatrix} \begin{bmatrix} \frac{1}{\sqrt{3}} & \frac{1}{\sqrt{3}} & \frac{1}{\sqrt{3}} \\ -\frac{1}{\sqrt{2}} & -\frac{1}{\sqrt{2}} & 0 \\ -\frac{1}{\sqrt{6}} & -\frac{1}{\sqrt{6}} & \frac{2}{\sqrt{6}} \end{bmatrix} \qquad 3\text{-}37$$

For a screw dislocation, when the *z* axis is parallel to the dislocation line, the normal stress components, the only ones contributing to equation (3-29) in cylindrical coordinates are [47]

$$\begin{aligned} \sigma_{xx} &= \frac{\mu b}{6\pi r}\left(\sqrt{6}\sin\theta - \sqrt{2}\cos\theta\right) \\ \sigma_{yy} &= \frac{\mu b}{6\pi r}\left(-\sqrt{6}\sin\theta - \sqrt{2}\cos\theta\right) \\ \sigma_{zz} &= \frac{\mu b}{6\pi r}\left(2\sqrt{2}\cos\theta\right) \end{aligned} \qquad 3\text{-}38$$

If $\varepsilon_{xx} = \varepsilon_{yy} = \varepsilon_{zz}$ in spherical symmetry, the interaction with the other defects is zero. Thus we find

$$W_{\mathrm{int}} = \frac{\mu b V\sqrt{6}}{6\pi}\left(\varepsilon_{xx} - \varepsilon_{yy}\right)\left(1 - \frac{\cot\theta}{\sqrt{3}}\right)\frac{\sin\theta}{r} \qquad 3\text{-}39$$

where b is the magnitude of Burgers vector, and V is the reference volume containing solute atoms.

3-9 The interaction energy – Edge dislocations

By considering the general tensor transformation for the stress tensor we will have

$$\boldsymbol{\sigma}' = \mathbf{Q}^{\mathrm{T}}\boldsymbol{\sigma}\mathbf{Q} = \begin{bmatrix} \frac{1}{\sqrt{3}} & -\frac{1}{\sqrt{2}} & -\frac{1}{\sqrt{6}} \\ \frac{1}{\sqrt{3}} & -\frac{1}{\sqrt{2}} & -\frac{1}{\sqrt{6}} \\ \frac{1}{\sqrt{3}} & 0 & \frac{2}{\sqrt{6}} \end{bmatrix} \begin{bmatrix} \sigma_{xx} & \sigma_{xy} & 0 \\ \sigma_{yx} & \sigma_{yy} & 0 \\ 0 & 0 & \sigma_{zz} \end{bmatrix} \begin{bmatrix} \frac{1}{\sqrt{3}} & \frac{1}{\sqrt{3}} & \frac{1}{\sqrt{3}} \\ -\frac{1}{\sqrt{2}} & -\frac{1}{\sqrt{2}} & 0 \\ -\frac{1}{\sqrt{6}} & -\frac{1}{\sqrt{6}} & \frac{2}{\sqrt{6}} \end{bmatrix} \qquad 3\text{-}40$$

The normal stress components after transformation are [47]

$$\begin{aligned} \sigma_{xx} &= -\frac{\mu b}{12\pi(1-\nu)r}\left((3+2\nu)\sin\theta + 2\sin^3\theta + 2\sqrt{6}\cos\theta\cos 2\theta\right) \\ \sigma_{yy} &= -\frac{\mu b}{12\pi(1-\nu)r}\left((3+2\nu)\sin\theta + 2\sin^3\theta - 2\sqrt{6}\cos\theta\cos 2\theta\right) \\ \sigma_{zz} &= -\frac{\mu b}{6\pi(1-\nu)r}\left((3+4\nu)\sin\theta - 2\sin^3\theta\right) \end{aligned} \qquad 3\text{-}41$$

If $\varepsilon_{xx} = \varepsilon_{yy} = \varepsilon_{zz}$ in spherical symmetry, the interaction with the other defects is purely through the hydrostatic stress component. In this case the interaction energy for the dislocation is

$$W_{\text{int}} = \left(\frac{\mu b(1+\nu)V}{3\pi(1-\nu)} \right) \frac{\sin\theta}{r} \qquad \text{3-42}$$

where $\frac{\mu b(1+\nu)v}{3\pi(1-\nu)}$ can be defined as one constant, μ is the shear modulus, b is the magnitude of Burgers vector ν is Poisson's ratio and V is the internal increment of expansion of the solute atom.

If $\varepsilon_{xx} > \varepsilon_{yy} = \varepsilon_{zz}$ for the general form of the interaction energy for the dislocation must be considered that there are three types of interstitial site with the appropriate stress field given by cyclic permutation which for two of them the same amount deduced. Accordingly, two forms for the interaction energy for three sites will be [47]

$$W_{\text{int}} = \frac{\mu b V\sqrt{6}}{12\pi(1-\nu)} \Big((3+2\nu)(\varepsilon_{xx}+\varepsilon_{yy}) + 2(3+4\nu)\varepsilon_{zz} \Big) \left(1 + \left(\frac{2(\varepsilon_{xx}+\varepsilon_{yy}) - 4\varepsilon_{zz}}{(3+2\nu)(\varepsilon_{xx}+\varepsilon_{yy}) + 2(3+4\nu)\varepsilon_{zz}} \right) \sin^2\theta \right) \frac{\sin\theta}{r}$$

3-43

$$W_{\text{int}} = \frac{\mu b V\sqrt{6}}{12\pi(1-\nu)} \Big(2(3+4\nu)\varepsilon_{xx} + (3+2\nu)(\varepsilon_{zz}+\varepsilon_{yy}) \Big) \left(1 + \left(\frac{-4\varepsilon_{xx} + 2(\varepsilon_{yy}+\varepsilon_{zz})}{2(3+4\nu)\varepsilon_{xx} + (3+2\nu)(\varepsilon_{zz}+\varepsilon_{yy})} \right) \sin^2\theta \right) \frac{\sin\theta}{r}$$

Evidently equations (3-43) reduces to equation (3-42) by $\varepsilon_{xx} = \varepsilon_{yy} = \varepsilon_{zz} = \frac{e}{3}$ for each site, which equals to the dilation component of strain.

3-10 The first and the second order interaction energies

As it mentioned in the previous part, the stress field due to hydrogen can have spherical symmetry $\varepsilon_{xx} = \varepsilon_{yy} = \varepsilon_{zz}$ or in general $\varepsilon_{xx} > \varepsilon_{yy} = \varepsilon_{zz}$. Therefore the interaction energy may be divided as first and second order. The first order interaction energy associated with a hydrogen atom introduced against the stress field, σ_{ij}^{a} of a defect is given by [49]

$$W_{\text{int}}^{1} = -\frac{\sigma_{kk}^{a}}{3}\Delta v' = -\frac{\sigma_{kk}^{a}}{3}\Delta v \qquad 3\text{-}44$$

Where $\Delta v'$ is the unconstrained volume dilatation and denotes the difference in volume of the hydrogen atom before its introduction into the lattice and that of the interstitial lattice space available to host the hydrogen atom [41], and $\Delta v = \Delta v'$ is the volume change of the host metal lattice per hydrogen atom. Δv is directly related to the partial molar volume of hydrogen, $V_H = \Delta v N_A$, where N_A is Avogadro's number. It is assumed that the solution is dilute and the hydrogen-induced strains are approximately purely dilatational.

In addition to the first order interaction energy, which arises from the volume change associated with the solute atom, the second order interaction energy [41,44] while the external loads, σ_{ij}^{a}, are held fixed can be written as

$$W_{\text{int}}^{2} = \frac{1}{2}\left(c'_{ijkl} - c_{ijkl}\right) \varepsilon'_{ij}\, \varepsilon^{a}_{kl}\, v_s \qquad 3\text{-}45$$

where v_s the volume over which the solute atoms alter the elastic stiffnesses, c_{ijkl} the strains, ε^{a}_{ij} are those caused by the external stress, σ^{a}_{ij} in the absence of the solute atom, and strains ε'_{ij} are the elastic strains inside the volume v_s after the solute atom has been introduced in the lattice in the presence of the external stresses σ^{a}_{ij} which are held constant. The primed stiffnesses correspond to those characteristics of the local stiffnesses in the presence of the solute atom, and the value of v_s is usually taken as the volume of the solute atom. In general, the second order interaction energy is much smaller than the first order interaction energy. In the vicinity of a dislocation, the second order interaction energy decreases with distance from the dislocation as $\frac{1}{\mathbf{r}^2}$, in contrast to the $\frac{1}{\mathbf{r}}$ dependence of the first order interaction energy.

In the case of an isotropic solid, the second order elastic interaction is manifest primarily through the dependence of the shear modulus and bulk modulus on the solute concentration. While the first order interaction dominates the solute interactions with edge dislocations, the dominant interaction term for screw dislocations is the second order interaction for those solutes having isotropic distortion fields (e.g. H interstitials), and the first order interaction for solutes having distortion fields with symmetries lower than cubic (e.g. C interstitials).

CHAPTER 4

The force on a singularity by surface tractions

A point singularity will naturally be defined as a solution of the elastic equations with vanishing $\sigma_{ij}n_j$ at the surface of the solid and becoming infinite in a prescribed way at a certain point.

By applying surface tractions $\sigma_{ij}^A n_j$ to Γ_o which results in producing displacement and stress σ_{ij}^A, u_i^A in the body in addition to the σ_{ij}^S, u_i^S already present [41]. If the singularity undergoes to a translation $\partial\xi$ parallel to the x_k axis as shown in Figure (3-4), the work done by the surface tractions is

$$\delta W = \delta\xi \int_{\Gamma_o} \sigma_{ij}^A \frac{\partial u_i^S}{\partial \xi} dS_j + O(\partial\xi)^2 \qquad 4\text{-}1$$

The force due to the applied surface traction can be obtained as

$$F_k^A = \lim_{\partial\xi\to 0} \frac{\delta W}{\partial \xi} = \int_{\Gamma_o} \sigma_{ij}^A \frac{\partial u_i^S}{\partial \xi} dS_j \qquad 4\text{-}2$$

By using equation (3-3) to (3-5) and knowing $\sigma_{ij}^{S} n_j = 0$ on Γ_o we can write

$$F_k^A = \int_{\Gamma} \left(\sigma_{ij}^A \frac{\partial u_i^S}{\partial \xi} - u_i^A \frac{\partial \sigma_{ij}^S}{\partial \xi} \right) dS_j \qquad 4\text{-}3$$

taken over the surface $\Gamma = \Gamma_o$. This integral can equally well be taken over any surface Γ in the body into which Γ_o can be deformed without entering Γ_s

$$F_k^A = \int_{\Gamma} \left(\sigma_{ij}^A \frac{\partial u_i^{\infty}}{\partial \xi} - u_i^A \frac{\partial \sigma_{ij}^{\infty}}{\partial \xi} \right) dS_j + \int_{\Gamma} \left(\sigma_{ij}^A \frac{\partial u_i^I}{\partial \xi} - u_i^A \frac{\partial \sigma_{ij}^I}{\partial \xi} \right) dS_j \qquad 4\text{-}4$$

By using equation (3-24)

$$\int_{\Gamma_1 - \Gamma_2} \left(\sigma_{ij} u'_{i,\mathrm{k}} - \sigma'_{ij} u'_{i,\mathrm{k}} \right) dS_j = 0 \quad if \;\; c_{ijkl,m} = 0 \qquad 4\text{-}5$$

The second term vanishes and simply

$$F_k^A = \int_{\Gamma} \left(u_i^A \sigma_{ij,\mathrm{k}}^{\infty} - \sigma_{ij}^A u_{i,\mathrm{k}}^{\infty} \right) dS_j \qquad 4\text{-}6$$

The simplest singularity is a center of dilatation in an isotropic body. If it is at the origin

$$u_i^{\infty} = \frac{\alpha x_i}{r^3}$$
$$r^2 = x_1^2 + x_2^2 + x_3^2 \qquad 4\text{-}7$$

where α is a constant. In order to find the force, a small sphere of radius *r* is taken about the origin. If the applied stress and displacement in a Taylor series are expanded, one can write

$$F_k^A = \sigma_{ij,\mathrm{k}}^A \int u_i^\infty dS_j + \sigma_{ij,\mathrm{k}\,m}^A \int x_m u_i^\infty dS_j - u_{i,\mathrm{k}}^A \int \sigma_{ij}^\infty dS_j - u_{i,\mathrm{k}\,m}^A \int x_m \sigma_{ij}^\infty dS_j + \ldots \qquad 4\text{-}8$$

where the *A* quantities are to be given their value at the origin. We have

$$\int u_i^\infty dS_j = \alpha r^{-4} \int x_i x_j dS = \alpha r^{-4} \delta_{ij} \int \frac{1}{2}\left(x_1^2 + x_2^2 + x_3^2\right) dS = \frac{4}{3}\pi\alpha\delta_{ij} \qquad 4\text{-}9$$

In a similar way one can find

$$\int \sigma_{ij}^\infty x_m dS_j = -\frac{16}{3}\pi\mu\alpha\delta_{mi} \qquad 4\text{-}10$$

The term in $\int \sigma_{ij}^\infty dS_j$ vanishes since the singularity is in equilibrium. The remaining terms are of order *r*. Since F_k^A is independent of the choice of r they can make no contribution whether we let r tend to zero or not. Thus

$$F_k^A = \frac{4}{3}\pi\alpha\left(\sigma_{ii,\mathrm{k}}^A + 4\mu u_{i,ik}^A\right) = 4\pi\alpha\frac{(1-\nu)}{(1+\nu)}\sigma_{ii,\mathrm{k}}^A \qquad 4\text{-}11$$

where $\nu = \dfrac{\lambda}{2(\lambda+\mu)}$ is Poisson's ratio. In general

$$F = -12\pi\alpha\frac{(1-\nu)}{(1+\nu)} grad\,\sigma^A \qquad 4\text{-}12$$

where $\sigma^A = -\dfrac{1}{3}\left(\sigma_{11}^A + \sigma_{22}^A + \sigma_{33}^A\right)$ is the applied hydrostatic pressure at the position of the singularity.

An elastic sphere of radius $(1+\beta)r_0$ is forced into a spherical hole of radius r_0 in an infinite block of the same material. If we regard this as a volume singularity we may take for Γ any sphere of radius $r > r_0$. The force must then be given by above equation since this expression did not depend on the size of the surface over which we integrated

For the two-dimensional problem of an infinite straight dislocation line along the x_3 axis with σ_{ij}^A, u_i^A independent of x_3 the force F_k^A can be calculated by taking a cylinder of radius r and unit length for Γ with its axis along x_3.

The Burgers vector can be calculated as

$$\oint u_{i,j}\ dx_j = b_i \qquad \text{4-13}$$

for any closed circuit embracing the dislocation line. This, however, does not completely define the singularity. Without altering above equation we could add single-valued line singularities (e.g. a line of dilatation) coincident with the dislocation line. They may be excluded by requiring that

$$\lim_{r\to 0} r u_i^{\infty} = 0 \qquad \text{4-14}$$

where *r* is the distance of the point x_i from the singular line.

If $\Delta u_i^{\infty} = b_i$ is considered and expanded, we will have

$$F_k^A = u_{i,\mathrm{k}}^A \int_\Gamma \sigma_{ij}^\infty \, dS_j + \varepsilon_{k3}\sigma_{ik}^A b_i + O(r) \qquad \text{4-15}$$

The first term vanishes since the dislocation is in equilibrium. Hence

$$F_k^A = \sigma_{2i}^A b_i \ , \ F_k^A = -\sigma_{ki}^A b_i \qquad \text{4-16}$$

For a pure screw dislocation with $\mathbf{b} = (0, 0, \mathrm{b})$

$$F_k^A = \sigma_{23}^A b \ \ , \ F_2^A = -\sigma_{13}^A b \qquad \text{4-17}$$

and for a pure edge dislocation with $\mathbf{b} = (b, 0, 0)$

$$\begin{aligned} &F_k^A = \sigma_{12}^A b \ \ , \ F_2^A = -\sigma_{11}^A b \\ &F_k^A = \frac{2}{\pi}\frac{\lambda+\mu}{\lambda+2\mu}\sigma_{12}^A b \end{aligned} \qquad \text{4-18}$$

Therefore for the general Surface singularity dislocations, the force can be obtained as

$$F_k^A = \int_S b_i \, \sigma_{ij,\mathrm{k}}^A \, dS_j \qquad \text{4-19}$$

4-1 Force between two dislocations

In the absence of hydrogen, the interaction force (Peach-Koehler force) per unit length between two dislocations can be calculated as [41]

$$\mathbf{F}_{1\to 2} = \boldsymbol{\sigma}_{1\to 2}\mathbf{b}_2 \times \boldsymbol{\xi}_2 \qquad \text{4-20}$$

where $\boldsymbol{\sigma}_{1\to 2}$ is the stress of dislocation 1 exerted to dislocation 2, $\mathbf{b}_2$ is the Burgers vector of dislocation 2, and ξ_2 is the unit vector along the dislocation line 2. The same force can be derived for $\mathbf{F}_{2\to 1}$. If we consider two dislocations with Burgers vectors along x and dislocation line direction along z on parallel planes, the force between two dislocations as shown in the Figure (4-1), will be $\mathbf{F} = \boldsymbol{\sigma}\mathbf{b} \times \boldsymbol{\xi}$.

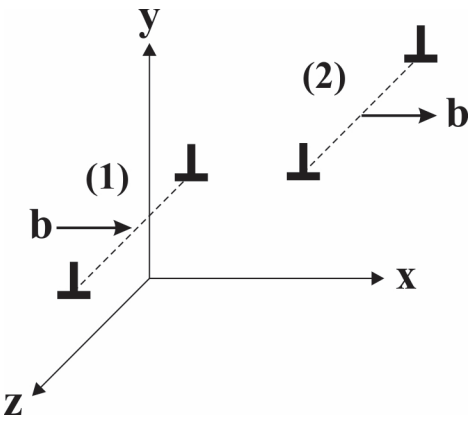

Figure 4-1 Two parallel edge dislocations

Where $\boldsymbol{\sigma}$ is given in equation (3-34) and (3-35) for edge dislocations.

$$\mathbf{b} = \begin{bmatrix} b \\ 0 \\ 0 \end{bmatrix}, \boldsymbol{\xi} = \begin{bmatrix} 0 \\ 0 \\ 1 \end{bmatrix} \Rightarrow \mathbf{F} = \begin{bmatrix} \sigma_{xx} & \sigma_{xy} & 0 \\ \sigma_{yx} & \sigma_{yy} & 0 \\ 0 & 0 & \sigma_{zz} \end{bmatrix} \begin{bmatrix} b \\ 0 \\ 0 \end{bmatrix} \times \begin{bmatrix} 0 \\ 0 \\ 1 \end{bmatrix}$$

$$F_x = \sigma_{xy} b_y = \frac{\mu b^2}{2\pi(1-\nu)} \frac{\mathrm{x}(x^2 - y^2)}{(x^2 + y^2)^2} \qquad \text{4-21}$$

$$F_y = F_z = 0$$

Parallel edge dislocations results in a repulsive force if the dislocations are of the same sign and on the same slip system. In this case, the force on dislocation 2 due to dislocation 1 is $\tau_D b_2$, where τ_D is the stress of dislocation 1 resolved along the slip plane and Burgers vector.

For screw dislocations

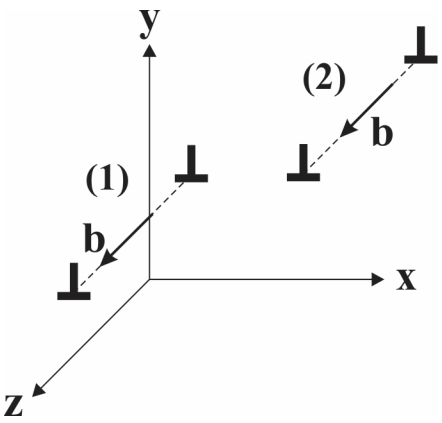

Figure 4-2 Two parallel screw dislocations

and by using equations (3-32) , (3-33) we will have

$$\mathbf{b} = \begin{bmatrix} 0 \\ 0 \\ b \end{bmatrix}, \boldsymbol{\xi} = \begin{bmatrix} 0 \\ 0 \\ 1 \end{bmatrix} \Rightarrow \mathbf{F} = \begin{bmatrix} 0 & 0 & \sigma_{xz} \\ 0 & 0 & \sigma_{yz} \\ \sigma_{zx} & \sigma_{zy} & 0 \end{bmatrix} \begin{bmatrix} 0 \\ 0 \\ b \end{bmatrix} \times \begin{bmatrix} 0 \\ 0 \\ 1 \end{bmatrix}$$

$$F_x = \sigma_{yz} b_z = \frac{\mu b^2}{2\pi} \frac{x}{(x^2 + y^2)} \qquad 4\text{-}22$$

$$F_y = \sigma_{xz} b_z = \frac{\mu b^2}{2\pi} \frac{y}{(x^2 + y^2)}$$

$$F_z = 0$$

4-2 Hydrogen Effect on the interaction between two edge dislocations

The hydrogen effect on the interaction between the dislocations 1 and 2 is assessed by calculating the hydrogen-induced change to the shear stress τ_D due to interactions between the hydrogen atmospheres surrounding the two dislocations. These hydrogen atmospheres are modeled by a continuous distribution of dilatation lines parallel to the dislocation lines each acting as a stress source which affects the shear stress τ_D.

4-3 The stress field of a single hydrogen dilatation line

In the displacement field caused by a point source of expansion, three perpendicular double forces produce a stress field typical of such a source. If f_i is kept constant (*M*) along unit cell axes, the total displacement in the *r* direction is [41]

$$u_r = \frac{M}{4\pi(\lambda + 2\mu)} \frac{1}{r^2} \tag{4-23}$$

This displacement is representative of a point of expansion with a strength

$$\delta v = 4\pi r^2 \delta r = 4\pi r^3 u_r = \frac{M}{\lambda + 2\mu} \tag{4-24}$$

If the source of expansion is at the origin of a free sphere of radius *R,* in order to obtain a displacement field u_r consistent with the free surface condition, a term αr must be added to make σ_{rr} vanish at $r = R$

$$u_r = \frac{\delta v}{4\pi r^2} + \alpha r \qquad 4\text{-}25$$

In spherical coordinates

$$\begin{aligned} \sigma_{rr} &= (\lambda + 2\mu)\frac{\delta u_r}{4\pi r^2} + \alpha r \\ \sigma_{\phi\phi} = \sigma_{\theta\theta} &= 2(\lambda + \mu)\frac{u_r}{r} + \lambda\frac{\partial u_r}{\partial r} \end{aligned} \qquad 4\text{-}26$$

Combining equations (4-23) to (4-25) and setting $\sigma_{rr} = 0$ at $r = R$

$$u_r(R) = \frac{3\lambda + 6\mu}{3\lambda + 2\mu}\frac{\delta v}{4\pi R^2} \qquad 4\text{-}27$$

Near the singularity, for $r << R$, the first term in Eq. (4-25) is dominant. In this region the dominant part of the internal stress is found from Eq. (4-26) to be

$$\begin{aligned} \sigma_{rr} &= -\frac{\mu\delta v}{\pi r^3} \\ \sigma_{\phi\phi} = \sigma_{\theta\theta} &= \frac{\mu\delta v}{2\pi r^3} \end{aligned} \qquad 4\text{-}28$$

The general analogy is sometimes used in the continuum theory of dislocations.

4-4 Plane strain condition

This model is consistent with the plane strain assumption for the dislocation strain field when the hydrogen concentration does not vary in the direction of the dislocation lines. The in-plane concentration of the dilatation lines n is directly related to the hydrogen concentration per unit volume C through [49]

$$n = Ch \qquad 4\text{-}29$$

where h is the distance between two successive hydrogen atoms along the dilatation line and the concentration n denotes the number of hydrogen atoms per unit area in the plane normal to the dilatation line. In the following subsections hydrogen effects on the constitutive moduli are neglected.

The line of dilatation associated with hydrogen atoms introduced into a stress-free lattice is produced in a continuum sense by replacing a cylindrical hole of infinite length and radius r_0 in an infinite lattice with a cylinder of the same material and radius $r_0 + \varepsilon r_0$ where ε is a small positive number related to the volume of solution of hydrogen. Relative to a polar cylindrical coordinate system r, ϕ, z, where the. Q axis coincides with the dilatation line, one may write the nonzero stress components of the plane strain axisymmetric field σ_{rr} at a distance r from the dilatation line as [49]

$$\sigma_{rr} = -\frac{\mu \Delta a}{\pi r^2} \ , \ \sigma_{\phi\phi} = \frac{\mu \Delta a}{\pi r^2} \qquad 4\text{-}30$$

where

$$\Delta a = \frac{\Delta a'}{2(1-\nu)} \qquad 4\text{-}31$$

denotes the strength of the dilatation line, and $\Delta a' = 2\pi r_0 \varepsilon$ is the unconstrained area of expansion. Due to combined axial symmetry and plane strain only the displacement, *u*, in the r direction in the *z* plane is nonzero and is given by

$$u = \frac{\Delta a}{2\pi r} \qquad 4\text{-}32$$

The strain field associated with *u* is incompressible and the area flux in the *z* plane through a circular boundary enclosing the dilatation line is $\Delta A = \Delta a$. The unconstrained area of expansion $\Delta a'$ can be evaluated in terms of the unconstrained volume change $\Delta v'$ of a hydrogen atom. Consistent with the plane strain assumption of the model, the unconstrained volume of the unit length cylinder $\Delta a'$ used to produce the dilatation line is equal to the total unconstrained volume $\frac{\Delta v'}{h}$ of the $\frac{1}{h}$ hydrogen atoms which make the unit length of the cylinder. Therefore $\Delta a' = \frac{\Delta v'}{h}$. In view of the fact that $\Delta v = \Delta v'$, one may

write $\Delta a' = \frac{\Delta v}{h}$. Since the volume change Δv is related to the partial molar volume of hydrogen in solution V_H, [49]

$$\Delta a' = \frac{V_H}{N_A h} \tag{4-33}$$

4-5 Interaction of a single dilatation line with an applied stress

Assume that a dilatation line is introduced in an infinite elastic solid subject to stresses σ_{ij}^a with corresponding displacements u_i^a caused by externally applied loads. The interaction energy per unit length between the stress field σ_{ij} of the dilatation line and the stress field σ_{ij}^a due to the external loads can be written as [46]

$$E_{\text{int}} = \oint_S \left(\sigma_{ij} u_i^a - \sigma_{ij}^a u_i \right) n_j \, dS = \frac{\sigma_{xx}^a + \sigma_{yy}^a}{2} \Delta a' \tag{4-34}$$

where *S* is any arbitrary curve on the *z* plane encircling the dilatation line, stress components σ_{ij}^a are measured in a Cartesian coordinate system whose axis *z* coincides with the hydrogen dilatation line, and n is the outward unit normal vector to the curve. In (3-29), which is the plane version of (4-34) dividing E_{int} by the total number of hydrogen atoms $\frac{1}{h}$ in the unit length of the dilatation line, one

finds the interaction energy per hydrogen atom as $W_{\text{int}} = E_{\text{int}} h$. Therefore, with use of (4-33) and (4-34), one obtains W_{int} as

$$W_{\text{int}} = \frac{\sigma_{xx}^a + \sigma_{yy}^a}{2} \frac{V_H}{N_A} \qquad 4\text{-}35$$

Equation (4-35) is used in (3-2) to calculate the hydrogen concentration *C* in equilibrium with an applied stress field σ_{ij}^a and (4-29), provides the density *n* of the dilatation lines in the plane normal to the dislocation lines. Since the stress field, σ_{ij}^a varies with position, so also do the fields *C* and *n*.

4-6 shear stress of hydrogen dilatation lines on a dislocation

Consider a Cartesian coordinate system of axes *x* and *y* centered at the core of the dislocation 2, as shown in Figure (4-3), and a single hydrogen dilatation line at a point with polar coordinates r, ϕ. The shear stress exerted at the core of dislocation 2 along the slip plane by the hydrogen dilatation line can be found from (4-30) as

$$\frac{\sigma_{xx}^a + \sigma_{yy}^a}{2} \sin 2\phi = -\frac{\mu \Delta a}{\pi r^2} \sin 2\phi \qquad 4\text{-}36$$

Using the principle of linear superposition and (4-36) one may calculate the shear stress $d\tau_H$ due to the dilatation lines of an infinitesimal area *dS* at (r, ϕ) as

$$d\tau_H = n\,dS\left(-\frac{\mu\Delta a}{\pi r^2}\right)\sin 2\phi \qquad 4\text{-}37$$

Substituting (4-29), (4-31) and (4-33) into (4-37) and then integrating over the entire area *S* occupied by the atmosphere, one finds the net shear stress τ_H induced by the hydrogen atmosphere as

$$\tau_H = -\frac{\mu}{2\pi(1-\nu)}\frac{V_H}{N_A}\int_0^{2\pi}\int_{r_2}^{R} C(r,\phi)\frac{\sin 2\phi}{r}\,dr\,d\phi \qquad 4\text{-}38$$

where r_2 is the inner cut-off radius of dislocation 2 and *R* is the outer cut-off radius of the atmosphere centered at dislocation 2. The core of dislocation 1 with cut-off radius *r*, is also excluded from the integration. A similar expression can be written for the resolved shear stress on dislocation 1 due to hydrogen.

According to (4-30), the stress field of a hydrogen dilatation line is purely deviatoric. Consequently, the interaction energy, as calculated from (4-35), between the hydrogen dilatation lines is zero, i.e. the introduction of a dilatation line into the lattice is energetically independent of the presence of the neighboring lines. Therefore, the hydrogen concentration $C(r,\phi)$ at any position (r,ϕ) is determined solely by the corresponding stress due to dislocations 1 and 2. Superposition of the singular linear elastic stress fields of the two dislocations [41] yields the in-plane hydrostatic stress as

$$\frac{\sigma_{xx}^{a}+\sigma_{yy}^{a}}{2}=-\frac{\mu}{2\pi(1-\nu)}\left(b_2\frac{\sin\phi}{r}+b_1\frac{\mathrm{r}\sin\phi-l\sin\omega}{r^2+l^2-2rl\cos(\phi-\omega)}\right) \qquad 4\text{-}37$$

where l,ω are the polar coordinates of the position of dislocation 1 Figure (4-3). Then, concentration $C(r,\phi)$ in (4-38) is calculated by combining (3-2), (4-35) and (4-38).

Equations (4-30) indicate that the stress field of a hydrogen dilatation line decays as $\frac{1}{r^2}$ with distance *r*. It is expected that the magnitude of the shear stress τ_{H} due to hydrogen on dislocation 2 will depend mainly on the dilatation lines close to the core of dislocation 2 and less on those which are remote from the core. This effect is seen in the integrand of (4-38) which diminishes as *r* increases and becomes zero at $r\to\infty$, where $C(r,\phi)=C_0$. In the calculations for the hydrogen distribution and stresses on the dislocation, for fixed relative dislocation positions (l,ω) the integral of (4-38) is computed numerically for an arithmetic progression of outer cut-off radii, *R*, differing by $20b_2$. The calculation is regarded as convergent when the relative error in the calculated shear stress for two successive radii is less than 10^{-3}.

Lastly, the corresponding shear stress, τ_D, resolved along the slip plane at the core of dislocation 2 due to dislocation 1 is given by

$$\tau_D = -\frac{\mu b_1}{2\pi(1-\nu)}\frac{\cos\omega\cos 2\omega}{l} \qquad 4\text{-}40$$

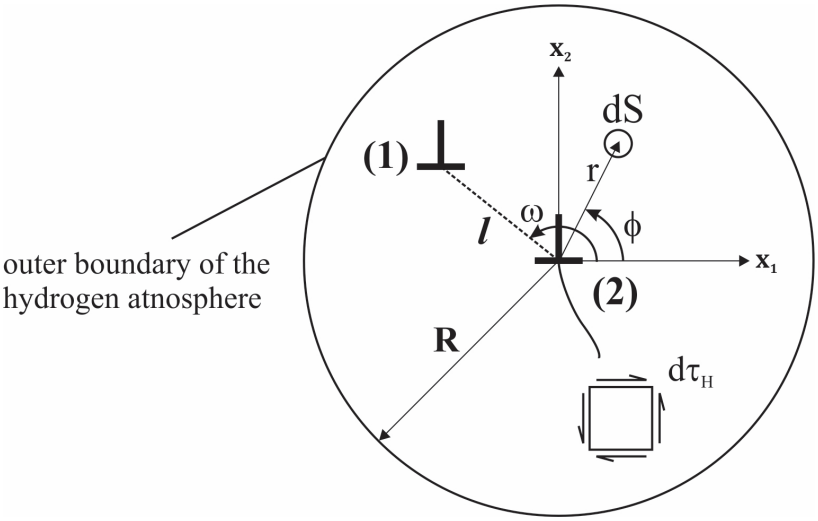

Figure 4-3 The shear stress $d\tau_H$, induced at the core of the dislocation 2 by the hydrogen dilatation lines [49]

The net shear stress exerted on dislocation 2 is equal to $\tau_D + \tau_H$.

CHAPTER 5

General finite element approach

We will formulate the finite element equations with respect to the current, or deformed, configuration, which is usually called an updated Lagrangian formulation [48]. The initial position of the material particle P within the element can be specified as

$$X(\xi,t) \approx \sum_{I=1}^{NNODE} N_I(\xi)\, X_I(t) \qquad 5\text{-}1$$

where NNODE denotes the number of finite element nodes, $N_I(\xi)$ represents the element shape functions and $X_I(t)$ indicates the initial positions of the finite element nodal points P_I , which are given in terms of the local element reference, (ξ_1,ξ_2) shown in Figure (5-1). Assuming that the material particle P remains attached to the same finite elements during the deformation, the current positions of the material particles are specified by

$$x(\xi,t) \approx \sum_{I=1}^{NNODE} N_I(\xi)\, x_I(t) \qquad 5\text{-}2$$

where $x_I(t)$ denotes the current positions of the finite element nodal points p_I. The displacements are assumed to be small and there are no rigid body rotations. $X(\xi,t)$ and $x(\xi,t)$ are therefore identical. For two-dimensional elements, two local reference frame independent variables are needed, (ξ_1,ξ_2), to specify position. The displacement field within each finite element is approximated as follows

$$u(\xi,t) \approx \sum_{I=1}^{NNODE} N_I(\xi)\, u_I(t) \qquad 5\text{-}3$$

The deformation gradient tensor is obtained by differentiating equation (5-2) with respect to the initial configuration as follows

$$\nabla_X N_I(\xi,t) = \frac{\partial N_I(\xi)}{\partial X(\xi,t)} = \left[\begin{array}{ccc} \frac{\partial N_I}{\partial X} & \frac{\partial N_I}{\partial Y} & \frac{\partial N_I}{\partial Z} \end{array}\right] \qquad 5\text{-}4$$

that are the derivatives of the shape functions N_I. The gradient term is ∇, and the dyadic product is $\otimes$. The derivative can be rewritten as follows

$$\nabla_X N_I(\xi,t) = \frac{\partial N_I(\xi)}{\partial X(\xi,t)} = \frac{\partial N_I(\xi)}{\partial \xi}\frac{\partial \xi}{\partial X(t)} = \frac{\partial N_I(\xi)}{\partial \xi}\left(\frac{\partial X(t)}{\partial \xi}\right)^{-1} \qquad 5\text{-}5$$

It is normally not possible to determine $\frac{\partial \xi}{\partial X}$ in Equation (5-5) directly since Equation (5-1) specifies X in terms of ξ. It is therefore necessary to determine $\frac{\partial X}{\partial \xi}$

instead and obtain the inverse. The derivative $\frac{\partial X}{\partial \xi}$ or the Jacobian relates infinitesimal quantities in the material configuration to those in the local element coordinate system. Therefore

$$\frac{\partial X(t)}{\partial \xi} = \frac{\partial N_I(\xi)}{\partial \xi} X_I(t) \qquad 5\text{-}6$$

where the members of $\frac{\partial X(t)}{\partial \xi}$ are given by

$$\frac{\partial X_i}{\partial \xi_j} = \sum_{I=1}^{NNODE} X_{iI} \frac{\partial N_I}{\partial \xi_j} \qquad 5\text{-}7$$

The small strain tensor can be approximated

$$\varepsilon(\xi, t) = \frac{1}{2}\left(\nabla u + (\nabla u)^T\right) \approx \frac{1}{2} \sum_{I=1}^{NNODE} \left(u_I(t) \otimes \nabla_X N_I(\xi) + \nabla_X N_I(\xi) \otimes u_I(t)\right) \qquad 5\text{-}8$$

The spatial derivatives with respect to the current configuration are obtained from the shape functions as

$$\nabla_x N_I(\xi, t) = \frac{\partial N_I(\xi)}{\partial x(t)} = \frac{\partial N_I(\xi)}{\partial \xi} \frac{\partial \xi}{\partial x(t)} = \frac{\partial N_I(\xi)}{\partial \xi} \left(\frac{\partial x(t)}{\partial \xi}\right)^{-1} \qquad 5\text{-}9$$

where members of the Jacobian, $\frac{\partial x(t)}{\partial \xi}$, are given by

$$\frac{\partial x_i}{\partial \xi_j} = \sum_{I=1}^{NNODE} x_{iI} \frac{\partial N_I}{\partial \xi_j} \qquad 5\text{-}10$$

The increment in the virtual work for an arbitrary virtual displacement δu will be

$$\delta W = \int_{\Omega} \sigma : \delta\varepsilon \, dV - \int_{\partial\Omega} t \cdot \delta u \, dA = 0 \qquad 5\text{-}11$$

where t is the stress vector, or traction, σ and ε are the stress and strain tensors respectively, and $\partial\Omega$ and Ω are domains of area, A and volume, V , respectively.

The first term in the right-hand side of (5-11) is the internal work per unit volume. A stress quantity is called work conjugate to the strain if their double contracted tensor product yields work. The co-rotational Cauchy, or true, stress is work conjugate to the true strain.

The spatial virtual work equation, (5-11), which describes the static equilibrium of the element can be rewritten in terms of the finite element discretization as

$$\delta W \approx \int_{\Omega} \sigma : \frac{1}{2} \sum_{I=1}^{NNODE} \left(\delta u_I \otimes \nabla_x N_I + \nabla_x N_I \otimes \delta u_I \right) dV - \int_{\partial\Omega} t \cdot \left(\sum_{I=1}^{NNODE} N_I \, \delta u_I \right) dA \qquad 5\text{-}12$$

As σ is a symmetric tensor, this reduces to

$$\delta W \approx \int_{\Omega} \sigma : \sum_{I=1}^{NNODE} \delta u_I \otimes \nabla_x N_I \, dV - \int_{\partial\Omega} t \cdot \left(\sum_{I=1}^{NNODE} N_I \, \delta u_I \right) dA \qquad 5\text{-}13$$

and as the nodal virtual velocities are independent of the integration, this may be rewritten to give

$$\delta W \approx \sum_{I=1}^{NNODE} \delta u_I \cdot \int_{\Omega} \sigma \nabla_x N_I \, dV - \sum_{I=1}^{NNODE} \delta u_I \cdot \int_{\partial\Omega} N_I t \, dA \qquad 5\text{-}14$$

The virtual work equation can finally be written in vector form as

$$dW \approx \sum_{I=1}^{NNODE} \delta u_I \cdot \left(f_I^{int} - f_I^{ext} \right) \qquad 5\text{-}15$$

by introducing expressions for the equivalent element nodal force vectors as follows

$$dW \approx \sum_{I=1}^{NNODE} \delta u_I \cdot \left(f_I^{int} - f_I^{ext} \right) \qquad 5\text{-}16$$

where

$$f_I^{int} = \int_{\Omega} \sigma \nabla_x N_I \, dV \qquad 5\text{-}17$$

and

$$f_I^{ext} = \int_{\partial\Omega} N_I \, t \, dA \qquad 5\text{-}18$$

where f_I^{int}, f_I^{ext} represent the internal, and the external element nodal forces, respectively. Since the discretized rate of virtual work, Equation (5-16) must be satisfied for all cases of the arbitrary virtual velocities, the element equation can be rewritten

$$f_I^{int} - f_I^{ext} = 0 \qquad 5\text{-}19$$

The nodal forces can be further assembled into global vectors (column matrices) by summing over all elements to give

$$f_I^{int} = \begin{bmatrix} f_1^{int} \\ f_2^{int} \\ \vdots \\ f_n^{int} \end{bmatrix} \quad , \quad f_I^{ext} = \begin{bmatrix} f_1^{ext} \\ f_2^{ext} \\ \vdots \\ f_n^{ext} \end{bmatrix} \tag{5-20}$$

where n is the total number of points used in the discretization. Finally, the finite element discretization can be expressed by the set of non-linear equilibrium equations as follows

$$f_I^{int}(u) - f_I^{ext}(u) = 0 \tag{5-21}$$

for the set (column matrix) of nodal displacements

$$u = \begin{bmatrix} u_1(t) \\ u_2(t) \\ \vdots \\ u_n(t) \end{bmatrix} \tag{5-22}$$

at time t .

We can rewrite Equation (5-19) in a more familiar way by considering the internal work term and writing it in terms of Voigt notation. We will assume small strain elasticity for simplicity. Returning to Equation (5-11), the internal work term originates from $\delta W^I = \int_\Omega \sigma : \delta\varepsilon \, dV$ and may be written using Voigt notation as

$$\delta W^I = \int_\Omega \sigma : \delta\varepsilon \, dV = \int_\Omega \delta\varepsilon^T \sigma \, dV \tag{5-23}$$

where

$$\varepsilon^T = \begin{pmatrix} \varepsilon_{xx} & \varepsilon_{yy} & 2\varepsilon_{xy} \end{pmatrix} \tag{5-24}$$

in which the off-diagonal terms (shear terms) are doubled to satisfy work conjugacy as specified in (5-23).

After some algebra, this can be written in Voigt notation as

$$\varepsilon = \begin{pmatrix} \varepsilon_{xx} \\ \varepsilon_{yy} \\ 2\varepsilon_{xy} \end{pmatrix} = \sum_{I=1}^{NNODE} B_I \cdot u_I = \sum_{I=1}^{NNODE} \begin{bmatrix} \frac{\partial N_I}{\partial x} & 0 \\ 0 & \frac{\partial N_I}{\partial y} \\ \frac{\partial N_I}{\partial y} & \frac{\partial N_I}{\partial x} \end{bmatrix} \begin{bmatrix} u_{x\,I} \\ u_{y\,I} \end{bmatrix} \tag{5-25}$$

so that from (5-23) the internal energy term becomes

$$\delta W^I = \int_\Omega \delta\varepsilon^T \sigma \, dV = \int_\Omega \left(\sum_{I=1}^{NNODE} B_I \cdot du_I \right)^T \sigma \, dV \tag{5-26}$$

If we assume purely elastic small deformation, then, we may write

$$\delta W^I = \int_\Omega \left(\sum_{I=1}^{NNODE} B_I \cdot du_I \right)^T C\varepsilon \, dV = \int_\Omega \left(\sum_{I=1}^{NNODE} B_I du_I \right)^T C \left(\sum_{J=1}^{NNODE} B_J du_J \right) dV \tag{5-27}$$

where C is the elastic material property matrix which can be obtained as

$$\sigma = \begin{pmatrix} \sigma_{xx} \\ \sigma_{yy} \\ \sigma_{xy} \end{pmatrix} = \begin{bmatrix} \lambda + 2\mu & \lambda & \lambda \\ \lambda & \lambda + 2\mu & \lambda \\ \lambda & \lambda & \mu \end{bmatrix} \begin{pmatrix} \varepsilon_{xx} \\ \varepsilon_{yy} \\ \gamma_{xy} \end{pmatrix} = C\varepsilon \tag{5-28}$$

where $\lambda = \dfrac{E\nu}{(1+\nu)(1-2\nu)}$ and $\mu = G = \dfrac{E}{2(1+\nu)}$ are the Lame constants. For the plain strain case where $\varepsilon_z = 0$ the normal stress out of plane will be

$$\sigma_z = \nu(\sigma_x + \sigma_y) \qquad 5\text{-}29$$

So that

$$\delta W^I = \delta u_I^T \left(\sum_{I,J=1}^{NNODE} \int_{\Omega} B_I^T C B_J \, dV \right) u_J \qquad 5\text{-}30$$

Equation (5-30) can be written as $\delta W^I = \delta u_I^T k \, u_I$ where

$$k = \sum_{I,J=1}^{NNODE} \int_{\Omega} B_I^T C B_J \, dV \qquad 5\text{-}31$$

for static problems,

$$f = ku \qquad 5\text{-}32$$

This equation, in general, is non-linear. This is because the stiffness matrix, k, depends upon the C matrix which is non-linear.

5-1 Four-Node rectangular elements

The shape functions for this element, as shown in Figure (5-1), are as follows

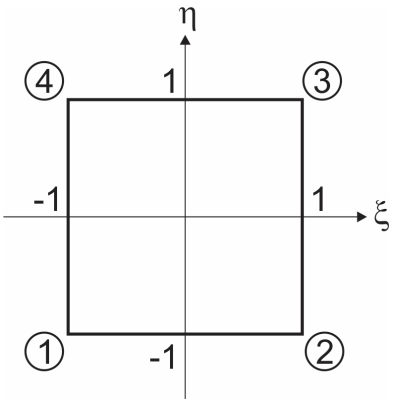

Figure 5-1 Element local coordinate system

$$
\begin{aligned}
N_1(\xi) &= \frac{1}{4}(1-\xi)(1-\eta) \\
N_2(\xi) &= \frac{1}{4}(1+\xi)(1-\eta) \\
N_3(\xi) &= \frac{1}{4}(1+\xi)(1+\eta) \\
N_4(\xi) &= \frac{1}{4}(1-\xi)(1+\eta)
\end{aligned}
\qquad 5\text{-}33
$$

In order to obtain the stiffness matrix we need to carry out integrations of the shape functions. Hence, we need to use a numerical technique. Often, in order to simplify the process, the integration is carried out with respect to a particular point in the element; this point is known as an integration point. The integration will be performed numerically using four integration points at $P(\xi,\eta) = P(\pm\frac{1}{\sqrt{3}},\pm\frac{1}{\sqrt{3}})$.

Integrals over the element domain of the type $I = \int_{\Omega} f(\xi, \eta)\, dV$ are expressed in the element local coordinate system by use of the Jacobian, J, as

$$I = \int_{-1}^{1}\int_{-1}^{1} f(\xi, \eta)\, \det J\, d\xi d\eta \qquad 5\text{-}34$$

where the Jacobian for a two-dimensional problem is given by

$$J = \begin{bmatrix} \frac{\partial X}{\partial \xi} & \frac{\partial X}{\partial \eta} \\ \frac{\partial Y}{\partial \xi} & \frac{\partial Y}{\partial \eta} \end{bmatrix} \qquad 5\text{-}35$$

The integral in (5-34) will be approximated using Gauss quadrature by

$$I \approx f(\xi, \eta) \int_{-1}^{1}\int_{-1}^{1} \det J\, d\xi d\eta \qquad 5\text{-}36$$

The shape function derivatives at the integration point $P(\xi, \eta) = P(\pm\frac{1}{\sqrt{3}}, \pm\frac{1}{\sqrt{3}})$ are obtained from

$$\frac{\partial N}{\partial X} = \frac{\partial N}{\partial \xi}\frac{\partial \xi}{\partial X} = \frac{\partial N}{\partial \xi}\left(\frac{\partial X}{\partial \xi}\right)^{-1} \qquad 5\text{-}37$$

5-2 Implicit integration to solve non-linear equations

Implicit integration schemes are often preferred to their explicit counterparts since they involve the determination of a residual force at each step and iteration within the step to minimize the residual force to within a specified tolerance. There are different techniques like the tangential stiffness method, the initial tangential stiffness method, and the Newton–Raphson method in order to solve non-linear equations.

5-2-1 Newton–Raphson method

The discretized static equilibrium equation given in (5-32), will not generally be satisfied unless a convergence occurs which can be expressed in terms of residual forces as follows

$$k(u)u - f = \Psi \neq 0 \qquad 5\text{-}38$$

The iteration starts from an initially guessed solution u_0 and the corresponding stiffness matrix $k(u_0)$. The residual forces at a given time step can be calculated as

$$\Psi = k(u)u - f \qquad 5\text{-}39$$

Using a Taylor expansion, Ψ may be approximated by

$$\Psi(u) + \frac{\partial \Psi(u)}{\partial u}\Delta u + O(\Delta u^2) = 0 \qquad 5\text{-}40$$

The matrix $J = \frac{\partial \Psi}{\partial u}$ is called the Jacobian, or effective tangent stiffness, and from (5-39) it can be seen that this comprises a term corresponding to the internal forces, termed the tangent stiffness matrix, and a further term corresponding to the 'external' forces, called the load stiffness matrix.

Equation (5-40) provides a linearization of (5-39) and may be written as

$$\Psi + J\Delta u = 0 \qquad 5\text{-}41$$

So that

$$J(u_n)\Delta u_n = -\Psi(u_n) \qquad 5\text{-}42$$

and the displacement is updated by $u_{n+1} = u_n + \Delta u_n$. The iteration continues until the tolerance limit on residual force is achieved.

5-3 Hydrogen effect on the elastic moduli of niobium

High frequency acoustic measurements [51,52] of the elastic constants C', C_{11} and C_L of the Nb-H(D) system were used to calculate the cubic moduli C_{11}, C_{22} and C_{44}. Over a wide range of hydrogen concentrations, the Nb-H system is elastically anisotropic with $C_{44} = \frac{C_{11} - C_{12}}{2}$.

This set of data allows the calculation of the Reuss and Voigt averages of the isotropic elastic moduli and these will be used in the calculations presented in a subsequent paper. In the present paper, the model material was assumed to be isotropic with bulk modulus, $B = \frac{C_{11} + 2C_{12}}{3}$, and shear modulus, $\mu = C_{44}$ which models the behavior in systems in which hydrogen increases the shear modulus.

Using this procedure, and the data from [51,52], the hydrogen effects on Young's modulus E, Poisson's ratio, ν, and shear modulus, μ, are described by

$$E = E_0(1 + 0.34c)\ ,\ \nu = \nu_0 - 0.025c\ ,\ \mu = \mu_0 \frac{1 + 0.34c}{1 - 0.0177c} \qquad 5\text{-}43$$

where $E_0 = 87.1\,\text{GPa}$, $\nu_0 = 0.415$, $\mu_0 = 30.8\,\text{GPa}$ are Young's modulus, Poisson's ratio and shear modulus respectively for the hydrogen-free material, and c can be calculated from equation (3-2).

The conclusions about the hydrogen effect on the mechanical behavior of the material are strongly associated with the assumed increase of the shear modulus

with increasing hydrogen concentration (which follows from the assumption $\mu = C_{44}$).

All parameters, mechanical and hydrogen related, were chosen for the BCC niobium system whose lattice parameter is a = 3.301 A with a corresponding Burgers vector magnitude, b = 0.285 $x10^{-9}$ m. The elastic behavior of the niobium was assumed to be isotropic with a shear modulus of 30.8 GPa and a Poisson's ratio of 0.415, values which correspond to the hydrogen-free material. Given the ratio of volume expansion per hydrogen atom to volume of the host lattice atom is 0.174 [52], one can calculate the partial molar volume of hydrogen as V_H = $0.188x10^{-5}$ m^3 mol^{-1}. The molar volume of the metal was V_M = 0.108 $x10^{-4}$ m^3 mol^{-1}, which corresponds to N_L = 0.555 x 10^{29} solvent lattice atoms per m^3 of host metal lattice. The parameter β was chosen equal to six interstitial lattice atoms per solvent atom corresponding to tetrahedral site occupancy, thus allowing for local hydrogen concentrations capable of forming the NbH structure at θ = l/6. The system's temperature was 300 K.

CHAPTER 6

Simulations and results

Solving equation (3-2) in order to find the concentration of solute atoms in the dislocation field is an iterative process because the interaction energy in this equation is a function of the elastic stress field associated with the introduction of hydrogen into the lattice. Furthermore, the elastic modulus of the lattice varies point to point according to equations (5-43). Therefore, non-linear finite element method with Newton-Raphson approach is used here to solve for the hydrogen concentration in the presence of dislocation fields.

In this chapter, the relaxed elastic stress field associated with the introduction of hydrogen into the lattice is calculated and the elastic moduli of the lattice are allowed to vary pointwise according to the local hydrogen concentration. In addition, relaxation of the standard singular dislocation for elastic stress field is accounted for, which is ignored in the literature due to an assumption indicating the small effect on the concentration. However, hydrogen in regions far from a

field is incapable of relaxing the dislocation for singular stress field because the stresses due to hydrogen decay rapidly by $\frac{1}{r^2}$. Later in this chapter we will show that this effect near the core cannot be ignored, and in some cases, this effect, substantially changes the results of the concentration in the field especially near the core.

In order to verify the computational scheme, the simulations have been done for a single edge dislocation with initial concentration of 0.1, two parallel edge dislocations of equal and opposite Burgers vectors with the distance of 6b, 8b, and 10b. For all simulations only the first order interaction energy (equation (3-44)) has been considered in order to compare the results with the results in reference [49].

In order to investigate the effect of initial concentration, three simulations for a single edge dislocation have been done for initial concentration of 0.1, 0.01, and 0.001.

Second order interaction energy introduced in equation (3-45), which is ignored in literature has been considered in the second set of simulations for a single edge dislocation with different initial concentrations.

Finally hydrogen concentration has been calculated for randomly-distributed dislocations. In these simulations, both the effect of the magnitude of the nominal initial concentration and second order interaction energy on concentration distributions due to diffused solute have been investigated.

6-1 Finite element simulation cell and imposed boundary conditions

A schematic simulation cell for all cases is shown in Figure (6-1), which is a square block with 50*b* dimension, where, *b* is the Burgers vector of niobium with the magnitude of 0.285×10^{-9} m .

Minimum boundary conditions avoiding rigid body motion are shown in Figure (6-1), where displacement in y direction u_2 and traction in x direction t_1 are assigned to be zero, in addition, the other sides are traction free surfaces (t=0).

The simulation cell sides are large enough that concentration is not affected by boundary conditions.

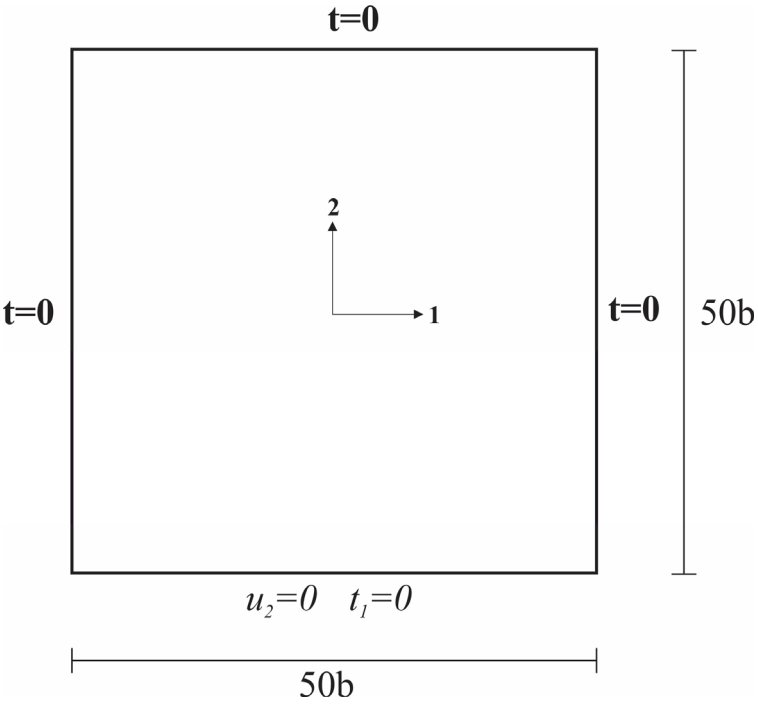

Figure 6-1 schematic of the simulation cell

6-2 Verification of computational scheme

In this section, nominal concentration of 0.1 at temperature 300 K considered for a single edge dislocation, and two parallel edge dislocations of equal and opposite Burgers vectors with a separation distance of 6b, 8b, and 10b. The results are compared with those in reference [49].

6-2-1 Single edge dislocation

The hydrogen atmosphere in equilibrium with the stress field of a single dislocation is shown in the form of normalized iso-concentration $\frac{c}{c_0}$, in Figure (6-2) at a nominal concentration $c_0 = 0.1$ hydrogen atoms per solvent atom. The atmosphere is symmetric with respect to the dislocation plane because of the corresponding symmetry in the hydrostatic stress field of the dislocation. There is a very good quantitative agreement between iso-concentration distributions shown in Figure (6-2) and those reported in reference [49].

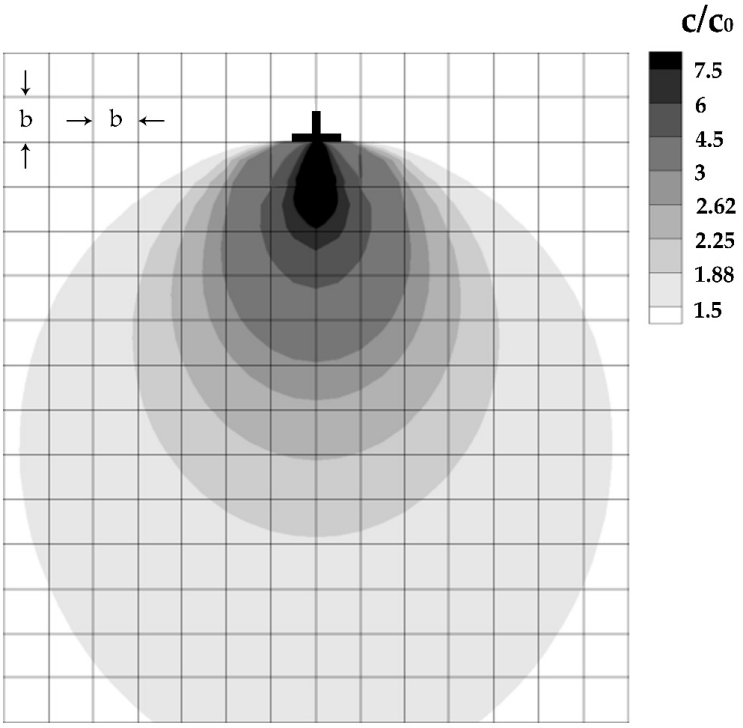

Figure 6-2 Contours of the normalized hydrogen concentration $\frac{c}{c_0}$ around a single edge dislocation at a nominal hydrogen concentration $c_0 = 0.1$ and temperature 300 K

The normal stresses are positive below the dislocation and negative above the dislocation, therefore, the hydrostatic stress field is positive below the slip plane and negative above it. The normal and shear stress distributions of the dislocation field affected by hydrogen are shown in Figure (6-3).

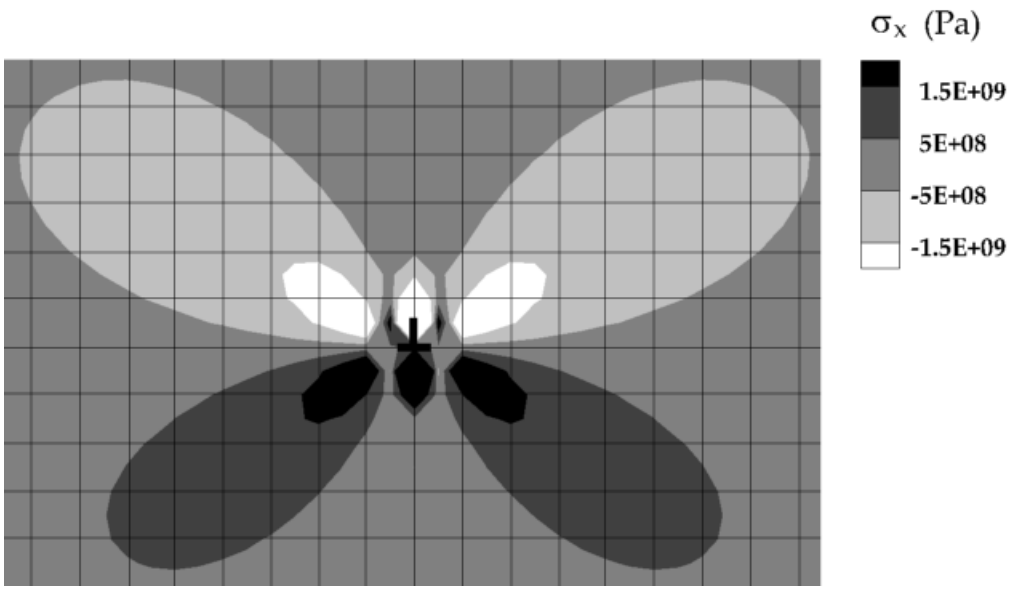

(a)

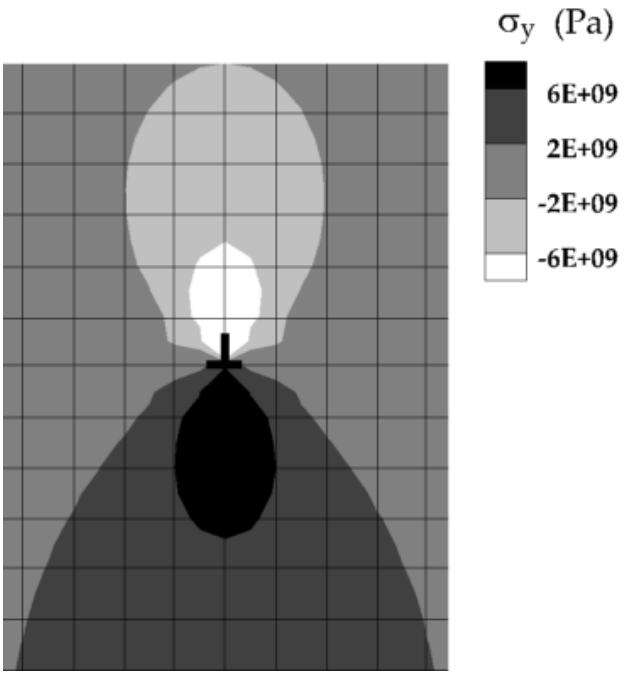

(b)

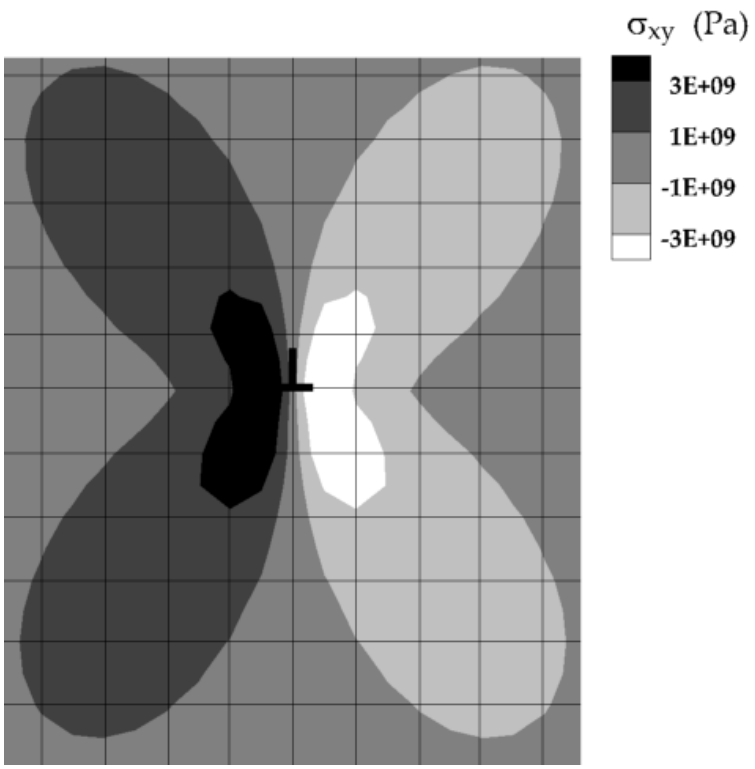

(c)

Figure 6-3 Contours of the normal and shear stresses around a single edge dislocation at a nominal hydrogen concentration, $c_0 = 0.1$, and temperature, 300K
a) Normal stress in the x direction b) Normal stress in the y direction
c) Shear stress on the xy plane

6-2-2 Two parallel edge dislocations with equal Burgers vectors

Under the same temperature and nominal hydrogen concentration, Figures (6-4) show the hydrogen atmosphere for dislocations 1 and 2 on the same slip system and at respective relative positions of 6, 8 and 10 Burgers vectors apart.

The hydrogen atmosphere in equilibrium with the stress field of two parallel dislocations having equal Burgers vectors for three separation distances between

the dislocations are shown in the form of normalized iso-concentration $\frac{c}{c_0}$, in Figure (6-4) at a nominal concentration $c_0 = 0.1$ hydrogen atoms per solvent atom.

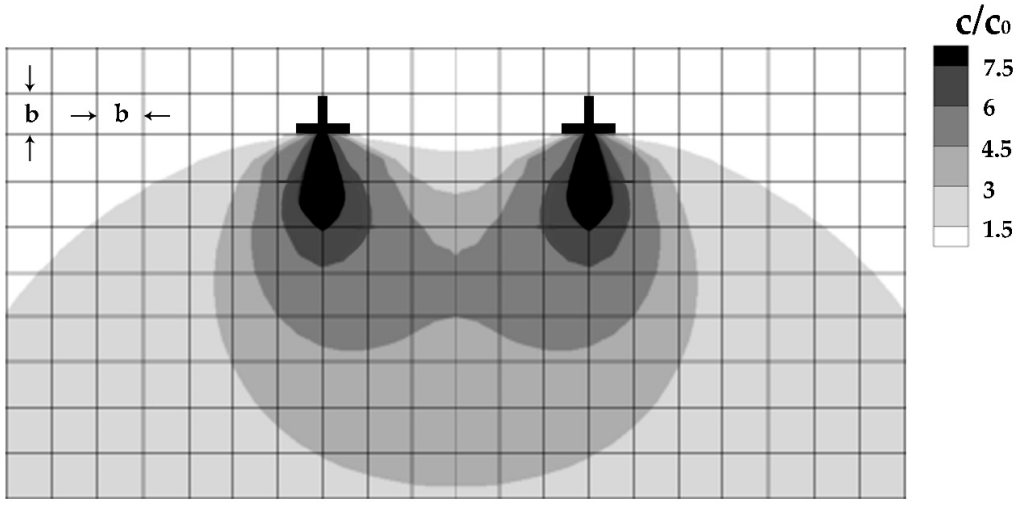

(a)

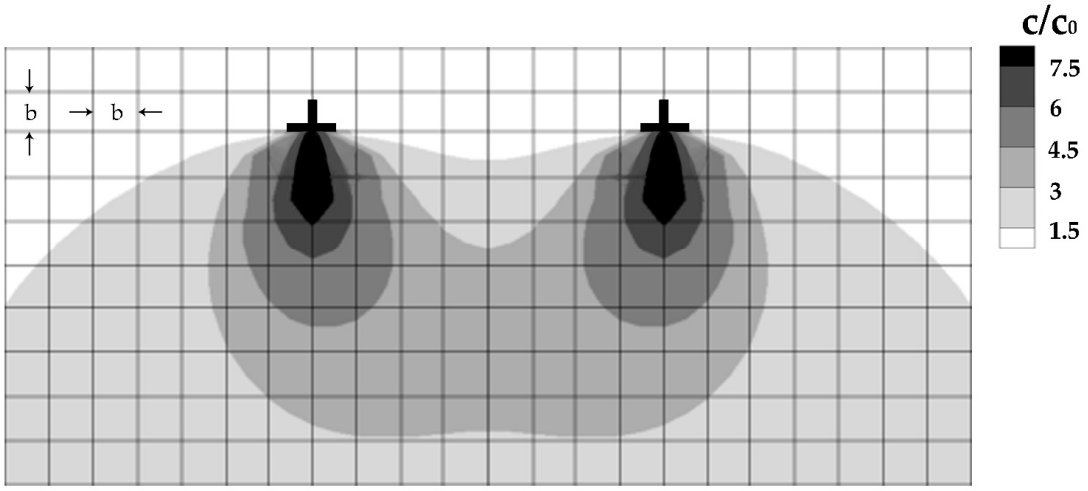

(b)

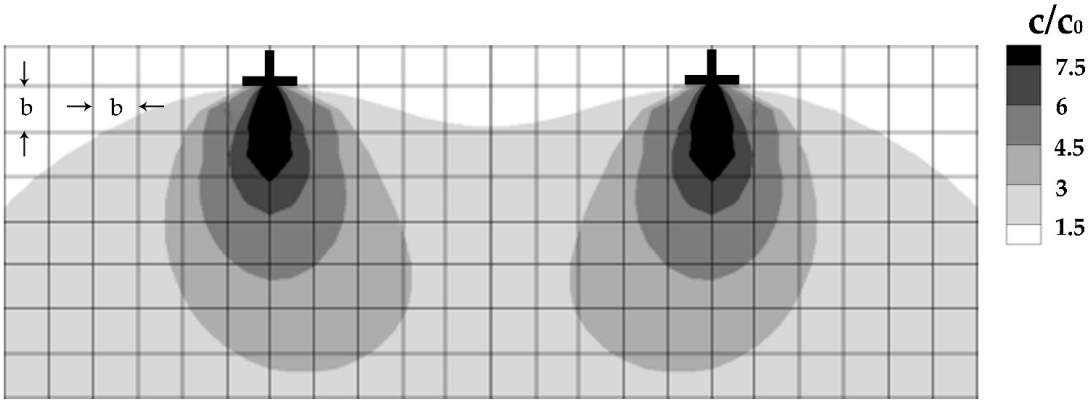

(c)

Figure 6-4 Contours of the normalized hydrogen concentration $\frac{c}{c_0}$ around two parallel edge dislocations with equal Burgers vectors at a nominal hydrogen concentration, $c_0 = 0.1$, and temperature, 300 K
The separation distances are a) 6b b) 8b c) 10b

The hydrostatic stress field is reinforced positively below the slip plane and negatively above the slip plane. For any given point in the area between the dislocations, this reinforcement increases as the dislocations approach each other. Consequently, the hydrogen concentration increases in the regions of positive stress enhancement and its value becomes larger than the concentration of the corresponding region in the atmosphere of a single dislocation. The normal and shear stress distributions for two parallel dislocations with equal Burgers vectors corresponding to dislocation distance of 6b, 8b, and 10b are shown in Figures (6-5)-(6-7). The normal stress distributions are symmetric, however, the magnitude

of these stresses decrease by increasing the distance of two dislocations. On the other hand, shear stress distribution is asymmetric, and is zero between two dislocations away from the cores.

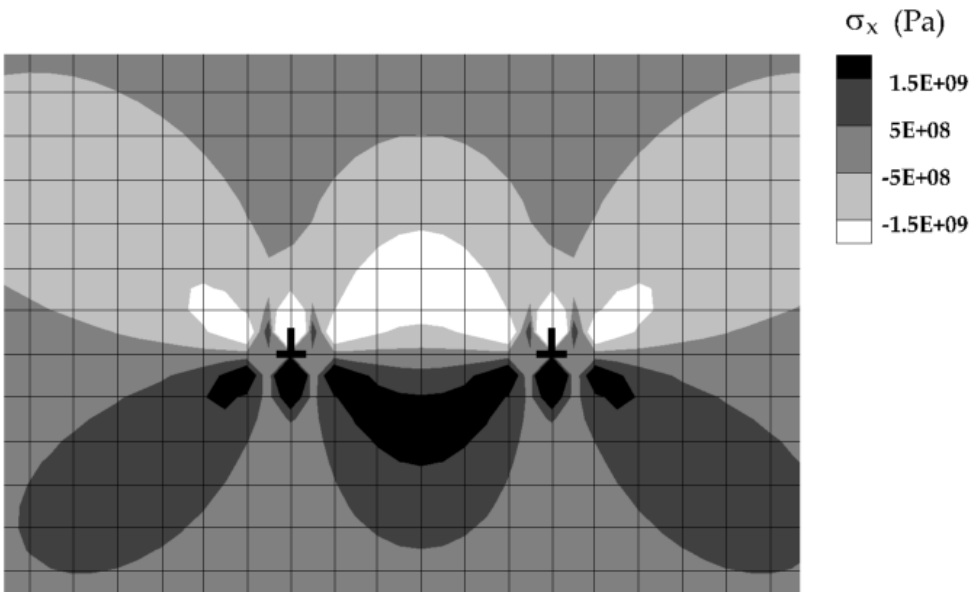

(a)

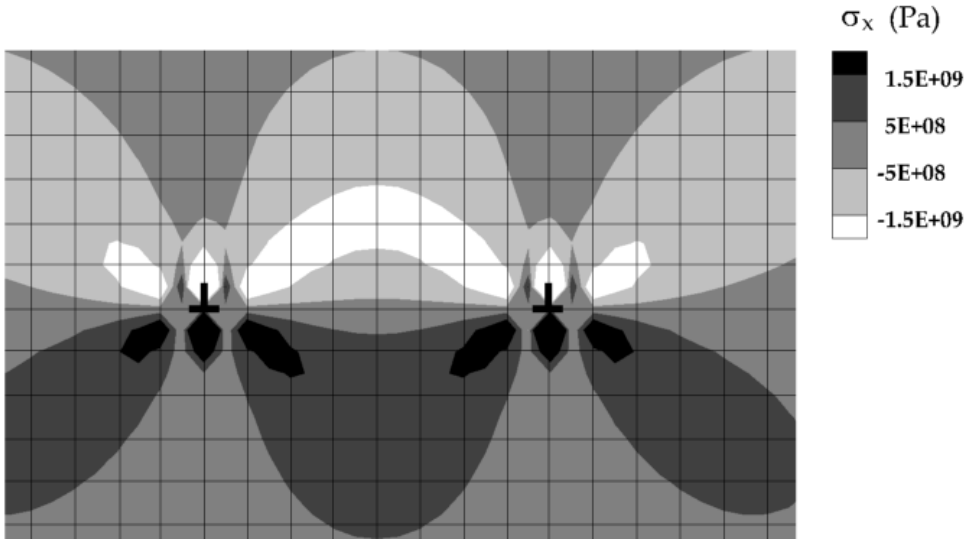

(b)

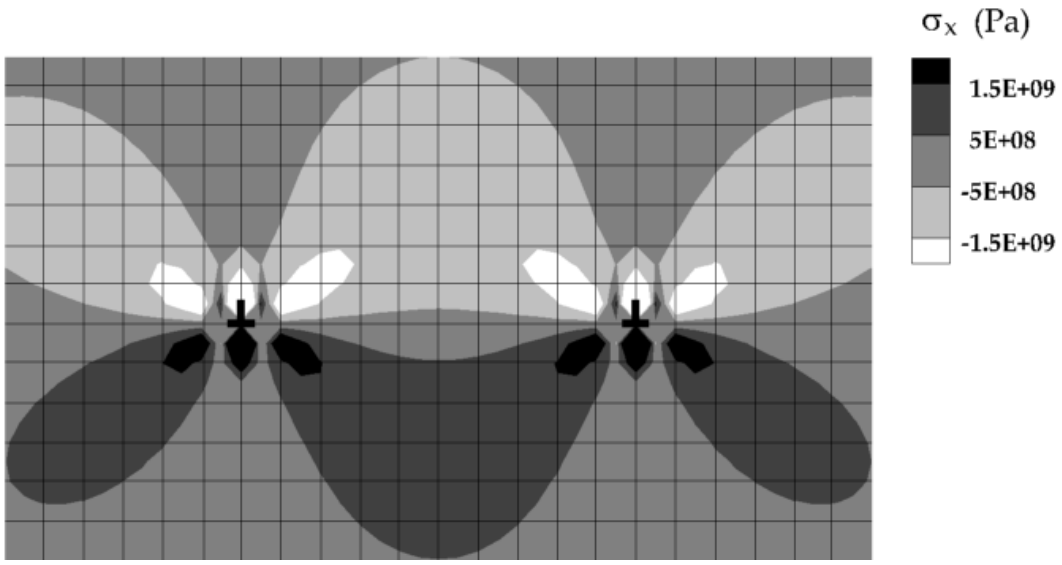

(c)

Figure 6-5 Contours of the normal stresses in the x direction around two parallel edge dislocations with equal Burgers vectors at a nominal hydrogen concentration, $c_0 = 0.1$, and temperature, 300 K

The separation distances of a) 6b b) 8b c) 10b

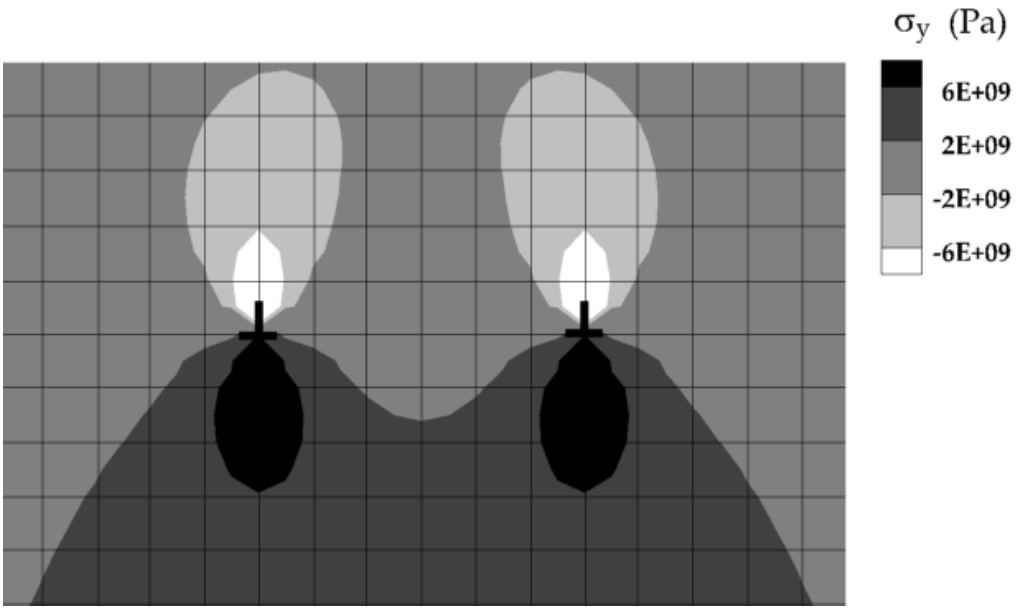

(a)

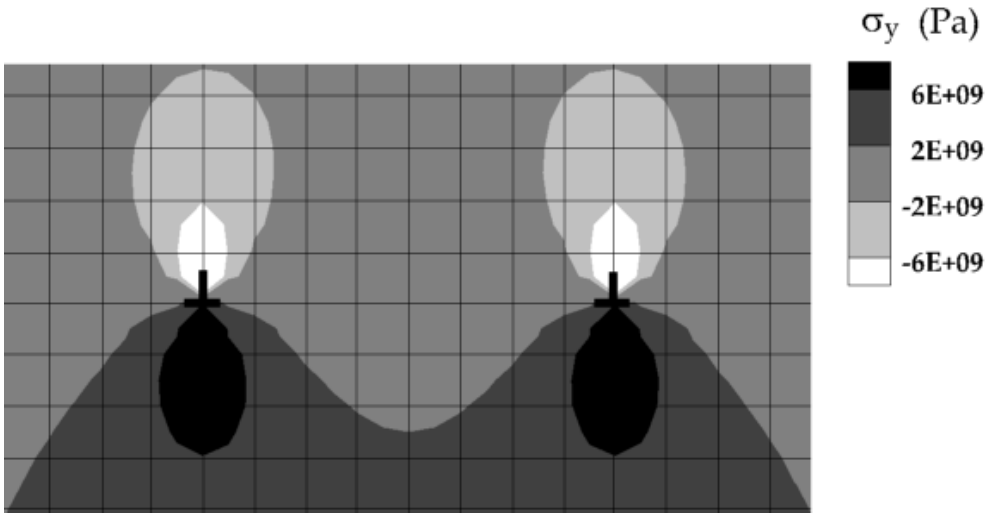

(b)

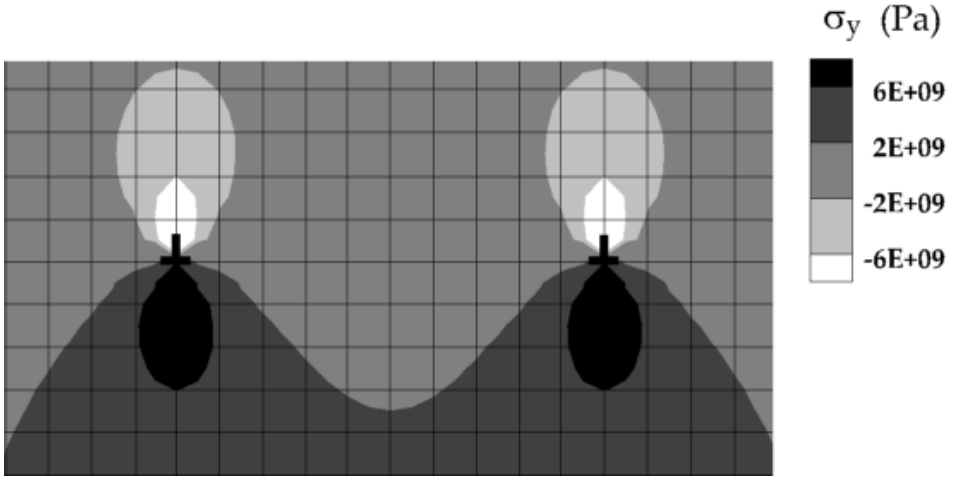

(c)

Figure 6-6 Contours of the normal stress in y direction around two parallel edge dislocations with equal Burgers vectors at a nominal hydrogen concentration, $c_0 = 0.1$, and temperature, 300 K

The separation distances are a) 6b b) 8b c) 10b

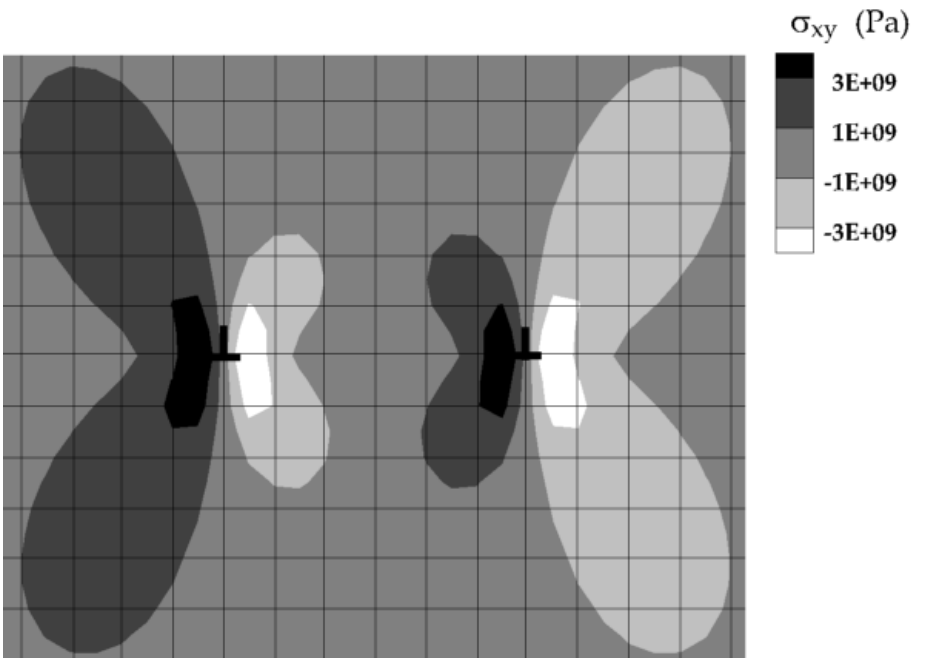

(a)

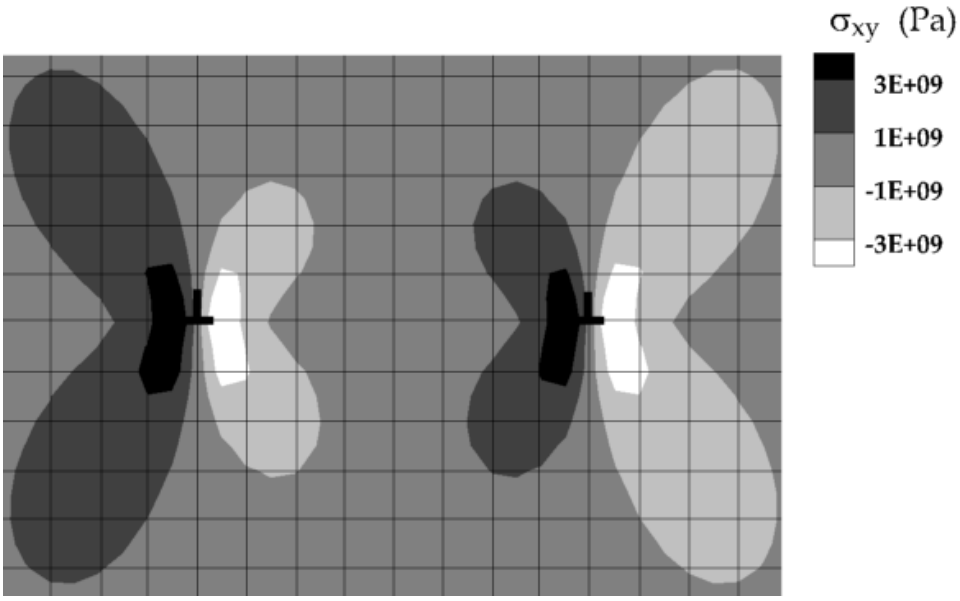

(b)

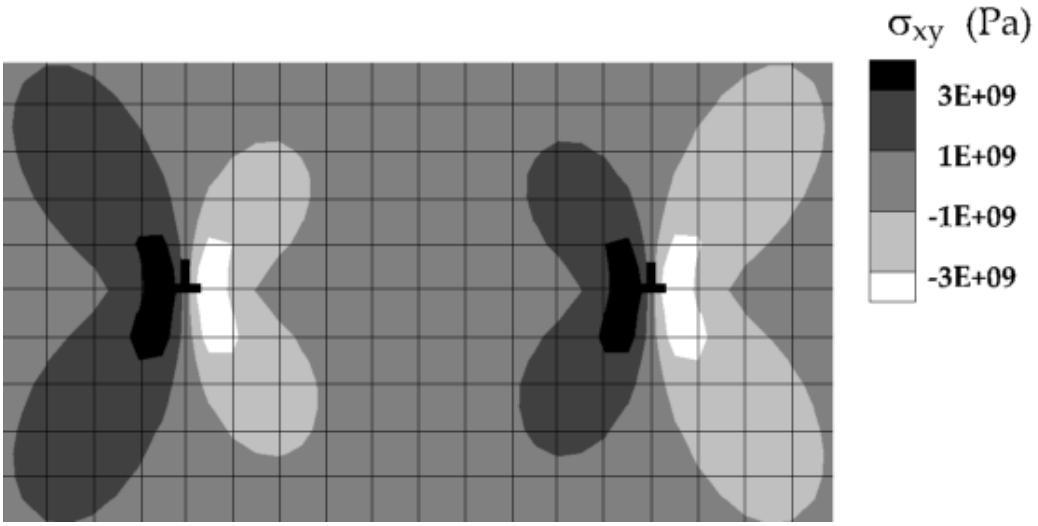

(c)

Figure 6-7 Contours of the shear stress on the xy plane around two parallel edge dislocations with equal Burgers vectors at a nominal hydrogen concentration, $c_0 = 0.1$, and temperature, 300 K
The separation distances are a) 6b b) 8b c) 10b

6-2-3 Two parallel edge dislocations with opposite Burgers vectors

In Figure (6-8), the hydrogen atmosphere in equilibrium with the stress field of two parallel dislocations with the opposite Burgers vectors for three separation distances of 6*b*, 8*b* and 10*b* between the dislocations are shown in the form of normalized iso-concentration $\frac{c}{c_0}$, under temperature, 300 K and nominal hydrogen concentration $c_0 = 0.1$. The hydrogen atmosphere around each dislocation is nonsymmetrical when compared with the atmosphere of the single dislocation shown in Figure (6-4). This is a direct result of the linear superposition in the stress field of the two dislocations.

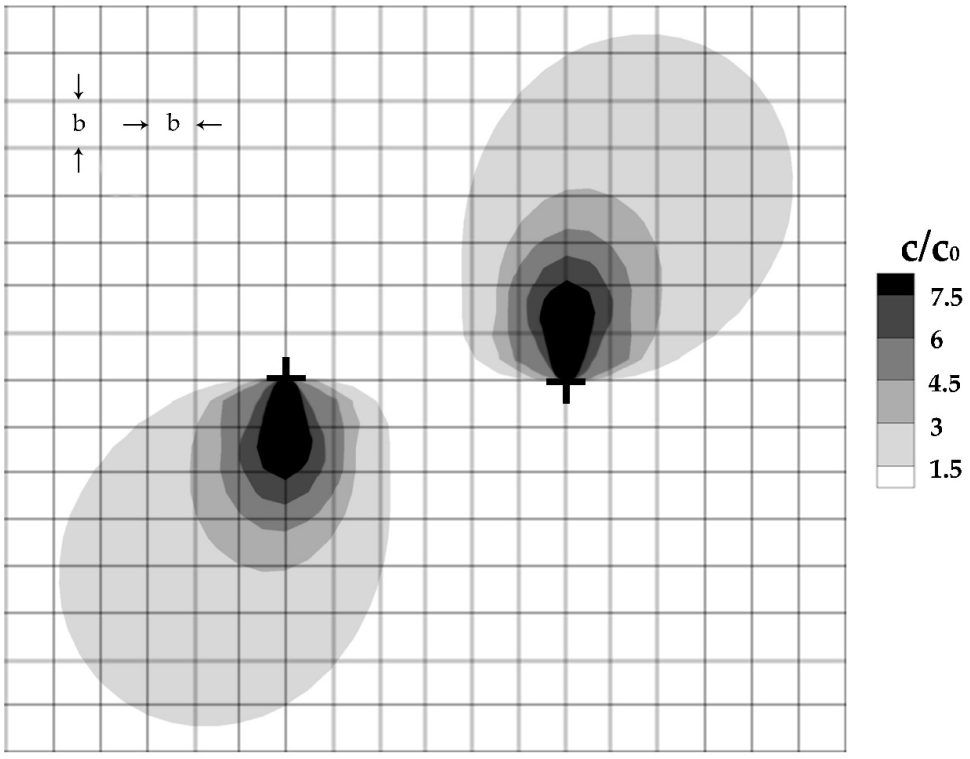

(a)

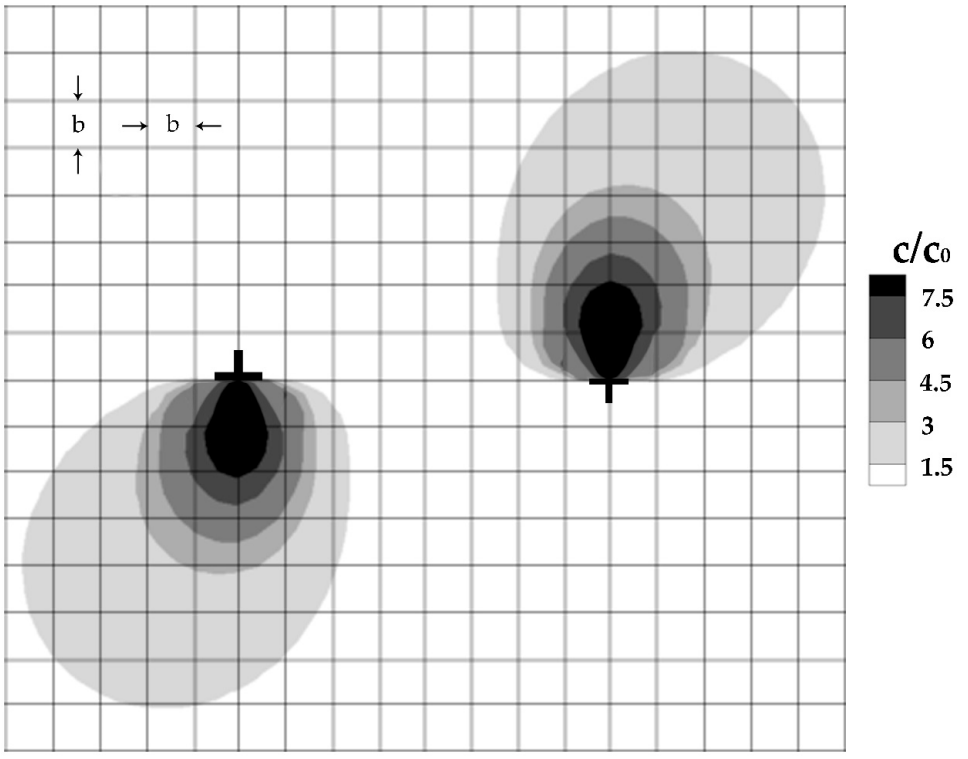

(b)

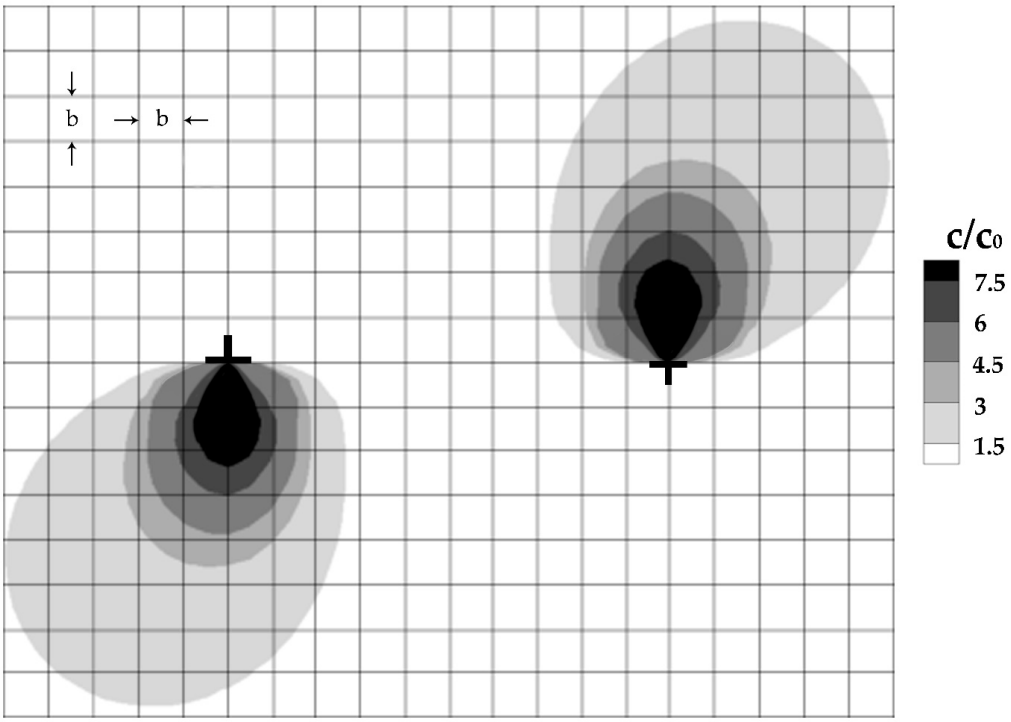

(c)

Figure 6-8 Contours of the normalized hydrogen concentration $\frac{c}{c_0}$ around two parallel edge dislocations with opposite Burgers vectors at a nominal hydrogen concentration, $c_0 = 0.1$, and temperature, 300 K
The separation distances are a) 6b b) 8b c) 10b

In the stress field of two parallel dislocations with opposite Burgers vectors, the positive hydrostatic stress field of each dislocation is weakened and the hydrogen concentration in the tensile regions of the two dislocations is less than that of a single dislocation alone. Figures (6-9) (a)-(c) to (6-11) (a)-(c) indicate the

distributions of the normal and shear stress corresponding to dislocation separation distances of 6*b*, 8*b*, and 10*b*. The normal stress distributions are asymmetric, however, the magnitude of these stresses are zero between two dislocations away from the cores of the dislocations. On the other hand, shear stress distribution is symmetric, the magnitude of these stresses decrease by increasing the distance of two dislocations.

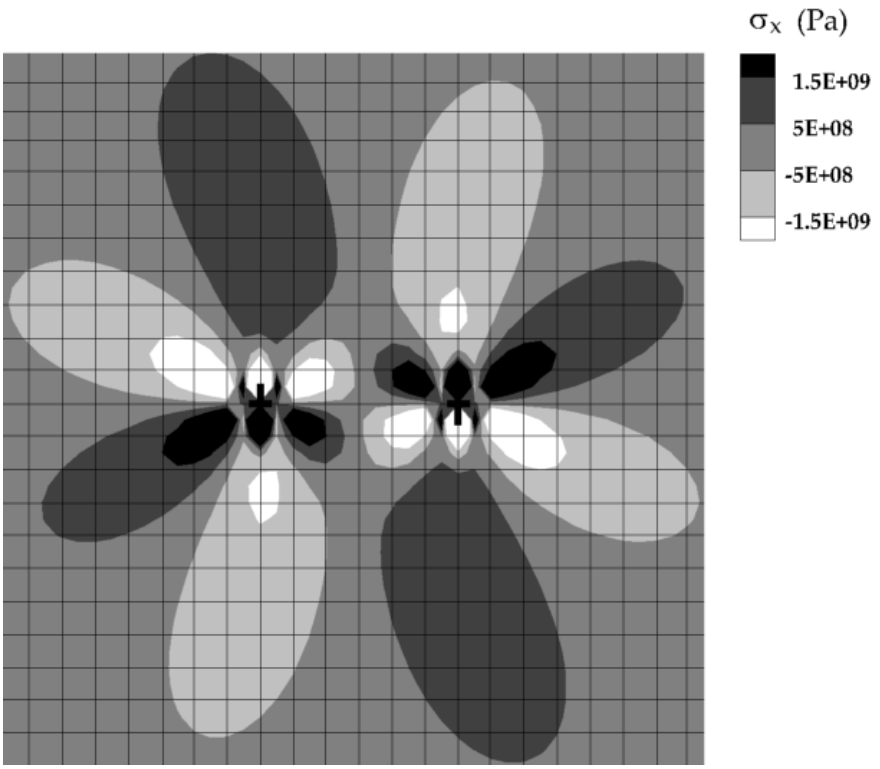

(a)

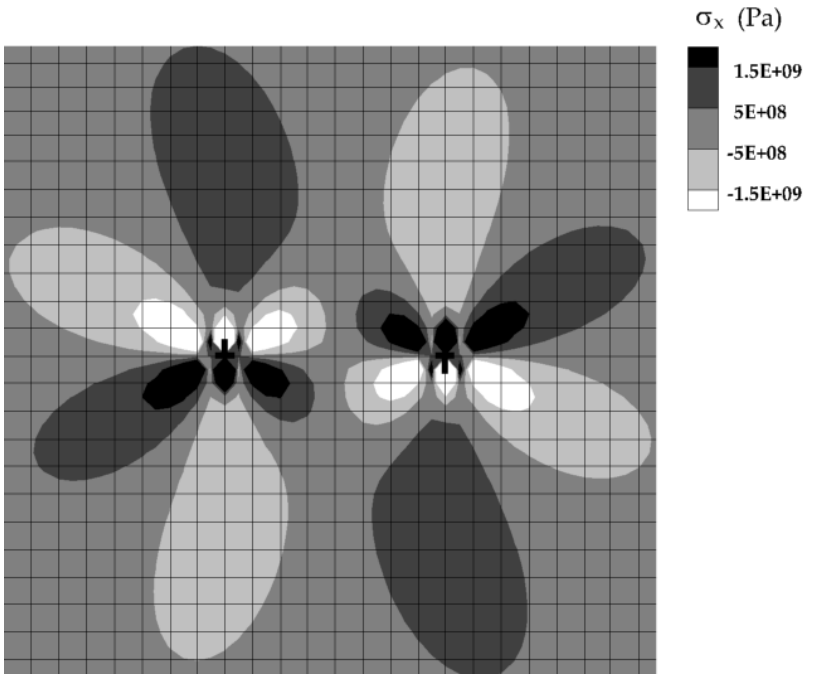

(b)

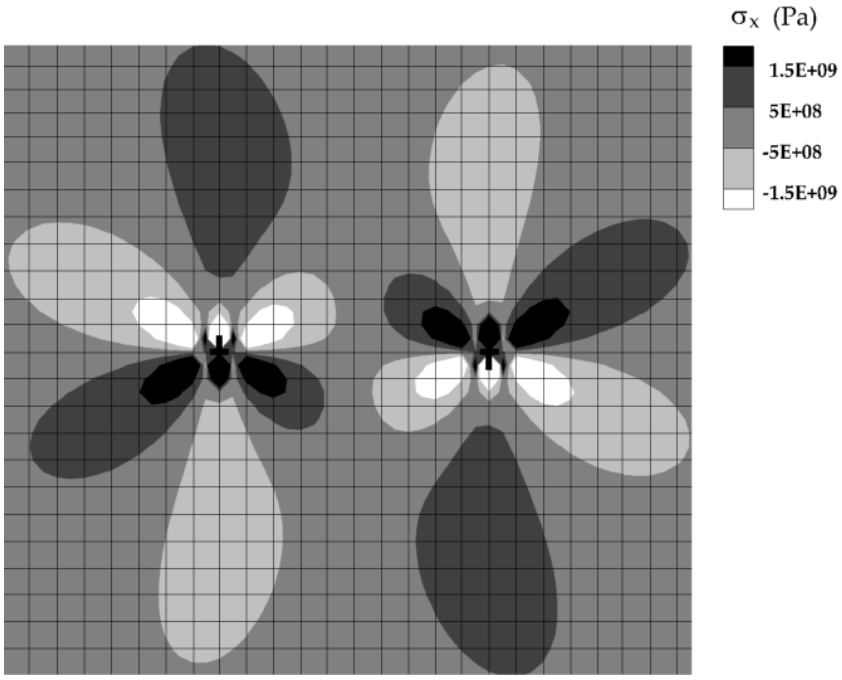

(c)

Figure 6-9 Contours of the normal stresses in x direction around two parallel edge dislocations with opposite Burgers vectors at a nominal hydrogen concentration, $c_0 = 0.1$, and temperature, 300 K

The separation distances are a) 6b b) 8b c) 10b

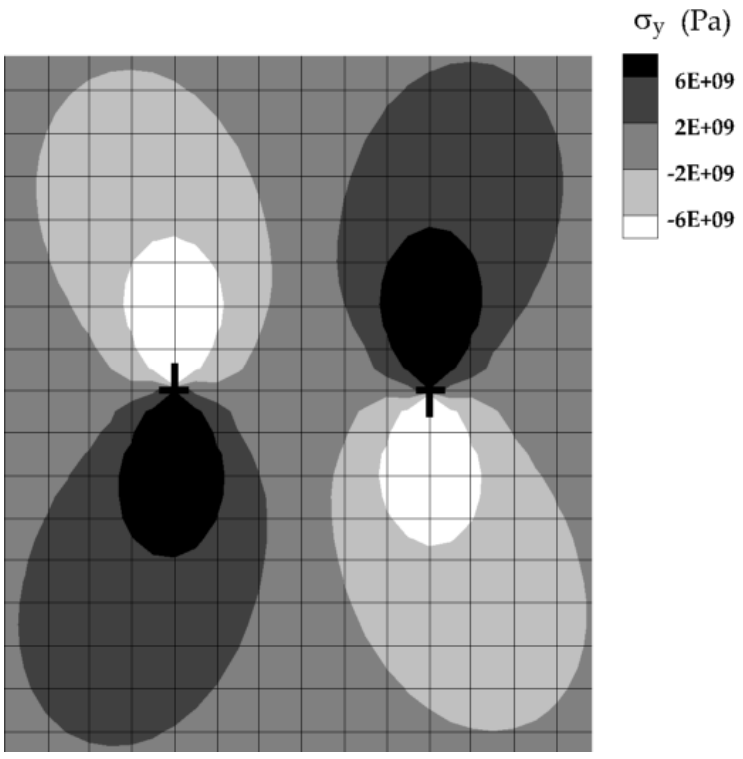

(a)

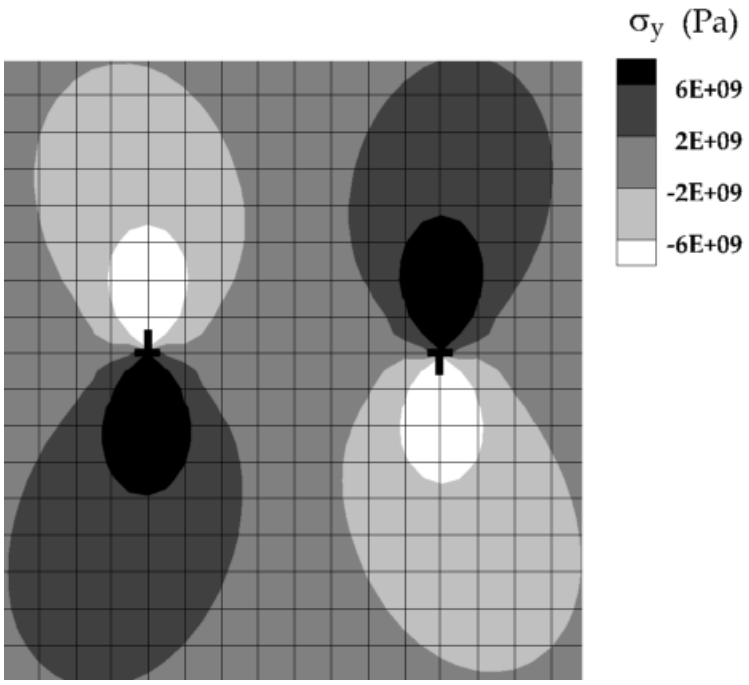

(b)

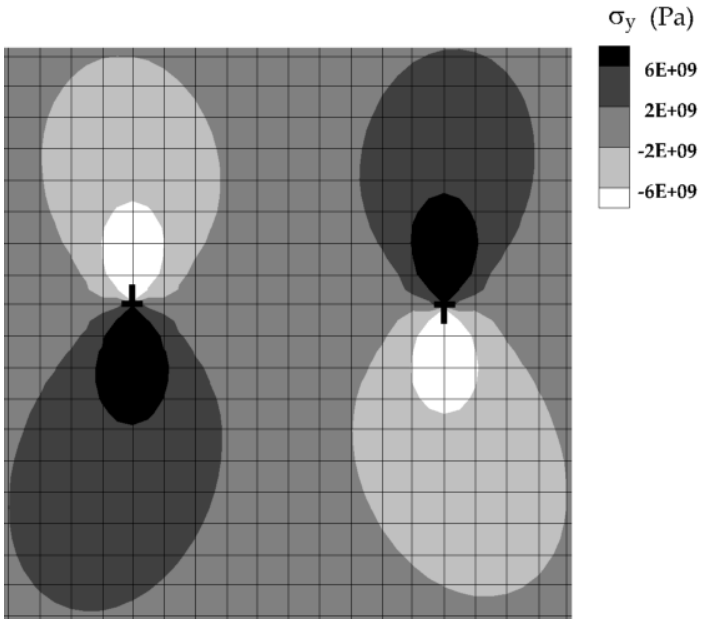

(c)

Figure 6-10 Contours of the normal stress in the y direction around two parallel edge dislocations with opposite Burgers vectors at a nominal hydrogen concentration, $c_0 = 0.1$, and temperature, 300 K

The separation distances are a) 6b b) 8b c) 10b

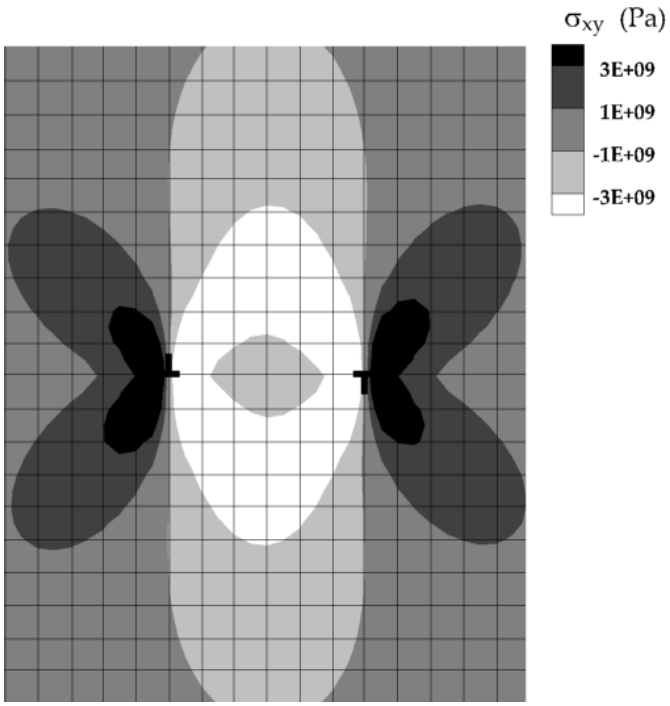

(a)

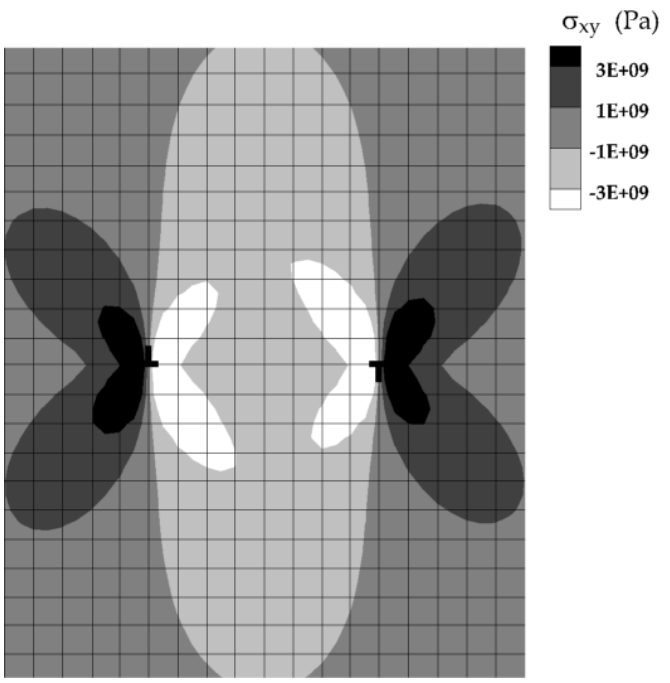

(b)

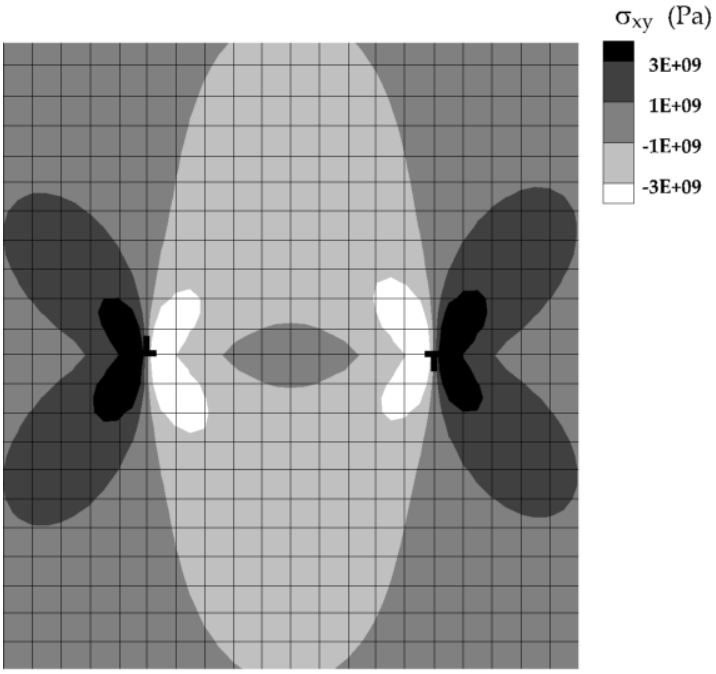

(c)

Figure 6-11 Contours of the shear stress on the xy plane around two parallel edge dislocations with opposite Burgers vectors at a nominal hydrogen concentration, $c_0 = 0.1$, and temperature, 300 K

The separation distances are a) 6b b) 8b c) 10b

6 -3 Extended studies

First, the effect of initial concentration on the hydrogen concentration distributing around a dislocation is studied in the case of a single edge dislocation for initial concentration of 0.1, 0.01, and 0.001.

Secondly, the effect of the second order interaction energy on concentration distribution is investigated, and as will be shown, in some cases this effect substantially changes the results of the concentration in the field especially near the dislocation core. The simulations are performed for a single edge dislocation with three initial concentrations of 0.1, 0.01, and 0.001.

Finally the hydrogen concentration is calculated for the case of randomly-distributed dislocations. Both effects of second order interaction energy and the magnitude of the initial concentration on concentration distribution are also investigated in this case.

6 -3-1 Effect of initial hydrogen concentration

In order to investigate the effect of initial concentration, three initial concentrations with magnitudes 0.1, 0.01, and 0.001 are considered in the case of a single edge dislocation. The results are shown in the form of normalized iso-concentration $\frac{c}{c_0}$,

under temperature 300 K in Figures (6-12) (a)-(c). The results show significant differences in the ratio of $\frac{c}{c_0}$ near the core, however, this difference diminishes for regions far from the core. In addition, the results for $c_0 = 0.01$ and $c_0 = 0.001$ are almost similar everywhere except the region very close to the core.

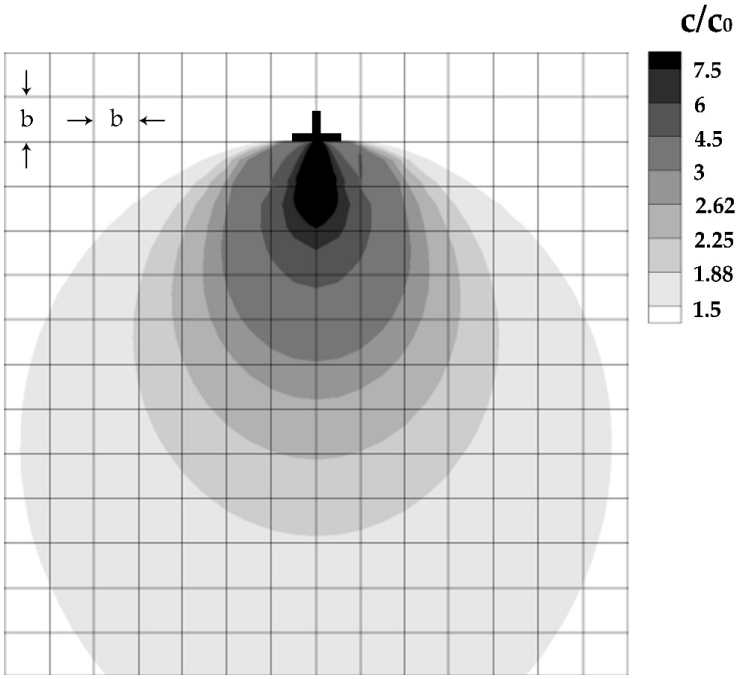

(a)

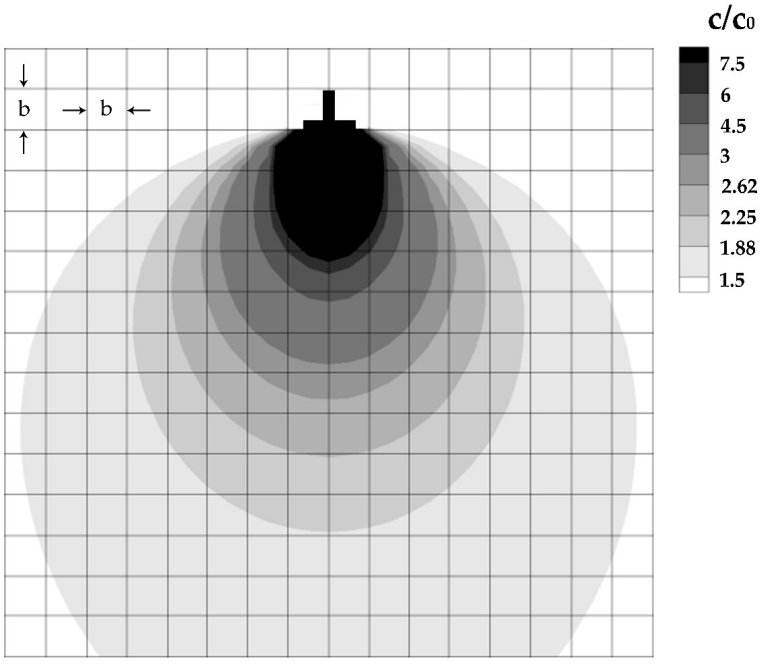

(b)

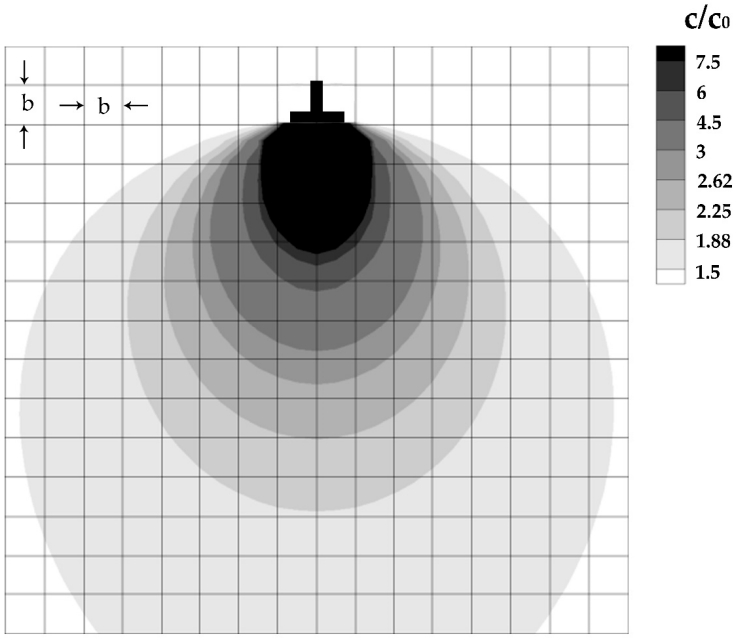

(c)

Figure 6-12 Contours of the normalized hydrogen concentration $\frac{c}{c_0}$ around a single edge dislocation for temperature 300 K and different nominal hydrogen concentrations a) $c_0 = 0.1$ b) $c_0 = 0.01$ c) $c_0 = 0.001$

6 -3-2 Effect of the second order interaction energy

To this point, only the first order interaction energy has been considered in all simulations, however, the second order interaction energy presented in equation (3-45) can alter the results. In this case, the effect of the second order interaction energy is investigated for three initial concentration of 0.1, 0.01 and 0.001 for the single edge dislocation.

The results are shown in the form of normalized iso-concentration $\frac{c}{c_0}$, under temperature 300 K in Figures (6-13) (a)-(c). These results can be compared with those in the previous section and it can be concluded that the change is noteworthy near the dislocation core. The differences vanish as the initial concentration decreases. As shown in the Figures (6-13) (b), (c) the changes of the effect of the second order interaction energy is negligible between 0.01 and 0.001 indicating almost no difference of considering 0.01 and 0.001 for an initial concentration.

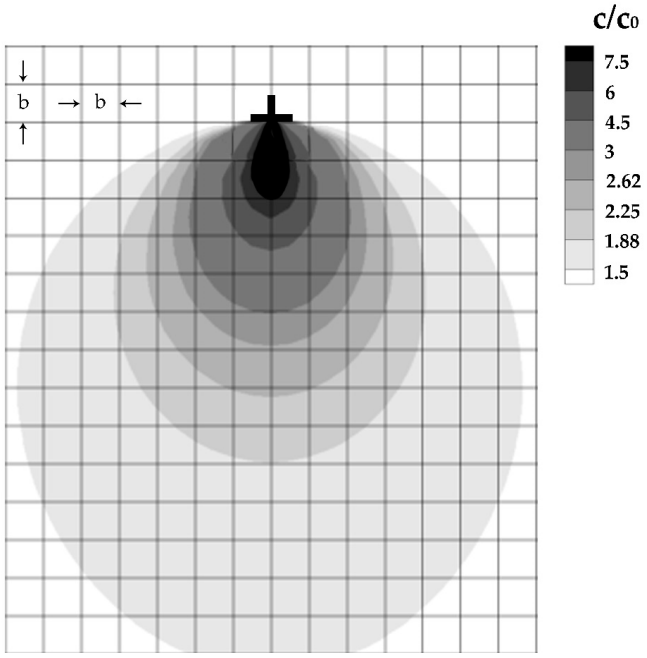

(a)

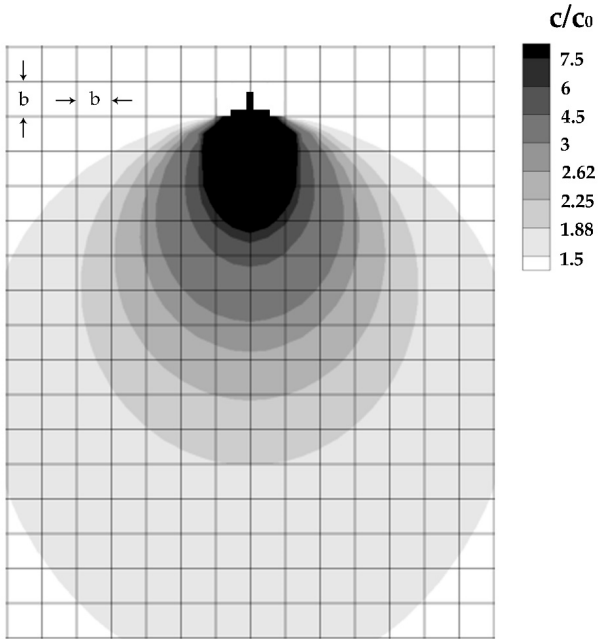

(b)

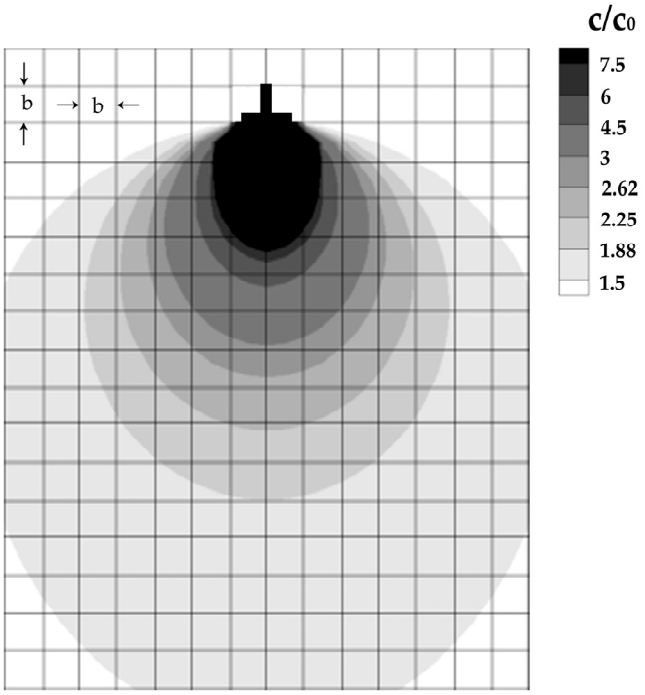

(c)

Figure 6-13 Contours of the normalized hydrogen concentration $\frac{c}{c_0}$ around a single edge dislocation with first and second order interaction energies for temperature, 300 K
The initial concentrations are a) $c_0 = 0.1$ b) $c_0 = 0.01$ c) $c_0 = 0.001$

In general, the second order interaction energy is smaller than the first order interaction energy, however, this is not the case for the vicinity of a dislocation. The second order interaction energy decreases with distance from the dislocation proportional to $\frac{1}{\mathbf{r}^2}$, in contrast to the $\frac{1}{\mathbf{r}}$ dependence of the first order interaction energy, therefore, the effect of this term is significant in the region close to the dislocation as shown in Figure (6-14). On the other hand, this effect diminishes by decreasing the magnitude of the initial concentration.

The distribution of the ratio of the second order to the first order interaction energy is shown in Figure (6-14) for three initial concentrations 0.1, 0.01, and 0.001.

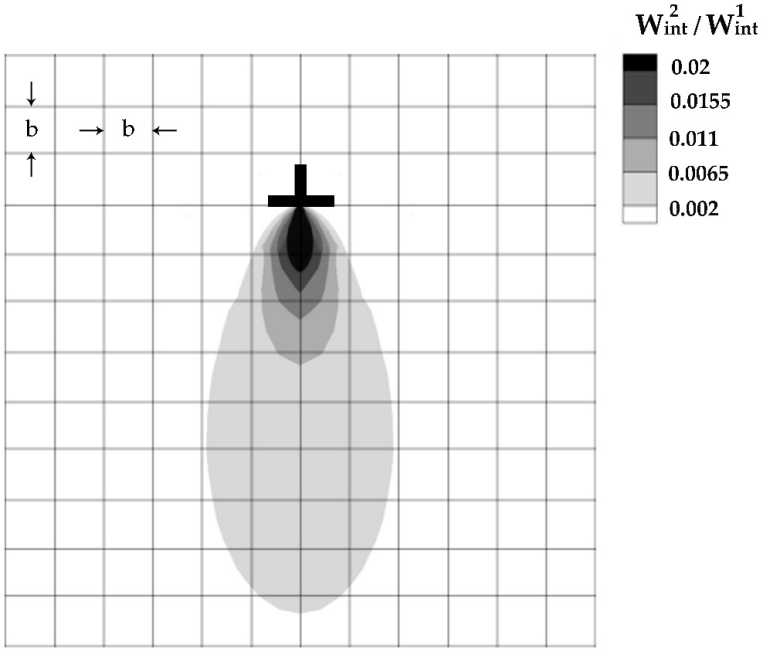

(a)

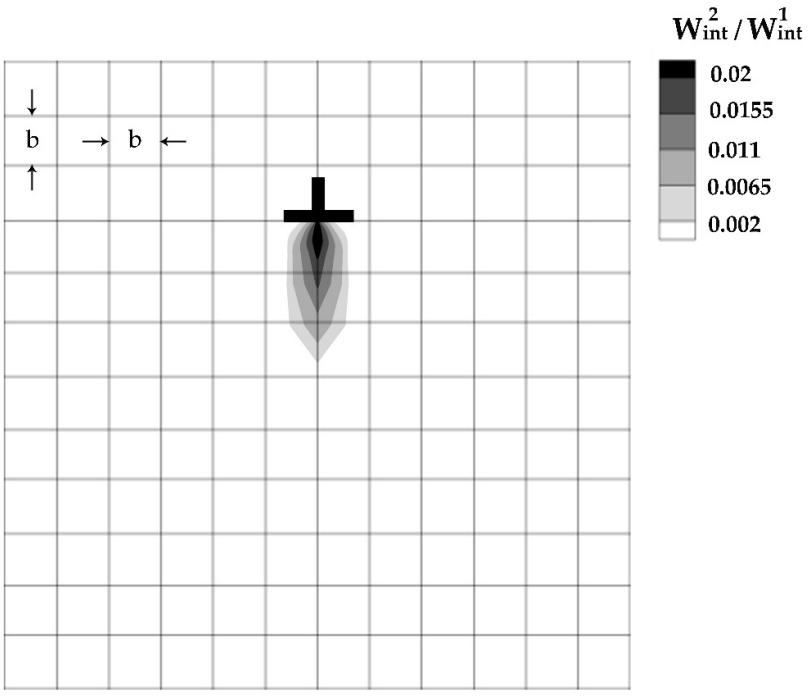

(b)

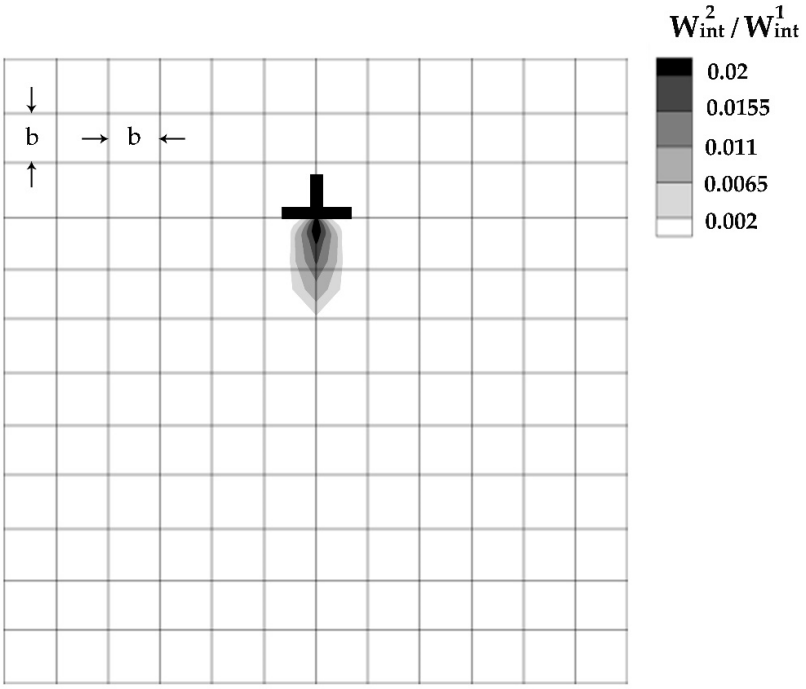

(c)

Figure 6-14 Contours of the ratio of the second order to the first interaction energy around a single edge dislocation for temperature, 300 K
The initial concentrations are a) $c_0 = 0.1$ b) $c_0 = 0.01$ c) $c_0 = 0.001$

6 -3-3 Randomly-distributed dislocations

In this subsection, the problem is extended to simulate the randomly-distributed dislocations network which mimics a more practical problem for distribution of hydrogen in the presence of dislocations. The simulation has been accomplished for both effects of the second order interaction energy and different initial concentrations. The dislocations are distributed randomly in the simulation cell introduced in Figure (6-1).

The Contours of the normalized hydrogen concentration distribution for the initial concentration of 0.1 with only first order and with both first and second order interaction energies are shown in Figure (6-15).

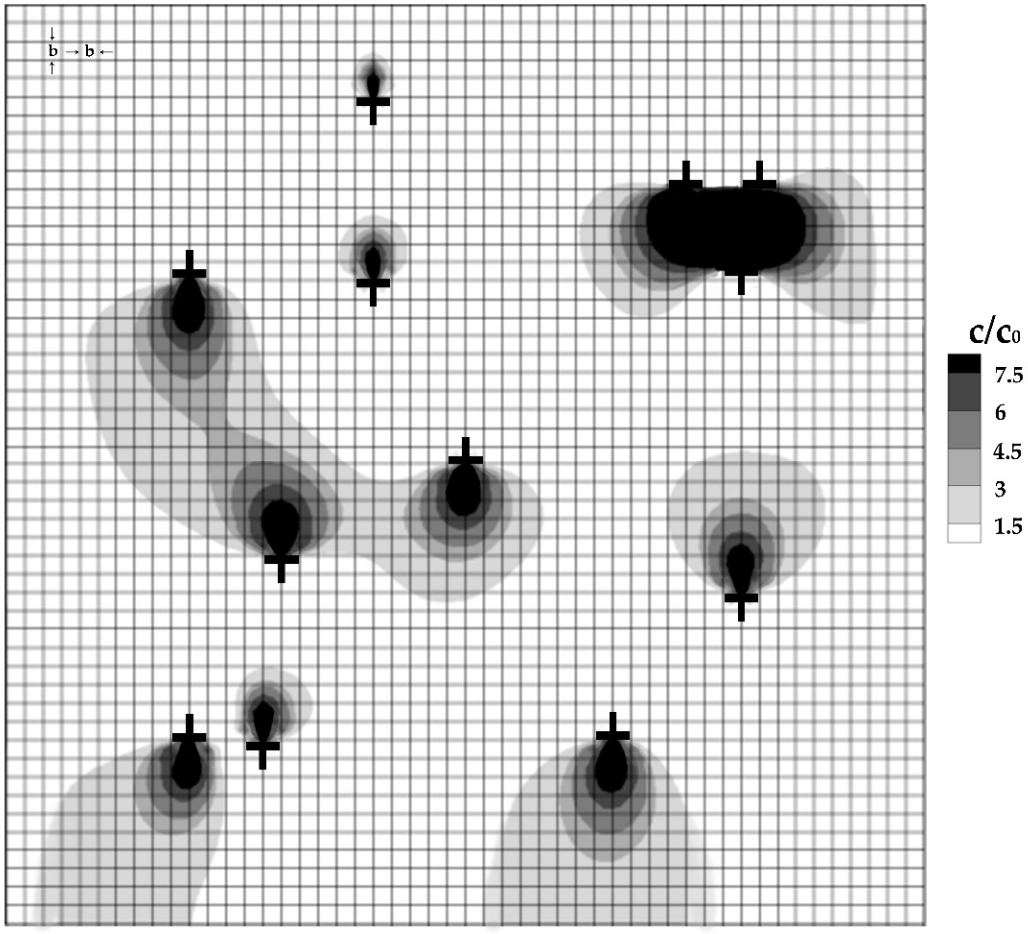

(a)

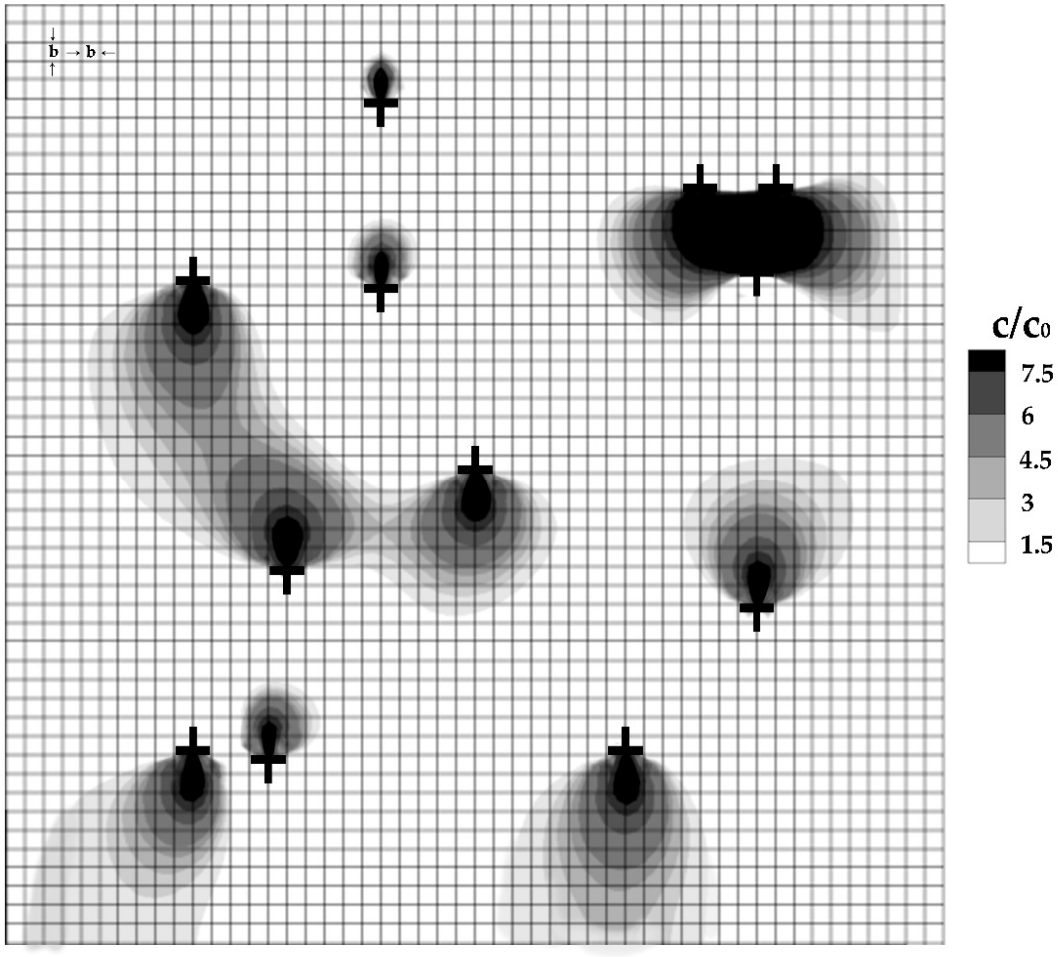

(b)

Figure 6-15 Contours of the normalized hydrogen concentration $\frac{c}{c_0}$ around randomly-distributed dislocations with the first and second order interaction energies and for initial concentration, 0.1 and temperature, 300 K
a) Only the first order interaction energy
b) Both the first and the second order interaction energies

Results for an initial concentration of 0.01 for only the first order and with both the first and the second order interaction energies are shown in Figure (6-16).

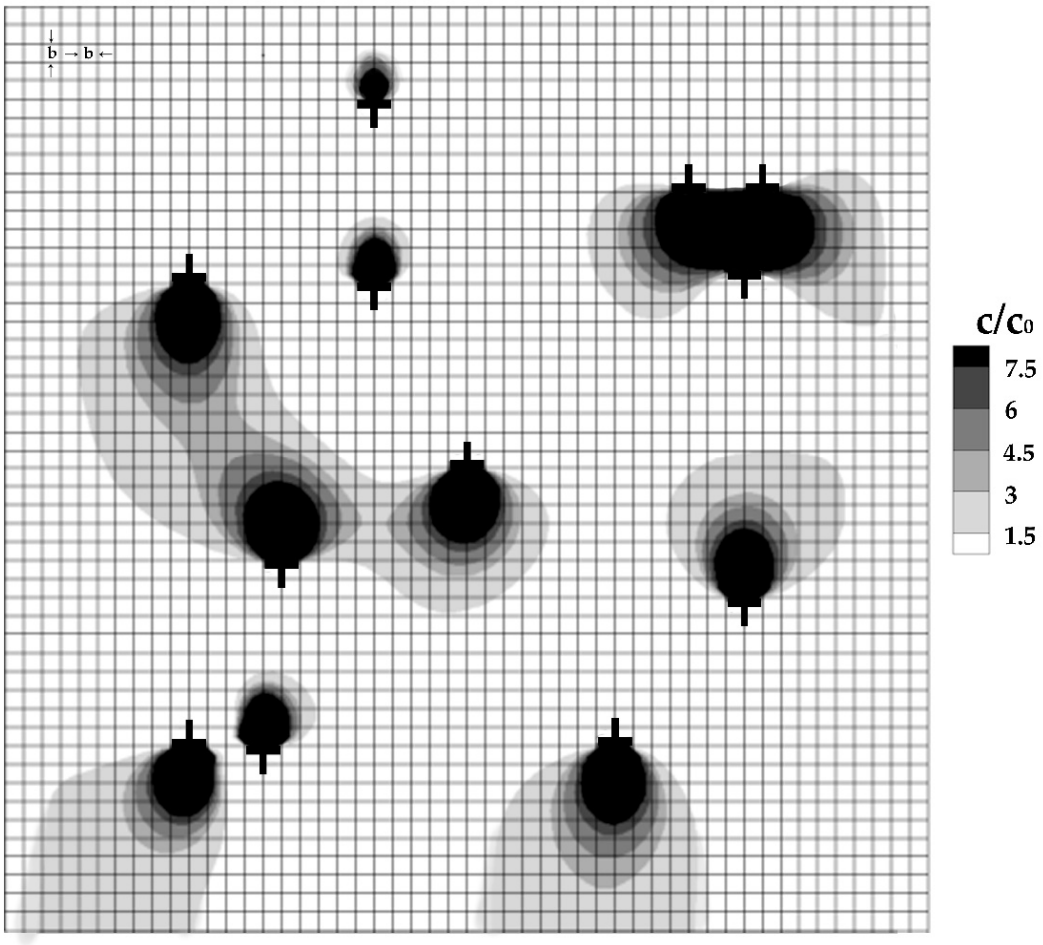

(a)

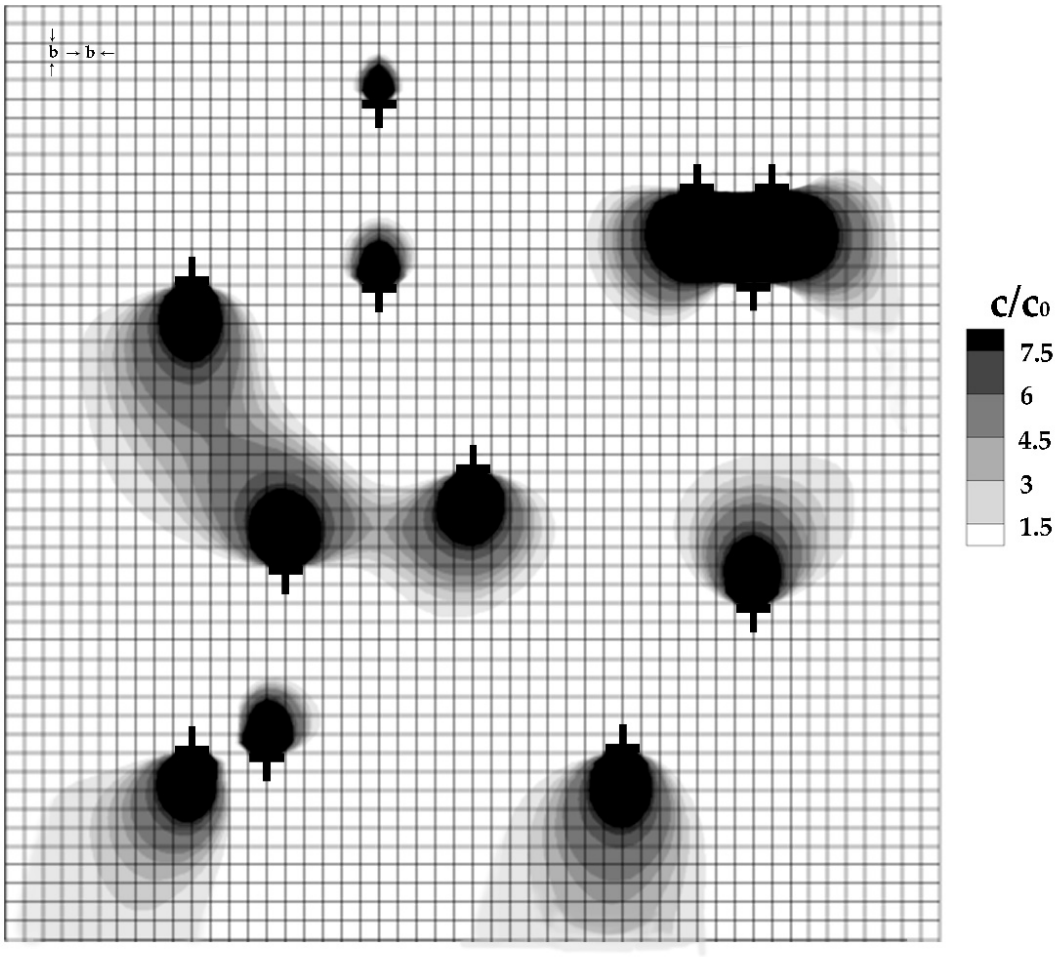

(b)

Figure 6-16 Contours of the normalized hydrogen concentration $\frac{c}{c_0}$ around randomly-distributed dislocations with the first and the second order interaction energies for initial concentration, 0.01 and temperature, 300 K
a) Only the first order interaction energy
b) Both the first and the second order interaction energies

6 -4 Closure

A method for calculating the effects of a mobile solute hydrogen, on the interaction between elastic centers has been developed. This method allows modeling of the lattice distortion induced by a single or a continuous distribution of interstitial atoms coupled with the distortion field of lattice defects such as dislocations. The method was applied using analytical and non-linear finite element methods to study the effects of hydrogen on the interaction between dislocations and solutes.

Model calculations were carried out for the case where hydrogen increased the elastic modulus of the system and in which the first and second order elastic interaction between the dislocations and hydrogen were considered.

The simulations were performed for three different nominal initial concentrations with the magnitude of 0.1, 0.01 and 0.001 for a single edge dislocation, two parallel edge dislocations with same and opposite Burgers vectors and randomly-distributed dislocations, indicating the increase of normalized hydrogen concentration in the field especially near the cores of dislocations by decreasing the initial values of nominal initial concentrations.

The effect of the second order interaction energy is significant for the region close to the core of a dislocation for the higher value of initial concentrations, however, it can be negligible for the distance faraway from dislocations.

References

[1] R. Thomson. "Brittle fracture in a ductile material with application to hydrogen embrittlement"; Journal of Material Science; 13 (1978) 128-142

[2] Joan B. Berkowitz, and Newton H. Emerson; NASA; SP-5114 (1972)

[3] M.R. Louthan Jr., G.R. Caskey Jr., J.A Donovan, and D.E. Rawl Jr.;"Hydrogen embrittlement of metals"; Material Science and Engineering; 10 (1972) 357-368

[4] B. J. Berkowitz, and R. D. Kane; "The effect of impurity on the hydrogen embrittlement of a high strength nickel based alloy in H_2S environment"; Corrosion; January 1980; Vol. 36; No. 1; pp. 24-29

[5] S. Gahr, H. K. Birnbaum; "Hydrogen embrittlement of niobium—III. High temperature behavior"; Acta Metallurgica; 26 (1978) 1781-1788

[6] www.dierk-raabe.com

[7] G. P. Tiwari, A. Bose, J.K. Chakravartty, S. L. Wadekar, M. K. Totlani, R. N. Arya, and R. K. Fotedar; "A study of internal hudrogen embrittlement of steels"; 286 (2000) 269-281

[8] Howard G. Nelson; "Environmental hydrogen embrittlement of an α-β titanium alloy: effect of hydrogen pressure"; Metallurgical Transaction; 4 (1973) 364-467

[9] Howard G. Nelson, Dell P. Williams, and James E. Stein; "Environmental hydrogen embrittlement of an α-β titanium alloy: effect of microstructure"; Metallurgical Transaction; 3 (1972) 473-479

[10] R. A. Oriani, and P.H. Josephic; "Equilibrium aspects of hydrogen-induced cracking of steel"; Acta Metallurgica; 22 (1974) 1065-1074

[11] W. A. Lanford, H. P. Trautvetter, J. F. Ziegler, and J. Keller; "New precision technique for measuring the concentration versus depth of hydrogen in solids"; Applied Physics Letters ; 28; (1976) 566

[12] M. Moser, V. Schmidt; "Fractography and mechanism of hydrogen cracking-The fisheye concept"; Academy of science GDR, Institute of solid state physics and electron microscopy; 1982

[13] C. D. Beachem; "A new model for hydrogen assisted cracking (hydrogen "embrittlement")"; Metallurgical Transaction; 3 (1972) 441-445

[14] http://app.aws.org

[15] C. D. Beachem; "The kinetics of hydrogen embrittlement: A quantitative diffusion model"; Engineering Fracture Mechanics; 3 (1972) 441-445

[16] Daniel S. Janikowski; "Condenser tube failure mechanisms"; Plymouth Tube Co.; 2011

[17] M. R. Louthan Jr.; "Hydrogen embrittlement of metals: A primer for the failure analyst"; Journal of Failure Analysis and Prevension; 8 (2008) 289-307

[18] Rob in News; “Hydrogen embrittlement-High strength steels Achilles heel”; 2013

[19] Max-Planck Institute research; www. Fkf.mpg.de

[20] Daniel P. Abraham and Carl J. Altstetter; “Hydrogen-Enhanced Localization of Plasticity in an Austenitic Stainless Steel”; Metallurgical and Materials Transactions; 26A (1995) 2859-2871

[21] V.N. Shivanyuk, B.D. Shanina, A.V. Tarasenko, V.G. Gavriljuk, and J. Foct; “Effect of Hydrogen on Atomic Bonds in Autenitic Stainless Steel”; Scripta Materialia; 44 (2001) 2765-2773

[22] A.G. Varias and A.R. Massih; “Hydride-Induced Embrittlement and Fracture in Metals – Effect of Stress and Temperature Distribution”. Journal of the Mechanics and Physics of Solids; 50 (2002) 1469-1510

[23] www.tms.org

[24] K. Sieradzki and P. Ficalora; "The Mechanism of Hydrogen Embrittlement Adsorption or Decohesion"; Scripta Metallurgica; 14 (1980) 641-644

[25] Wolfgang Losch; "Hydrogen Embrittlement: A New Model for the Mechanism of Reduction of Metallic Cohesion"; Scripta Metallurgica; 13 (1979) 661-664

[26] A. Toshimitsu Yokobori Jr., Takenao Nemoto, Koji Satoh, and Tetsuya Yamada; "The Characteristics of Hydrogen Diffusion and Concentration Around a Crack Tip Concerned With Hydrogen Embrittlement"; Corrosion Science; 44 (2002) 407-424.

[27] Solanki research group; Multiphysics lab; Multiphysics.lab.asu.edu

[28] Pekka Nevasmaa; "Predictive Model for the Weld Metal Hydrogen Cracking in High-Strength Multipass Welds"; Acta University of Oulu; 191 (2003)

[29] Y. Liang, D.C. Ahn, P. Sofronis, R.H. Dodds Jr., D. Bammann; "Effect of Hydrogen Trapping on Void Growth and Coalescence in Metals and Alloys"; Mechanics of Materials; 40 (2008) 115-132

[30] I.M. Robertson; "The Effect of Hydrogen on Dislocation Dynamics"; Engineering Fracture Mechanics; 64 (1999) 649-673

[31] P. Sofronis, Y. Liang, and N. Aravas; "Hydrogen Induced Shear Localization of the Plastic Flow in Metals and Alloys"; European Journal of Mechanics A/solids; 20 (2001) 857-872.

[32] http://www.nde-ed.org

[33] Cristian Teodosiu; "The elastic field of point defects"; Elastic models of crystal defects; (1982) 287-316

[34] Helmut Mehrer; "Diffusion in solids"; Springer series in solid state science; ISBN 978-3-540-71486-6

[35] Aloke Paul, Tomi Laurila, Vesa Vuorinen, and Sergiy V. Divinski; "Thermodynamics, diffusion and Kirkendall effects in solids"; Springer; ISBN 978-3-319-07461-0

[36] Devendar Gupta; "Diffusion processes in advanced technological materials"; William Andrew, Inc; ISBN 0-8155-1501-4

[37] E. L. Cussler; "Diffusion- mass transfer in fluid systems"; Cambridge University; ISBN 0-521-56477-8

[38] Cottrell, A. H. and Bilby, B. A.; "Dislocation theory of yielding and strain ageing of iron"; Proc. Phys. Soc.; 1949; A62; 49-62

[39] D. N. Besher; "On the distribution of impurity atoms in the stress field of a dislocation"; Acta Metall.; 1958; 521-523

[40] W. Beck, J. O'M. Bockris, J. McBreen and L. Nanis, B. A.; " Hydrogen Permeation in Metals as a Function of Stress, Temperature and Dissolved Hydrogen Concentration"; Proc. R. Soc.; 1966; A290, 220.

[41] Hirth, J. P. and Lothe, J.; "Theory of Dislocations" John Wiley; 1982; New York.

[42] Eshelby, J. D.; " The Force on an Elastic Singularity"; Phil. Trans.; 1951; A244, 87.

[43] V. Volterra; " Sur l'equilibre des crops elastiques multiplement connexes"; Ann. Ec. Norm.; 1907; t. 24, 401-517.

[44] Eshelby, J. D. "The determination of the elastic field of an ellipsoidal mclusion and related problems." ; 1957; Proc. R. Sot. A241, 376-396.

[45] Love, A. E. H. "Theory of elasticity"; 1927; Cambridge University Press.

[46] Eshelby, J. D. "The continuum theory of lattice defects." Solid State Physics (ed. F. Seitz and D. Turnbull), 1956; Vol. 3, pp. 79-144. Academic Press, New York.

[47] Hirth, J. P. and Carnahan, B. "Hydrogen adsorption at dislocations and cracks in Fe." 1978; Acta Metall.; 26, 1795-1803.

[48] F. Dunne, N. Petrinic "Introduction to Computational Plasticity" 2004; Oxford University Press.

[49] P. Sofronis, H. K. Birnbaum; "Mechanics of the hydrogen-dislocation impurity interactions-I. Increasing shear modulus"; J. Mech. Phys. Solids; 1995; pp 49-90.

[50] Mazzolai, F. M. and Birnbaum, H. K. "Elastic constants and ultrasonic attenuation of the α-α' phase of the N&H(D) system. I : Results." 1985a; J. Phys. F: Met. Phys.; 15, 507-523.

[51] Mazzolai, F. M. and Birnbaum, H. K. “Elastic constants and ultrasonic attenuation of the α-α′ phase of the N&H(D) system. II : Interpretation of results.” 1985b; J. Phys. F: Met. Phys.; 15, 525-542.

[52] Peisl, H. “Lattice strains due to hydrogen in metals. Hydrogen in Metals I, Topics in Applied Physics (ed. G. Alefeld and J. Volkl)” 1978; 28, pp. 53-74. Springer, New York.

Vita

Zara Molaeinia was always passionate about science, art, literature, and sports. She learned to read and write when she was four. The enthusiast of learning directly was inside her since then. In the beginning time of her life, she found herself attracted to some branches of sports and has had some accomplishments in basketball, swimming, skiing, and fitness. She went to NODT schools, and was on top of her classes all the time till she got the opportunity to enter to university and work on advanced science concepts. Meanwhile, she was as well pursuing her passion in arts, and could set up several exhibitions in painting, calligraphy, interior design, and piano recitals. In schools, she was working on computational mechanics in different fields, and got the opportunity to establish several journal papers and conference proceedings, write three mathematics books, and teach in several schools at undergraduate and partly graduate.

She is willing to continue chasing her dreams in all aspects she loves till the life time allows.